A Preliminary Habitat Suitability Model for Devil Rays in the Western Indian Ocean

Gency Guirhem[1], Haritz Arrizabalaga[1], Leire Lopetegui[1], Hilario Murua[2], Nerea Lezama Ochoa[3], Shane Griffiths[4], Jon Ruiz Gondra[5], Philippe S. Sabarros[6,7], Jose Carlos Baez[8], Maria Jose Juan-Jordá[1]

[1]AZTI, Marine Research Division, Basque Research and Technology Alliance (BRTA), Pasaia, Gipuzkoa, Spain
[2]International Seafood Sustainability Foundation (ISSF), Washington, DC, United States of America
[3] Institute of Marine Sciences, University of California Santa Cruz, Santa Cruz, CA, USA
[4]Inter-American Tropical Tuna Commission, Ecosystem and Bycatch Program, La Jolla, CA, USA
[5]AZTI, Marine Research Division, Basque Research and Technology Alliance (BRTA), Sukarrieta, Vizcaya, Spain
[6]MARBEC, Univ Montpellier, CNRS, Ifremer, IRD, Sète, France
[7]IRD, Ob7, Sète, France
[8]Instituto Español de Oceanografía, Centro Oceanográfico de Málaga, Fuengirola, Málaga, Spain

Summary

The European tropical tuna purse seine fishery incidentally captures three highly migratory and endangered species of devil rays, spinetail devil ray *Mobula mobular*, sicklefin devil ray *M. tarapacana*, and bentfin devil ray *M. thurstoni* in the Indian Ocean. Due to their global decreasing populations, understanding the factors of their spatial and temporal distributions and the associated environmental conditions are fundamental for their management and conservation. Yet, the spatial and temporal distribution of devil rays in the Indian Ocean is poorly understood. Here we developed a habitat suitability model for devil rays in the Western Indian Ocean depicting the seasonal and interannual changes in their spatial distributions and underlying environmental conditions. We used bycatch data collected between the period 2010-2020 by the EU tropical tuna purse seine observer programs to determine which environmental variables influence the occurrence of devil rays using generalized additive models. A separate modelling was done for the spinetail devil ray, and for the three species of devil rays combined, since many individuals are only recorded at the genus level. The environmental variables associated with the presence of devil rays were chlorophyll, sea surface height and sea surface temperature fronts. When modelling the habitat suitability for spinetail devil ray, the most influential environmental variables were net primary production of phytoplankton and sea surface temperature fronts. Both the interannual and seasonal variability in habitat suitability of devil rays were explained by these environmental variables. We also showed that devil rays are associated to permanent hotspots in the Mascarene Plateau and Central Indian Ridge, and to seasonal hotspots in the Western Arabian Sea and Equatorial regions where there is a high occurrence of devil rays during winter monsoon. We found that setting on large tuna schools decreases the chances of devil ray bycatch. Both models predicted a higher probability of incidental catch of devil rays in fishing sets on free swimming schools of tunas than in sets on fish aggregating devices. The identified hotspots and associated environmental characteristics provide information about the habitat use and ecology of the devil rays in the Western Indian Ocean. Furthermore, the habitat suitability models, and biological hotspots identified in this study could also to be used to inform the development of future spatial management measures, including time-area closures, to minimize the interaction of pelagic fisheries with these vulnerable species.

Keywords: devil rays, *Mobula*, bycatch, species distribution models, tuna fisheries, Indian ocean

1. Introduction

Tuna fisheries constitute a significant portion of the total fishery volume and value globally. In 2018, the industry contributed 5.2 million metric tons of volume, amounting to a value of approximately US$11.7 billion (McKinney et al. 2020). Consequently, tuna fisheries are crucial for providing food security and livelihoods, generating socio-economic benefits for many developed and developing countries around the world (Galland et al. 2016; McKinney et al. 2020). Despite this valuable provision of goods and benefits, sustainably managing tuna fisheries still faces many challenges in protecting vulnerable species interacting with these fisheries. Tuna fisheries can have large impacts on incidentally caught species of sharks, rays, sea turtles, sea birds and marine mammals (here referred as bycatch species), some of which can be particularly sensitive to overexploitation due to their intrinsic low productive rates (Duffy et al. 2019). Effective governance of bycatch is necessary to avoid the ecological consequences of fishing on marine ecosystems and undesirable socio-economic consequences on fisheries (Gilman et al. 2014).

Regional Fisheries Management Organizations (RFMOs) in charge of managing fisheries targeting tunas, billfishes and some oceanic sharks have had limited progress governing bycatch of vulnerable species throughout the years (Juan-Jordá et al. 2018). While tuna RFMOs have adopted a wide range of management and conservation measures to control and mitigate bycatch on vulnerable species, these measures have been perceived as insufficient, difficult to enforce and considered piecemeal since their joint implementation do not consider potential conflicts among them as well as their potential mutual benefits (Gilman et al. 2014). The management measures to mitigate bycatch of vulnerable species adopted in the five tuna RFMOs have mostly focused on either changing gear configuration and fishing methods to reduce bycatch or by establishing best handling and release practices to increase their probability of post-release survival (Clarke et al. 2014). In contrast, the establishment of bycatch limits and time-area closures for fisheries to reduce bycatch impacts have been very limited to none in tuna RFMOs (Hall et al. 2013; Clarke et al. 2014). Bycatch limits have only been applied to limit dolphin mortality in purse seine fisheries in the eastern Pacific Ocean (Juan-Jordá et al. 2018). Moreover, the small number of cases where area-time closures have been established in tuna fisheries have the main objective of reducing the catch of main target tunas, such as juvenile yellowfin and bigeye tunas in purse seine fisheries and juvenile swordfish in longline fisheries (Boerder et al. 2019).

There is increasing need to understand the spatial, temporal and environment factors determining high bycatch of vulnerable species interacting with tuna fishery operations. Furthermore, it is also important to examine to what extent the use of fixed or temporal time area closures would be an effective complementary measure in reducing bycatch in tuna RFMOs (Boerder et al. 2019). Towards this aim, Species Distribution Models (SDM), also known as ecological niche models, have increasingly been developed to understand the relationships between the presence and abundance of a vulnerable species caught in tuna fisheries and its environment predictors using a wide range of statistical learning methods (Sequeira et al. 2014; Montero et al. 2016; Cruz et al. 2018; Stock et al. 2019; Thorne et al. 2019; Lezama-Ochoa et al. 2020a; Lezama-Ochoa et al. 2020b; Lopez et al. 2020; Navarro et al. 2020; Stock et al. 2020; Díaz-Delgado et al. 2021). Having good knowledge of the species distribution and their habitat use is essential to minimize the interaction of fisheries with the most vulnerable species, and potentially useful to inform effective management regulations involving time area closures. SDMs have been developed for target tunas (Arrizabalaga et al. 2015), yellowfin tuna *Thunnus albacares* (Lan et al. 2017), skipjack tuna *Katsuwonus pelamis* (Druon et al. 2017; Putri et al. 2019), and non-target species including sailfish *Istiophorus platypterus* (Martinez-Rincon et al. 2015), whale sharks (Sequeira et al. 2014), silky shark *Carcharhinus falciformis* and rough triggerfish *Canthidermis maculata* (Lezama-Ochoa et al. 2016), olive ridley *Lepidochelys olivacea* (Montero et al. 2016) and spinetail devil ray (Lezama-Ochoa et al. 2019; Lezama-Ochoa et al. 2020a; Lezama-Ochoa et al. 2020b). These studies have mostly used fisheries dependent data such as the catch in log books (Oyafuso et al. 2017; Forrestal et al. 2019) and are increasingly using fisheries observer data from onboard commercial vessels (Sequeira et al. 2014; Lezama-Ochoa et al. 2016; Montero et al. 2016; Lezama-Ochoa et al. 2019; Lezama-Ochoa et al. 2020a; Lopez et al. 2020; Martinez-Rincon et al. 2015), with Generalized Additive Models (GAMs) being the most frequent statistical method used for modeling the distribution and environmental preferences of large pelagic fish and non-fish species.

The application of SDM to vulnerable species interacting with large scale tuna fisheries in the open ocean, has traditionally been challenging. This is due in part by the large spatial distributions of these migratory species, the lack of recorded occurrences, and the low observer coverage rates required in most of these fisheries (Hall et al. 2013; Gilman et al. 2014). However, in contrast to longline fisheries, the level of observer coverage in purse seine

fisheries has considerably increased in the last 10-20 years, from the minimum mandatory 5% observer coverage for all pelagic fisheries to sometimes 100% observer coverage all year round in some of RFMOs such as the Western and Central Pacific Fisheries Commission (WCPFC) and Inter American Tropical Tuna Commission (IATTC) or during specific periods such as during Fishing Aggregating Device (FAD) moratoriums or for specific fisheries (bluefin tuna fisheries) in other RMFOs such as International Commission for the Conservation of Atlantic Tunas (ICCAT) (ICCAT 2019). Moreover, some tuna purse seine fleets, such as the EU tropical tuna purse seine fleet, have also been increasing voluntarily its observer coverage to close to 100% using a combination of human observers and Electronic Monitoring System (EMS), with the objective to obtain ecolabel certifications among others (Ruiz et al. 2018). In this study, we take advantage of the recent increases in the observer coverage in the EU tropical tuna purse seine fishery operating in the Western Indian Ocean to advance our understanding on the spatial, temporal and environment factors determining high bycatch rates of vulnerable species interacting with this fishery.

In the Western Indian Ocean, the purse seine fishery targets tropical tuna species and incidentally catches diverse bycatch species (Lezama-Ochoa et al. 2015). Purse seine fisheries, relative to other fishing method, have broad spatial coverage, high intensity of effort, and high bycatch documentation (Martin 2020; Orue et al. 2020). In this type of fishing gear, tuna is targeted in either Free-Swimming Schools (FSC) or Fish Aggregating Devices (FADs) depending on the location of fishing sets (Davies et al. 2014). FSC sets are sets of mono or pauci-specific schools of tuna detected by birds, sonar marks, jumpers, or breezes in surface waters, while drifting FADs sets are done either on natural or man-made floating objects that attract tuna and other species (Lezama-Ochoa et al. 2015). The main targeted tuna species are skipjack *Katsuwonus pelamis*, yellowfin *Thunnus albacares*, and bigeye tuna *T. obesus* (Davies et al. 2014). Baez et al. (2018) reported that the average targeted tuna species composition of the tuna catches of Spanish purse seiners in 2017 was dominated by skipjack 84432t (56%), followed by yellowfin 54513t (36%), and bigeye 12345t. The bycatch species includes those non-targeted neritic tunas, billfishes, other bony fishes, sharks, rays, whale shark, cephalopods, and turtles (Ruiz et al. 2018). Among the rays, several *Mobula* species are incidentally caught in the European purse seine fishery in the Western Indian Ocean including *Mobula mobular, M. tarapacana, M. thurstoni,* and *M. birostris*. This recorded *Mobula* species can be divided into devil rays (*Mobula mobular, M. tarapacana, M. thurstoni*) and manta ray (*M. birostris*) (White et al. 2018; Hosegood et al. 2020). All of them are classified as endangered in the International Union for Conservation of Nature (IUCN) Red List of Threatened Species. They are also listed in the Appendix II of the Convention International Trade of Endangered Species of Wild Fauna and Flora (CITES) (IUCN 2018a; IUCN 2018b; IUCN 2018c; IUCN 2018d; IUCN 2019). To regulate the species international trade, they are also listed in Appendices I and II under Convention on the Conservation of Migratory Species of Wild Animals (CMS) (Lawson et al. 2017). Because of their global steep population declines, there has been increasing research for manta rays in the past years (Hacohen-Domené et al. 2017; Couturier et al. 2018; Beale et al. 2019; Thovyan et al. 2020). Yet research has been limited for devil rays which has focused mainly on spinetail devil ray *Mobula mobular* in the Pacific and Atlantic Oceans (Fortuna et al. 2014; Lezama-Ochoa et al. 2019; Lezama-Ochoa et al. 2020a). In contrast, basic research on the ecology, distributions and habitat use of devil rays in the Indian Ocean has lagged behind (Stewart et al. 2018; Lawson et al. 2017) . Therefore, this study focused on advancing our knowledge on the spatio-temporal distributions of devil rays in the Indian Ocean.

Population declines of devil rays in the Indian ocean have been reported by Indian Ocean Tuna Commission (IOTC), the tuna RMFOs in charge of managing tunas and tuna-like species in the Indian Ocean. Large declining trends for the population of spinetail devil ray *Mobula mobular* with increasing fishing effort have been documented in several areas of the Indian Ocean while the population status of sicklefin devil ray *M. tarapacana* and bentfin devil ray *M. thurstoni* remains unknown due to poor data availability (O'Malley et al. 2017; Shahid et al. 2018; Flounders 2020; Martin 2020; Lawson et al. 2017; Moazzam 2018). The four main drivers of decline in devil rays' populations are their high catchability in different fishing gear, high market demand, their intrinsic biology, and aggregation mechanisms, which makes them highly vulnerable to fisheries. Firstly, they are susceptible in a wide range of fishing gears including industrial longliners and purse seiners as targeted or incidental catch (Shahid et al. 2018) and also in artisanal or small-scale fisheries mainly using drift gillnets (Temple et al. 2019). Thus, their overlapping distribution with tuna species which are capture in different fishing gears, made devil rays to be highly susceptible to fisheries (Martin 2020). Secondly, the high fishing pressure on these species is driven by the high demand of their meat, skin, and gill plates. The dried gill plates of devil rays are used as the main ingredient of immune boosting tonic in Asian market (Lawson et al. 2017). Based on a survey conducted in fishers and traders of mobulid gill plates, gill plates became difficult to source despite increasing fishing effort (O'Malley et al. 2017). Thirdly, devil rays are also exceptionally susceptible to overexploitation because of their slow growth, long maturation and presumed high longevity (Croll et al. 2016; Stewart et al. 2018). Moreover, their fecundity is extremely low producing only one pup at a time every one to three years (Couturier et al. 2012). Furthermore, because of their k-selected life history, the populations are unlikely to withstand current

levels of fishing mortality and that their ability to recover from high fishing pressure is also likely to be low (Dulvy et al. 2014). Lastly, their aggregations, slow movement, and fragmented populations has likely contributed to several severe population declines (Couturier et al. 2012) . The formation of devil rays aggregations may be determined by an optimal set of environmental factors which affect primary productivity, or by courtship and breeding during specific periods (Couturier et al. 2012). In addition, substantial site fidelity has been observed (Couturier et al. 2012; Rohner et al. 2017b). All these factors may be contributing to population declines of devil rays raising the need to better identify their spatial and temporal distribution and associated environmental factors, together with their overlap with fisheries for designing appropriate conservation and management measures.

The feeding, aggregation and migration behaviors of devil rays have been associated to different environmental variables and processes (Fortuna et al. 2014; Stewart et al. 2018; Lezama-Ochoa et al. 2019; Lezama-Ochoa et al. 2020a) . Devil rays are generally attracted to highly productive regions with high concentration of chlorophyll and primary production. This is because of their passive filter-feeding planktivorous behavior with a diet mainly on zooplankton. Moreover, they may also exhibit some piscivorous behavior consuming some fish and crustaceans (Couturier et al. 2012; Rohner et al. 2017a). Because of this behavior, devil rays can be viewed as indicator species (Fadool 2020) and that their removal on marine environments can result in significant, cascading species composition changes (CMS 2016). Regarding the spatial and temporal distributions of devil rays, predictable aggregations have mainly been associated with local productivity, food availability, current circulation patterns, seawater temperature, or mating behavior (Rohner et al. 2013; Hacohen-Domené et al. 2017; Lezama-Ochoa et al. 2019; Lezama-Ochoa et al. 2020a). Furthermore, *Mobula* species have been associated to coastal areas and continental shelves (Alfaro-Cordova et al. 2017; Hacohen-Domené et al. 2017; Lezama-Ochoa et al. 2019; Lezama-Ochoa et al. 2020a; Peel et al. 2020), current patterns (Barr et al. 2019), El Niño–Southern Oscillation (ENSO)-related climate phenomena (Beale et al. 2019), daylight hours (Venables et al. 2020) ,lower sea surface height (Lezama-Ochoa et al. 2019; Lezama-Ochoa et al. 2020a), moon illumination (Couturier et al. 2012), seamount and islands (Mendonça et al. 2018), shallow depth (Palacios et al. 2021), shallow mixed layers or cold sides of thermal fronts (Graham et al. 2012; Belkin 2021), and upwelling zones (Lezama-Ochoa et al. 2019; Lezama-Ochoa et al. 2020a). These environmental conditions affect both the spatial distribution of their food (plankton) which in turn influence their behavior and distribution (Barr et al. 2019; Martin 2020). However, most of these studies have been conducted in the Pacific and Atlantic Oceans. The feeding, aggregation, and migration behaviors of devil rays in the Indian Ocean remain largely understudied.

The IOTC have adopted several management and conservation measures such as 2019 Resolution 19/03 on the conservation of mobulid rays caught in association with IOTC fisheries and best handling and release practices to minimize bycatch of devil rays in the Indian Ocean (Poisson et al. 2012; IOTC 2019a; Maufroy et al. 2020) . But still, the release strategies upon capture of devil rays cannot guarantee their survival given the current handling practices (Swimmer et al. 2020). Moreover, there is limited information available about their post-release survival, which based on anecdotal evidence, it may be very low (Francis et al. 2017; Martin 2020). Due to limited data on post release survival of devil rays, the bycatch of species belonging to this group are considered as mortality by the IOTC even if released (Martin 2020). The unknown post-release survival magnify the pressing concern to identify areas of aggregation and ultimately limit fishing activities in these areas (Francis et al. 2017). As such, understanding the key factors governing their distributions and interactions with fisheries is critically needed to be able to effectively mitigate the impacts of fishing on devil rays in the Indian ocean (Stewart et al. 2018; Martin 2020).

Here, we developed a habitat suitability model for devil rays in the Western Indian Ocean and modelled the seasonal and interannual changes in their spatial distributions. For this purpose, we used the bycatch data collected by the EU tropical tuna purse seine observer program between the period 2010-2020 to determine which environmental variables influence the occurrence of devil rays bycatch using a GAM modelling approach. Habitat modelling can improve our knowledge on the ecology and habitat use of devil rays across large spatial and temporal scales. We hypothesize that the spatio-temporal distribution of devil rays is associated with seasonal productive regions in the Western Indian Ocean. The predicted habitat suitability maps can be used to detect hotspot areas of high incidental bycatch of devil rays which can contribute to inform more holistic spatial management strategies to reduce bycatch of vulnerable and threatened species caught by pelagic fisheries in the Western Indian Ocean.

2. Material and Methods

2.1 Study area

The ocean circulation in the Western Indian Ocean (between 37ºW-83ºE, and 22ºN-30ºS) is mainly driven by two currents systems, the North Equatorial Current (NEC) or the monsoon current, and the South Equatorial Current (SEC) (Figure S1). The north hemisphere is characterized by the NEC or monsoon current while the southern hemisphere by the SEC. SEC is a current that moves westward and is largely supplied by the Indonesian Throughflow (ITF). The SEC splits to form the Northeast and Southeast Madagascar Currents (NEMC, SEMC) at the east coast of Madagascar at 17ºS. NEMC when approaching the Northern Coast of Mozambique splits into Mozambique channel eddy (flowing south) and East African Coastal Current (EACC, flowing north). SEMC can make westward eddies towards Southern Mozambique Channel (Schott et al. 2001; Schott et al. 2009).

Wind monsoon regulated the seasonal variation in the current circulation in Western Indian Ocean (Schott et al. 2001; Schott et al. 2009). During summer monsoon (Figure S1a), the northward Somali current are being supplied by both SEC and EACC. Somali current can become a different gyre system when it recirculates into the equator and become the Southern Gyre (SG). The second gyre is called the Great Whirl (GW) which is formed north of SG. The third gyre is called Socotra Eddy, which frequently appears in the Northeast of Socotra. Summer blooms arise because of the strong upwelling in coastal waters of Somalia and Arabia during the summer monsoon (Schott et al. 2009). Furthermore, other mesoscale processes such as eddies, filaments, fronts, and whirls can also increase the primary production controlled by chlorophyll abundance and variability brought by eddies and filaments (Tew-Kai & Marsac, 2009). During winter monsoon (Figure S1b), the previously northward Somali current flows southward and meets the EACC which flows northward at 2 to 4 ºS and is supplying the South Equatorial Counter Current (SECC). The SECC is present year-round however it becomes subsurface due to overlying westward Ekman transport during the summer monsoon. The winter monsoon blooms occur in the Western Arabian Sea, because of enhanced evaporation and reduced incoming solar radiation. Moreover, the high salinity (~36) in surface waters initiates convective mixing and transports nutrients from the upper nutricline to the surface layer (Prasanna Kumar et al. 2009). In the Southern hemisphere, the Mascarene Plateau have upwelling and nutrient enrichment in winter monsoon which is brought by westward zonal flow of the South Equatorial Current (Gallienne et al. 2004).

2.2. Fisheries Data

We analyzed the fisheries data collected in the fisheries observer programs of the European Union (EU) tropical tuna purse seine fleet operating in the Western Indian Ocean between 2010 and 2020. The EU with the Common Fishery Policy initiated a mandatory fishery data collection program in 2002 (Dörner et al. 2018). This EU Data Collection Framework originated from Council Regulations (EC) No 1534/2000, 1639/2001, 199/2008 and Commission Implementing Decision EU 2016/1251 (Ruiz et al. 2018). Accordingly, France and Spain started human observer programs in 2003 and 2005 respectively, to monitor the EU tropical tuna purse seine fisheries in the Indian Ocean. The *Institut de Recherche pour le Developpement* (IRD) manages observer programs for the French fleet and both the Instituto Español de Oceanografía (IEO) and AZTI for the Spanish fleet (Amandè et al. 2012). In addition to EU-funded observer programs that generally allow to cover 5 to 15% of the total fishing effort, industry-funded programs have been implemented to increase the observer coverage, such as OCUP since 2014 (*Observateur Commun Unique et Permanent*; financed by producer organization ORTHONGEL) for the French fleet. The total human observer coverage in 2010 was between 5-10% of total sets and it has increased around 50-60% in the most recent years (Ruiz et al. 2018).

The EU purse seine fishery targets tropical tuna species (skipjack *Katsuwonus pelamis*, yellowfin *Thunnus albacares*, and bigeye tuna *T. obesus*) using two types of fishing modes or sets in the Western Indian Ocean (Davies et al. 2014). For the purpose of this study, the purse seine fishing grounds in the Western Indian Ocean were divided in different areas (Figure S2) following the work of Lezama and colleges with minor modification (Lezama-Ochoa et al. 2015).The sets in these fishing areas were either associated to drifting Fish Aggregating Devices (FADs) or sets associated to free swimming aggregations of tunas (FSC) depending on the fishery strategy (Davies et al. 2014). The fisheries data analyzed in the current study contained a total of 26, 523 fishing sets observed between 2010-2020, of which 23,166 (87.34%) were FAD sets and 3357 (12.66%) were free school sets (Figure S3).

Initially the EU purse seine observer program was covered only by human observers onboard, but since 2015 it is being supplemented with Electronic Monitoring Systems (EMS) installed onboard. The fishing sets analyzed contains data mostly collected by human observers (85% of the total sets analyzed) which is increasingly being complemented by sets observed with the EMS installed onboard (15% of the total sets analyzed) (Figure S4). EMS are only provided by AZTI for Spanish fleets while for French fleets, IRD collected EMS data but are not validated at this stage. They were therefore not provided for this study. We used all the observer data collected by human observers in the EU purse seine fleet between 2010-2020 and in addition the observer data obtained with the EMS administered by AZTI between 2015 to 2020. The EMS tracks vessels position and activity, obtains reliable catch information and composition, and monitors and collect data on the target catch, non-target and bycatch species (Murua et al. 2020). It has been observed that the EMS can underestimate the catch of bycatch species compared with estimations obtained from the human observers, yet both systems perform well estimating the total catch of large bodied species, such as tunas and billfishes (Ruiz et al. 2015). Regarding the data collection for the bycatch of devil rays, the EMS can identify with a high degree of accuracy between devil rays (*Mobula mobular, M. tarapacana, M. thurstoni*) and manta rays (*Mobula birostris, Manta alfredi*) and it has difficulty to identify devil rays at the species level (as per coms Jon Ruiz AZTI, 2021). Throughout the period, human observers may also have had difficulties to identify devil rays at the species level.

The fisheries data recorded by the observer program include information about all fishing activities conducted during the trip: set day and hour, set type, set position, and catch of target (tunas) and bycatch species (in number or weight). Bycatch groups include neritic tunas, billfishes, other bony fishes, sharks, rays, sea turtles, cephalopods, and marine mammals. There are three devil ray species incidentally caught by the EU purse fleet in the Western Indian Ocean: spinetail devil ray *Mobula mobular* (RMM), sicklefin devil ray *M. tarapacana* (RMT), and bentfin devil ray *M. thurstoni (*RMO) (Figure S5). Moreover, the giant oceanic manta ray *M. birostris* (RMB) is also incidentally caught by the EU purse seine fishery. In the past, the devil rays and giant mantas were considered two distinct genera (genera *Mobula* included the devil rays and genera *Manta* included the giant mantas), but now all devil rays and giant mantas are classified into the *Mobula* genera (White et al. 2018). This early distinction is still reflected in the way fishery data is organized in the fishery observer programs database for AZTI and IEO, while for IRD some recorded presences identified in genus level are *M. birostris*. Over the years, the number of individuals of devil rays have been increasingly identified to the species level with the implementation of observer program training and the development of improved identification guides. However, their occurrences are still often recorded at the genus level (*Mobula* spp.). The category of *Mobula* spp. in the fishery dataset has traditionally excluded the giant mantas which were originally identified in a different genera (*Manta*) (IOTC 2019b).

We explored all occurrences identified to the species level for the three species of devil rays: *Mobula mobular, M. tarapacana, M. thurstoni* and all the occurrences identified to the genus level (*Mobula* spp., which mainly contained devil rays' occurrences identified at the genera level) collected in the EU purse seine observer program between 2010-2020. *Mobula japanica* (RMJ) occurrences were considered occurrences of *Mobula mobular* (RMM), as currently, *M. japanica* and *M. rancurelli* are considered junior synonyms of *M. mobular* (White et al. 2018; Hosegood et al. 2020).

A total of 378 combined presences of devil rays were recorded between 2010-2020, 118 individuals of *Mobula mobular* (Figure S5a), 25 of *Mobula tarapacana* (Figure S5b) and 9 of *Mobula thurstoni* (Figure S5c), and 226 individuals recorded at the genera level *Mobula* spp. (Figure S5d). Since we are modelling presence-absence of devil rays, in those sets were more than one individual was present (9 individual sets), only presence of devil ray was subjected to further analysis. As such, we analyzed a total number of 369 occurrences of devil rays. Moreover, due to the low number (118, 0.44%) of spinetail devil ray *Mobula mobular* occurrences (Figure S5a), we considered two separate modelling approaches. One approach modelled the occurrences of spinetail devil ray *Mobular mobular* (Figure S5a, Figure S5e) (referred as the spinetail devil ray habitat modelling analysis) and the second approach modelled the combined occurrences of all devil ray's species (Figure S5e) (referred as the devil ray's habitat modelling analysis). Therefore, the devil ray's habitat analysis contains all the occurrences from *Mobula mobular* (RMM), *Mobula tarapacana* (RMT) *Mobula thurstoni* (RMO) and *Mobula* spp. (RMV). Out of 26,523 fishing sets recorded, there were 369 (1.39%) occurrences of devil rays, 247 (66.94%) of which were associated to FAD sets and 122 (33.06%) associated to FSC sets. While for spinetail devil ray *Mobula mobular*, 118 (0.44%) occurrences were recorded, 72 (61.02%) of which were associated to FAD sets and 46 (38.98%) to FSC sets.

2.3. Predictor variables

2.3.1. Environmental variables

We considered the following environmental variables as potential predictor variables for the habitat modelling including chlorophyll-a concentration (Chl), net primary production of phytoplankton (NPPV), nitrate (NO_3), oxygen (O_2), phosphate (PO_4), silicate (Si), salinity (Salinity), sea surface height (SSH), mixed layer depth (MLD), sea surface temperature (SST), current velocity (Vel), eddy kinetic energy (Ke), heading of the current (Heading), sea surface temperature fronts (SSTfronts), and chlorophyll fronts (Chlfronts) (Table 1). The eddy kinetic energy (Ke), current velocity (Vel), and heading (Heading) of the current were derived using the eastward (Uo) and northward (Vo) velocity vectors. Sea surface temperature fronts (SSTfronts) and chlorophyll (Chlfronts) were also calculated using the previously extracted Chl and SST data using the front detection algorithm (Belkin & O'Reilly, 2009).

We chose different environmental covariates as a proxy of biological, chemical, and physical processes in the Western Indian Ocean that can be linked with the occurrences of devil rays. Chlorophyll and Net Primary Production of phytoplankton were considered as a proxy of highly productive and upwelling regions (Burt et al. 2018). Nitrate is one of the nutrient essential for photosynthesis of phytoplankton, and in some areas it is a limiting nutrient (Harms et al. 2019). Silicate is needed by silicious phytoplankton and could be a limiting nutrient in oligotrophic water (Sospedra et al. 2018). Moreover, the limitation of silicate and nitrate can often terminate blooms (Vonnahme et al. 2021). Salinity reflects the biological preference of organisms and excessively low salinity means freshwater input from lands (Velasco et al. 2019). Oxygen concentrations reveal if the area is hypoxic or well oxygenated (Giomi et al. 2019). Phosphate is also a macronutrient that is needed for photosynthesis (Martiny et al. 2019). Lower sea surface heigh is associated with upwelling areas (Lezama-Ochoa et al. 2019). Colder temperature and a deep MLD is a sign of productive region (Somavilla et al. 2017). Low sea surface temperature is also associated with upwelling areas (Harris et al. 2020). Current flow (current velocity, eddy kinetic energy, current heading) could be link to nutrient supply and plankton distribution (Thovyan et al. 2020). Sea surface temperature fronts are linked with foraging movements of species and broad thermal fronts off an upwelling zone (Graham et al. 2012). Chlorophyll fronts are associated with elevated primary and secondary productivity and fisheries (Belkin 2021).

Table 1 Environmental variables used in the species distribution models for devil rays and spinetail devil ray *Mobula mobular* obtained from Copernicus Marine Environment Monitoring Service (CMEMS) in the period 2010-2020.

Variable	Symbol	Units	Mean	Min	Max	Source
Chlorophyll	Chl	mg m^{-3}	0.20	0.06	1.59	NRT 001_028, RAN 001_029
Net Primary Production of Phytoplankton	NPPV	mg m^{-3} day^{-1}	10.75	0.60	79.60	
Nitrate	NO_3	mmol m^{-3}	0.16	0.00	3.77	
Oxygen	O_2	mmol m^{-3}	203.10	191.40	221.80	
Phosphate	PO_4	mmol m^{-3}	0.10	0.00	0.57	
Silicate	Si	mmol m^{-3}	1.81	0.41	12.72	
Salinity	Sal	psu	35.31	32.36	37.05	NRT 001_024, RAN 001_030
Sea Surface Height	SSH	m	0.37	0.06	0.91	
Mixed Layer Depth	MLD	m	18.47	9.78	104.51	
Sea Surface Temperature	SST	^oC	28.57	22.94	31.68	
Current Velocity	Vel	m/s	0.36	0.00	1.99	$\sqrt{u^2+v^2}$ *
Eddy Kinetic energy	Ke	m/s	0.09	0.00	1.97	$\frac{u^2+v^2}{2}$ *
Heading of the current	Heading	degrees	178.52	0.00	359.98	$atan\frac{u}{v}\frac{360}{2\pi}$ *
Sea Surface Temperature fronts	SSTfronts	^oC/km	0.02	0.00	0.10	(Belkin et al. 2009)
Chlorophyll fronts	Chlfronts	ratio	0.02	0.00	1.33	(Belkin et al. 2009)

*u is the eastward current velocity; v is northward current velocity.

We derived all the environmental variables from the EU Copernicus Marine Environment Monitoring Service (CMEMS) (http://marine.copernicus.eu) from the marine ocean products (http://marine.copernicus.eu/services-portfolio/access-to-products/). The Copernicus platform aggregates information from different databases on the physical state, variability and dynamics of the ocean and marine ecosystems worldwide (EU Copernicus, 2020). We selected models over in-situ observation and satellite products because they offered more spatial and temporal coverage and they are not affected by cloud cover. This study used both Near Real Time (NRT) and in the past (RAN) data. Since the marine ocean product RAN only covers the period between 2010-2018, NRT product with data between 2019-2020 was also used to complete the whole study period. We matched all the environmental variables with the operational fishing set data (latitude and longitude, observation date, catch information).

2.3.2. Spatial and temporal fisheries variables

We also consider some spatial and temporal variables such as latitude (Latitude), longitude (Longitude), year (Year), week (Week) and timing of the sets framed as hours from sunrise (Sunrise) as potential predictor variables for the habitat modelling. Week was considered to account for seasonal variations driven by the monsoon regime. Hours from sunrise was explored to account for behavioral thermoregulation and social interactions devil rays that usually happen before sunrise or early morning (Couturier et al. 2018) . Type of fishing set was also accounted as to identify what type of sets this species are in association with. Other variables are also explored because they may help identify variability and ecological processes occurring at varying spatial and temporal scales in Western Indian Ocean (Lopez et al. 2020). Therefore, to account for the effect of the community size associated to the type of fishing operation (FSC or FADs), the catch of the target tuna and the catch of non-target fish species (total catch of rays, sharks, billfishes, and other bony fishes) was also included in the analysis (Lopez et al. 2020).

2.4. Modelling approach

2.4.1. Generalized Additive model (GAMs)

We used GAMs to model presence-absence of both devil rays and spinetail devil rays *Mobula mobular* in relation to environmental characteristics in the Western Indian Ocean and the fisheries characteristics of the fishing operations, assuming a binomial distribution and a logit link function. In one model, the presence-absence of devil rays were modelled (369 presences, 1.39% of the total sets) and in the second model the presence-absence of spinetail devil ray *Mobula mobular* (118 presences, 0.44% of the total sets) were modelled.

GAMS were fitted as follows:

$$\mathbf{g}(\mu\mathbf{i}) = \boldsymbol{\alpha} + \boldsymbol{f_1}(\boldsymbol{x_{1i}}) + \boldsymbol{f_2}(\boldsymbol{x_{2i}}) + \boldsymbol{f_3}(\boldsymbol{x_{3i}}) \ldots + \boldsymbol{f_n}(\boldsymbol{x_{ni}})$$

g is the link function (logit for binomial family), μi is the expected response variable (presence-absence), α is the intercept, f_n are smooth functions, and X_n are the covariates (Wood 2017; Lezama-Ochoa et al. 2019)

A binomial distribution GAM was used in the modelling process. It is a family that models the presence and absence of the species and provides probability indices of occurrence, irrespective of their abundance (Wood 2017; Lezama-Ochoa et al. 2019; Lezama-Ochoa et al. 2020a; Lopez et al. 2020). The binomial family was chosen because majority of the sets contained either no presences of devil rays (zeros) or when present, the presences were dominated by one or few individuals (2,3 individual per set) (Figure S6). Other type of distribution such as Poisson and negative binomial were not explored.

We also conducted univariate binomial GAMs for each covariate considered in the study as an additional exploratory analysis (Figure S7). These univariate models were purely informative and provided information on both the potential functional shape of each covariate on the response variable (Lopez et al. 2020).

To avoid additional overfitting, we restricted the degrees of freedom of the smooth functions for each explanatory variable. Each smooth term had basis functions (k) which was set to k = 6 for the main effects and to k = 20 for first order interaction effects (Giannoulaki et al. 2013; Lezama-Ochoa et al. 2019). We fitted the GAMs using (i) thin plate regression splines for non-linear covariates, (ii) cyclic cubic regression spline for week and heading of the current to account for cyclical effects and (iii) a duchon spline to account for spatial effects (latitude, longitude) considering Euclidian distance (Miller et al. 2014). GAMs were fitted using the mgcv package v 1.8 (Wood 2017; Wood 2021).

2.4.2. Correlation and collinearity

We considered two measures to reduce correlation and collinearity and overfitting between variables (Figure S8). First, we examined all predictor covariates using Pearson's rank correlation to assess highly correlated variables (Figure S8a). Only one of the correlated variables (Pearson correlation $r > 0.6$) were subjected to modelling selection process at a time (Lezama-Ochoa et al. 2019). Second, we calculated the Variance Inflation Vector (VIF) (Figure S8b) to assess multicollinearity among the predictor variables with a cut-off value of 5 (Hahlbeck et al. 2017a) using the function vif from usdm package v 1.1-18 (Naimi 2017). Because of high correlation and collinearity, we only included one variable from these four groups of covariates: 1) "chlorophyll, NPPV, oxygen, sea surface temperature", 2) "chlorophyll and nitrate", 3) "NPPV and nitrate" and 4) "eddy kinetic energy and velocity of the current" in the selection process and habitat models at a time. A total of 8 combination of variables were subjected to variable selection (Table S1).

2.4.3. Variable and Model selection

We applied a combination of forward and backward stepwise variable selection procedure to select the final model covariates (Wood, 2017). Variables were selected if they improved the model Akaike's Information Criterion (AIC) value of 2.0 in the selection process (forward variable selection) (Giannoulaki et al. 2013). Moreover, as an additional measure to avoid overfitting in the selection process, only significant variable ($p < 0.05$) was kept, and non-significant variables were dropped one at a time (backward variable selection) (Lezama-Ochoa et al. 2019). We followed this approach until all the variables in the model were significant. We then compared the AICs of all best-fit models, and the lowest AIC were subjected to model evaluation (Table S1). When modelling devil rays, Models 1 and 3 had the lowest AIC, therefore both models were subjected to model evaluation.

2.4.4. Model evaluation

We validated the final models using a k-fold cross-validation method (with $k = 5$). The k-fold cross-validation method was used to evaluate the reliability and the predictive performance of the final models. This method consists of using independent data sets for model building (we use 80% of the data as training data) and model validation (we use 20% of the data as testing data), where data is partitioned into k equally sized segments or folds through random resampling. Model performance is assessed by successively removing each subset, re-establishing the model on the retained data, and predicting on the omitted data (Elith et al. 2009). Hold-out validation avoids the overlap between training data and test data, yielding a more accurate estimate for the generalization performance of the algorithm (Villarino et al. 2015).

We assessed model predictions through a confusion matrix using the 'PresenceAbsence' package v1.1.9 in R (Freeman 2012). We calculated the Area Under the receiver-operating Curve (AUC), the 'specificity, the 'sensitivity' and the mean True Skill Statistic (TSS) indices from the confusion matrix (Pearson 2010). The AUC provides an overall measure of accuracy that is threshold independent and ranges from 0 to 1. Values around 0.5 indicate that the prediction is as good as random, and values close to 1 indicate perfect prediction. This index measures the ability of the model to correctly predict where a species is present or absent (Elith et al. 2009; Lezama-Ochoa et al. 2019). Specificity is an index depicting the proportion of observed absences correctly predicted and sensitivity illustrates proportion of observed occurrences correctly predicted. Thus, sensitivity is the ability of the model to correctly identify areas with devil rays. The TSS is an alternative measure of accuracy, and it is calculated as sensitivity plus specificity minus 1, which ranges from -1 to $+1$. A TSS of 0 indicates no predictive skill while TSS of $+1$ indicates perfect agreement and the values in between zero or less indicate a performance no better than random (Brodie et al. 2015; Lezama-Ochoa et al. 2019).

The sensitivity, specificity and TSS indices are threshold-dependent, therefore, it is necessary to select a threshold to transform the probabilities into binary predictions (presence/absence) (Jiménez-Valverde et al. 2007). We explored two methods to select the threshold probability values (sensitivity is equal to specificity, and maximization of sensitivity plus specificity). At the end the sensitivity is equal to specificity threshold was used as it gives the most accurate predictions in cases where the dataset has a low prevalence and avoids omissions (false negative) errors (Liu et al. 2005; Jiménez-Valverde et al. 2007).

We repeated the validation procedure five times (5-fold) and the performance scores obtained were averaged to validate the prediction performance of the species distribution models (Lopez et al. 2020). We used the performance scores from the four indices in combination to evaluate the predictive performance of the species distribution models.

2.4.5. Prediction

Using the best fit models, we produced habitat suitability predictions for devil rays and spinetail devil ray *Mobula mobular* for the Western Indian Ocean using the environmental conditions present during the 10-year period (environmental values were downloaded every seven days between 2010- 2020) with a spatial resolution of 1 × 1° grid cells using the 'predict.gam' function of the 'mgcv' package v 1.8-36 (Wood 2017). For these predictions, the predictor variable of total tuna catches (Tuna) which was selected in the final model was set to mean levels for each 1x1º grid cell. To estimate the probabilities of each grid cell, prediction maps were averaged (and the standard deviation calculated) across the weekly predictions for the whole period (2010−2020). To assess temporal changes, we also calculated mean prediction by season following the monsoon regime and calculated by year. The four seasons describing the monsoon region consider were the winter monsoon, spring intermonsoon, summer monsoon and autum intermonsoon. Weeks 1-12 and week 49-53 were averaged for the winter monsoon predictions, week 13-20 into the spring intermonsoon, week 21-39 into the summer monsoon, and week 40-48 into the autumn intermonsoon. We also checked the ranges for the weekly environmental values for the whole study period used for the predictions to ensure those values were within the environmental envelope used to calibrate the species distribution models. Only 0.42% and 0.21% of the environmental data used in the predictions were outside the range of environmental values used to build the species distribution models for devil rays and spinetail devil ray *Mobula mobular* respectively. Model building, evaluation and predictions were performed using R version 4.0.2 (R Core Team 2020).

3. Results

3.1. Spatial and temporal patterns of EU purse seine fleet and devil ray's bycatch

The EU purse seine fleet fishing grounds vary by season (Figure 1). The spatial distribution of the fleet coincides with changes in monsoon. Generally, we observed that most of the fishing effort 21,645 (82%) was in South Somalia, Northwest Seychelles, and Southeast Seychelles fishing area (Figure S2). During winter monsoon (Figure 1, Figure S2), the fleet covers the North Somalia (20ºN) extending to Mozambique channel (30ºS) reaching the Maldives Chagos fishing ground (70-80ºE). The observed fishing sets (9215 sets) during winter monsoon are more concentrated in the equatorial region (3085 sets) between 0º to 5º S in the Northwest Seychelles fishing ground. The spatial coverage of the sets during the Spring intermonsoon (3810 sets) are similar to the winter monsoon but there is a decrease of sets in South Somalia, Southeast Seychelles and Maldives-Chagos fishing grounds. During summer monsoon, the fishing sets (8505 sets) are located more in the north than during the previous monsoon seasons. The fishing coverage is from 25ºN extending to 15ºS. During this season the highest sets are found between 5ºN to 0ºS (3274 sets). Compared to winter monsoon, half of the Mozambique channel fishing grounds were lost as well as the Maldives Chagos fishing ground. During autumn intermonsoon the fishing sets (4993 sets) are restricted to <20ºN. In addition, sets are absent in the Mozambique channel. The sets are scattered all throughout the area as there is no prominent area where the fishing fleets aggregate. We found that the highest number of total sets (sets with presence and no presence of devil rays) per month (1420 sets) were made during the winter monsoon in January (Figure 2a).

The EU purse seine fishing sets with the occurrence of devil rays (Figure 1a) and spinetail devil ray *Mobula mobular* (Figure 1b) also appears to be variable in space and time. We identified a total of 369 devil rays occurrences incidentally caught in the EU purse fishery between 2010 and 2020; 247 individuals (66.94%) were caught in FAD sets and 122(33.06%) in FSC sets. During the winter monsoon the sets with presences of devil rays (Figure 1a) are concentrated South Somalia and Northwest Seychelles fishing area. There are also occurrences in Southeast Seychelles, Maldives-Chagos and Mozambique channel fishing areas. The spatial distributions of devil rays during spring intermonsoon are mostly restricted to South Somalia, Northwest, and Southeast Seychelles fishing area with at most two individuals in Mozambique channel and Arabian Sea fishing area. During summer monsoon, devil rays are more restricted in South Somalia fishing area. There are also individuals identified in Northwest Seychelles, Southeast Seychelles, North Somalia, and Arabian sea fishing area. There are no individuals present in Mozambique channel and Maldives Chagos fishing area. Lastly, during autumn intermonsoon the sets are more scattered utilizing all fishing areas except Mozambique Channel and Maldives Chagos fishing grounds. There is a higher number of FADs in this season compared to the rest of the seasons. We discovered that the individuals recorded in the Arabian sea, are captured in FADs sets throughout all-monsoon regime. On the other hand, considering only individuals identified as Spinetail devil ray *Mobula mobular*, we found a total of 118 (0.44%) presences were recorded; 72 (61.02%) in FAD sets and 46 (38.98%) in free school sets (Figure 1b). The spatial and temporal patterns of the recorded individuals are very similar to the patterns identified for devil rays. However, spinetail devil rays *Mobula mobular* have no recorded occurrences in the Arabian sea from ~15º N and above. We also found that the highest recorded individual occurrences were both observed also in January (Fig 2b-c) with presences of 71 and 19, for devil rays and spinetail devil ray *Mobula mobular*, respectively.

3.2. Generalized Additive Models

3.2.1. Effects of predictor variables on devil rays and spinetail ray bycatch

After we study all the possible combinations of covariates (8 candidate models for devil rays and 8 models for spinetail devil ray *Mobula mobular*, Table S1), the final models were chosen based on the lowest AIC value and the higher sensitivity values from model evaluation. Explanatory variables included a) spatial variables (Latitude-Longitude interaction), b) temporal variables (Week), c) type of fishing mode in sets (Type as factor), d) environmental variables (chlorophyll, sea surface heigh, sea surface temperature fronts for devil rays, and net primary productivity of phytoplankton, sea surface temperature fronts for spinetail devil ray *Mobula mobular*), and e) target tuna catch data. We presented models with similar AIC (Table S1) values given that they have selected almost the same variables including only one of correlated variable set (Chl, NPPV, SST, O_2). The difference for the highest and lowest AIC values for the candidate models is 5 in both the devil rays and spinetail devil rays *Mobula mobular* modelling.

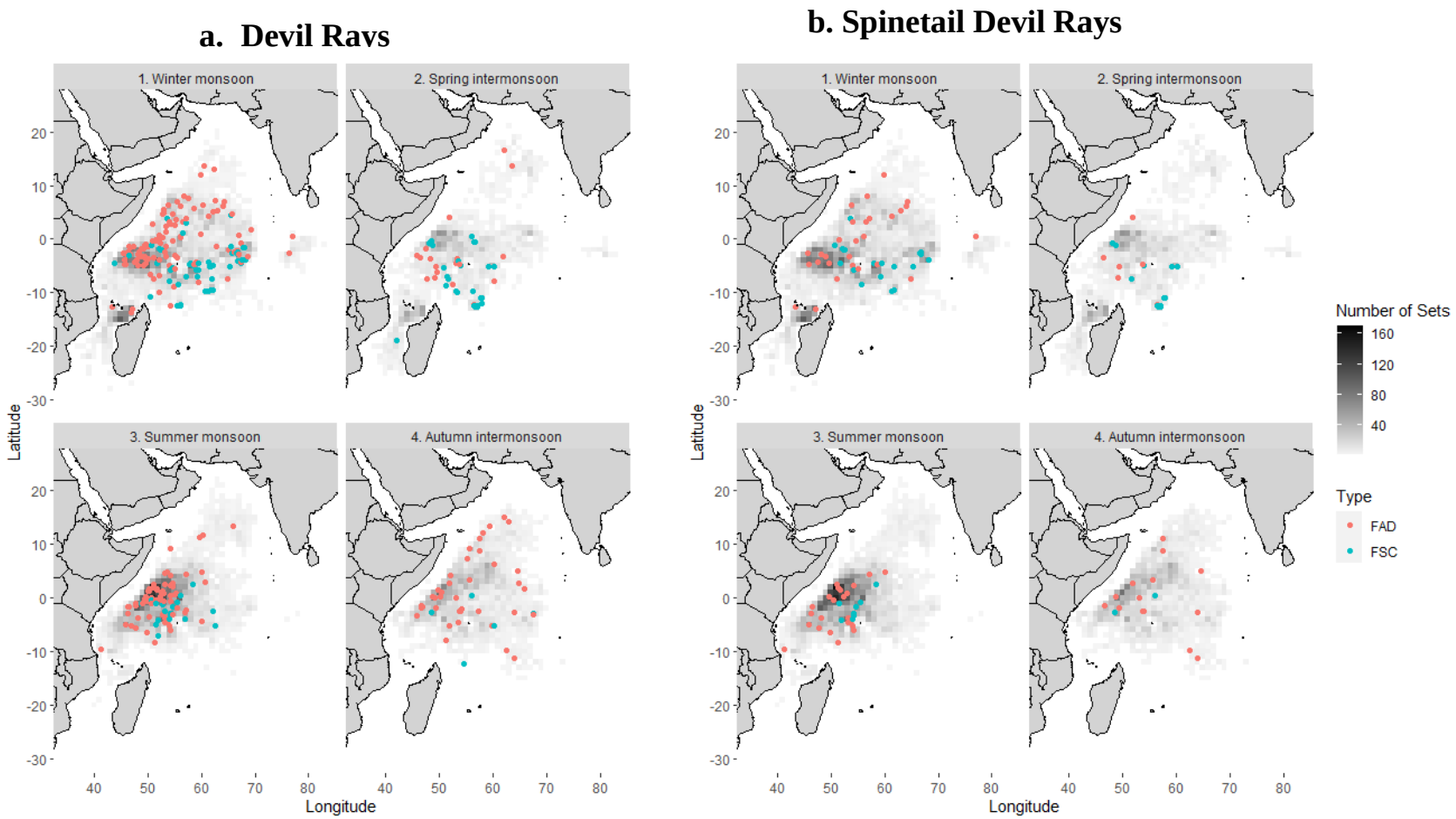

Figure 1 Distribution of observed sets with presence of a) Devil rays and b) Spinetail devil ray *Mobula mobular* between the years 2010−2020 in fishing aggregating devices (FADs) (pink dots) and free school sets (skyblue dots) by monsoon regimes from the EU tropical tuna purse sine fishery in the western Indian Ocean. Total number of observed sets in the fishery is represented in shades of gray. Maps were created using ggplot2 in R studio version 4.0.2 (R Core Team 2020).

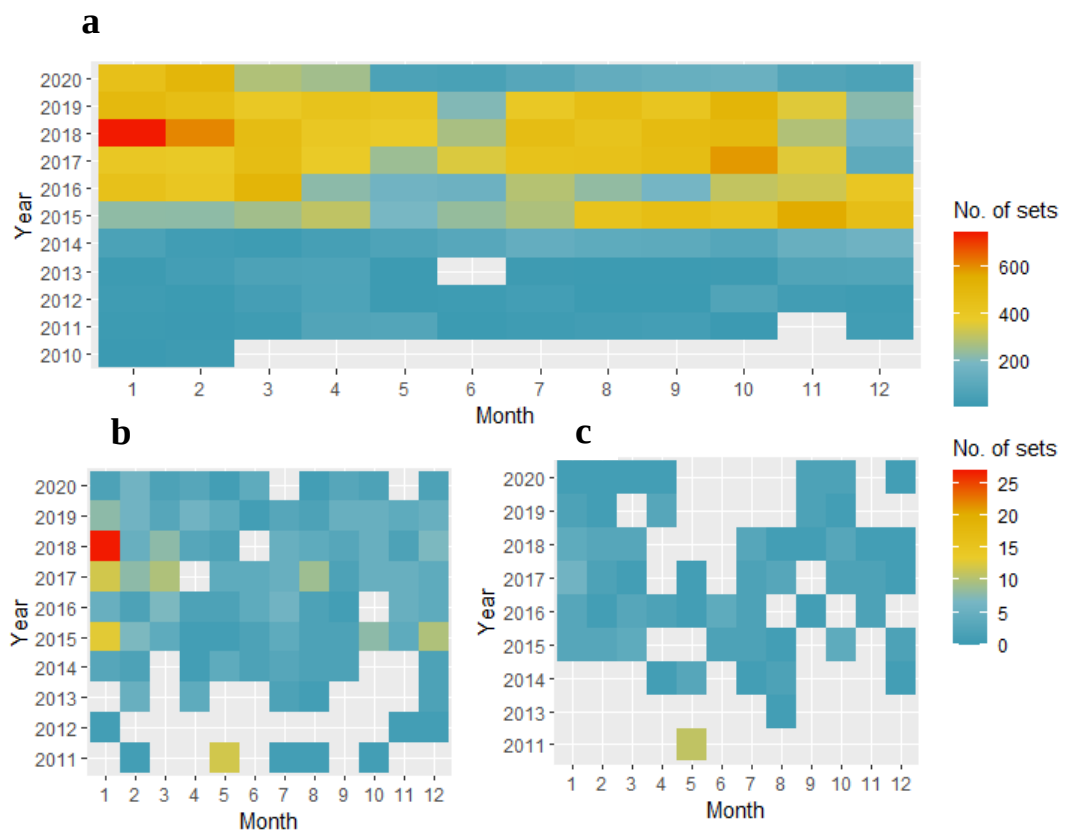

Figure 2 Distribution of observed sets in the EU tropical tuna purse seine fishery in the Western Indian Ocean between 2010-2020. a) Total number of sets in the fishery between 2010-2020 on the y-axis and months (1–12) on the x-axis. b) Total number of sets with presence of Devil rays between 2010–2020 and months (1–12). c) Total number of sets with presence of Spinetail devil rays *Mobula mobular* between 2010–2020 and months.

The final model for devil rays explained 7.38% of the total deviance (adjusted r^2=0.019). This model included as predictor variables a) spatial variables (Latitude-Longitude interaction), b) temporal variables (Week), c) type of fishing (set type as factor), d) environmental variables (chlorophyll, sea surface heigh, sea surface temperature fronts, and e) target tuna catch (Table 2). When considering only simple terms in the univariate GAMs, Latitude and Longitude had a percent deviance of 2.77% followed by Type (2.70%), Week (1.17%), Sea Surface Height (1.66%), Chlorophyll (0.46%), Tuna (0.40%) and Sea Surface Temperature fronts (0.15%).

The final model for the Spinetail devil ray *Mobula mobular* explained 8.01% of the total deviance (adjusted r^2 of 0.011). This model included a smaller number of predictor variables, including a) spatial variables (Latitude-Longitude interaction), b) type of fishing mode (Type as factor) and c) environmental variables (net primary production of phytoplankton, sea surface temperature fronts) (Table 3). When considering only simple terms, the most important variable was Type (3.45%), Latitude and Longitude (3.25%), Tuna (0.94%), Net Primary Production of phytoplankton (0.62%) and Sea Surface Temperature fronts (0.42%).

Both the devil ray model and the Spinetail devil ray *Mobula mobular* model included the spatial covariates (Latitude, Longitude) and the environmental variable (Sea Surface Temperature fronts), and total tuna catch (Tuna). However, the net primary production of phytoplankton was chosen when modelling spinetail devil ray *Mobula mobular* while sea surface height and chlorophyll were chosen when modelling all devil rays. Moreover, we found that the temporal covariate (Week) was not significant in the spinetail devil ray modelling. The piecewise construction of best fit model for devil rays and spinetail devil rays modelling is also provided in Table S2 presenting how variables in the final model improve the AIC.

Table 2 Final generalized additive model selected to model the presence of Devil rays in the Western Indian Ocean between 2010 and 2020 with estimated degrees of freedom (edf) using a binomial family with log as a link function. The model has an adjusted r^2= 0.02 and a deviance explained of 7.38% using a sample size of n = 26,521. Intercept is significant (p <0.05)

Variables	edf	p	% Deviance
Type			2.70%
Latitude, Longitude	16.69	< 0.001	2.77%
Week	3.79	< 0.001	1.17%
Chlorophyll	2.97	< 0.01	0.46%
Sea Surface Height	1.01	< 0.001	1.66%
Tuna	3.74	< 0.05	0.40%
SSTfronts	1.01	< 0.05	0.15%

Table 3 Final generalized additive model selected to model the presence of Spinetail devil rays in the Western Indian Ocean between 2010 and 2020 with estimated degrees of freedom (edf) using a binomial family with log as a link function. The model has an adjusted r^2= 0.01 and a deviance explained of 8.01%, using a sample size of n = 26,521. Intercept is significant (p <0.05)

Variables	edf	p	% Deviance
Type			3.45%
Latitude, Longitude	10.55	< 0.01	3.25%
NPPV	2.30	< 0.01	0.62%
Tuna	3.03	< 0.05	0.94%
SSTfronts	1.04	< 0.05	0.42%

We present the predictor variables included in the final model for devil rays (Figure 3a-g) and spinetail devil rays *Mobula mobular* (Figure3h-l) in Figure 3. The interaction of Longitude and Latitude (Figure 3a for devil rays; Figure 3h for spinetail devil ray *Mobula mobular*) suggested several potential hotspots with high incidental catches of devil rays and spinetail devil ray. The variable of week showed that there is a relevant temporal pattern in the distribution of devil rays' bycatch (Figure 3b), but it was not selected when modelling spinetail devil ray *Mobula mobular*. Moreover, we discovered based on the final model, that devil rays' presence is generally associated with productive systems, particularly in areas of 0.3-0.5 mmol m^{-3} chlorophyll (Figure 3c) or relatively high net primary production of phytoplankton (10-30 mg m^{-3} day^{-1}) (Figure 3i) for spinetail devil rays. Additionally, the sea surface height (Figure 3d, Animation S1) variable selected only in the devil ray model suggested devil rays are found in near to zero sea surface height (0.4m). Both models also suggested a higher probability of presence in areas with sea surface temperature fronts of about 0.02-0.03 ^{o}C km^{-1} (Figure 3f for devil rays, Figure 3k for spinetail devil ray *Mobula mobular*). We detected in both models, a higher probability of devil rays' presence in fishing operations setting on FSC than on FADs (Figure 3g for devil ray, Figure 3l for spinetail devil ray *Mobula mobular*). Moreover, we observed a decrease (20% probability) of both devil rays (Figure 3e) and spinetail devil ray *Mobula mobular* (Figure 3j) probability of catch in sets of big fish schools (sets in >50tons of total catch of targeted tuna).

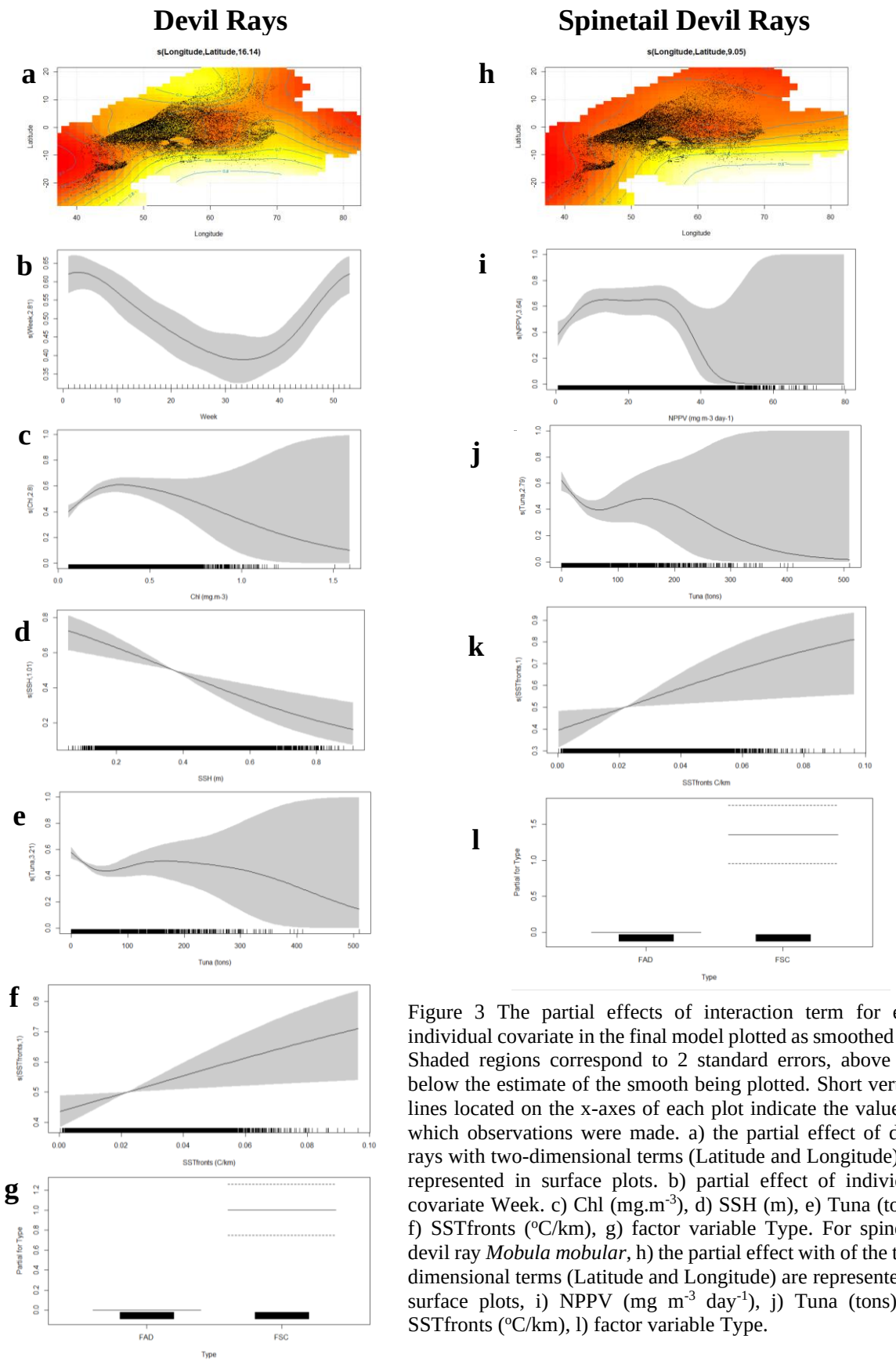

Figure 3 The partial effects of interaction term for each individual covariate in the final model plotted as smoothed fits. Shaded regions correspond to 2 standard errors, above and below the estimate of the smooth being plotted. Short vertical lines located on the x-axes of each plot indicate the values at which observations were made. a) the partial effect of devil rays with two-dimensional terms (Latitude and Longitude) are represented in surface plots. b) partial effect of individual covariate Week. c) Chl ($mg.m^{-3}$), d) SSH (m), e) Tuna (tons), f) SSTfronts ($^oC/km$), g) factor variable Type. For spinetail devil ray *Mobula mobular*, h) the partial effect with of the two-dimensional terms (Latitude and Longitude) are represented in surface plots, i) NPPV ($mg\ m^{-3}\ day^{-1}$), j) Tuna (tons), k) SSTfronts ($^oC/km$), l) factor variable Type.

3.2.2 Model performance

We showed in this study that the ability of the model to predict both devil ray's presence and spinetail devil ray *Mobula mobular* presences was acceptable AUC≥ 0.7 (Mandrekar 2010), given the very low number of presences in the data set used (Table 4, Table 5). For devil ray model (Table 4), the sensitivity was 0.71 and specificity was 0.56. while for spinetail devil ray *Mobula mobular* (Table 5) sensitivity was 0.31 with specificity value of 0.92. The TSS scores were 0.27 and 0.23 respectively.

Table 4 Accuracy indices including Sensitivity, Specificity, Area Under the Curve (AUC), and True Skill Statistic (TSS) to evaluate the performance of the model for Devil rays.

k	AUC	Sensitivity	Specificity	TSS
1	0.72	0.81	0.47	0.28
2	0.74	0.52	0.84	0.36
3	0.68	0.74	0.48	0.22
4	0.65	0.70	0.53	0.23
5	0.71	0.79	0.47	0.26
Mean	0.70	0.71	0.56	0.27

Table 5 Accuracy indices including Sensitivity, Specificity, Area Under the Curve (AUC), and True Skill Statistic (TSS) to evaluate the performance of the model for spinetail devil rays *Mobula mobular*.

k	AUC	Sensitivity	Specificity	TSS
1	0.74	0.37	0.92	0.29
2	0.66	0.32	0.90	0.22
3	0.73	0.27	0.92	0.19
4	0.69	0.28	0.92	0.20
5	0.70	0.33	0.93	0.26
Mean	0.70	0.31	0.92	0.23

1. *3.2.3 Predicted spatial distribution of devil rays and spinetail devil ray*

We identified four hotspots (Mascarene plateau, Central Indian Ridge, Equatorial region, Western Arabian Sea) in three of the fishing areas (Southeast Seychelles, South Somalia, and Arabian Sea) with higher habitat suitability for devil rays (Figure4, Animation S2) and two hotspots (Mascarene plateau, Central Indian Ridge) in one of the fishing areas (Southeast Seychelles) for spinetail devil ray *Mobula mobular* (Figure 4, Animation S3). Devil rays showed a higher presence between 10˚-20˚N and 50-60 ˚E in the Arabian sea fishing area specifically in the Western Arabian Sea hotspot; 10˚-20˚ S and 55-75º E in the Southeast Seychelles fishing area specifically in Mascarene Plateau hotspot (55-60 ºE) and Central Indian Ridge hotspot (65-75 ºE); and between 5N to 5S between 40-60ºE in the South Somalia fishing ground specifically in equatorial region hotspot (Figure 4a, FSC: Figure S9a, FADs: Figure S2). We observed a high variability in the presence of devil ray in the Arabian Sea extending to Somalia fishing area and in Mozambique channel fishing area (Figure 4b, FSC: Figure 9b, FADs. Figure S2). The resulting prediction maps for spinetail devil ray *Mobula mobular* have the same two (out of four) hotspots also identified for devil rays (Fig 4c, FSC; Figure S9c, FADs). The two hotspots are found in the Southeast Seychelles fishing ground specifically in Mascarene Plateau and Central Indian Ridge. The spinetail devil ray model failed to identify the Western Arabian Sea and the equatorial region hotspots. However, we observed a high variability (Figure 4d, FSC: Figure S9d, FADs) in the areas from 25ºN to 5ºS near the coastal areas in western

part of Arabian Sea, Somalia, Seychelles and Maldives fishing area, which overlapped with the identified Western Arabian Sea and equatorial region hotspots for devil rays.

The seasonal prediction maps for devil rays show that the presence of devil rays vary seasonally driven by the seasonal upwelling events characteristic of the Western Indian Ocean. We revealed that the probability of occurrence for devil rays (Figure 5, FSC; Figure S10, FAD) is higher during the winter monsoon period, in all four identified hotspots, compared to the rest of the monsoon regimes. During spring intermonsoon there is an abrupt decrease in the probability of occurrence for devil rays in the Western Arabian Sea and the equatorial region hotspots suggesting a seasonal decrease in habitat suitability. The highest probability of occurrence is found around the Mascarene Plateau and the Central Indian Ocean ridge hotspots. During the summer monsoon the probability of occurrence for devil rays decreases further, now the areas with higher probabilities get more contracted around the Mascarene plateau hotspot. During the Autumn intermonsoon period, the probability of finding devil rays in the Western Arabian Sea hotspot starts to increase again while the probability in both Mascarene plateau and Centra Indian Ridge hotspot continue to decrease. The seasonal prediction maps for spinetail devil ray *Mobula mobular* (Figure 5b, FSC; Figure S10b, FAD) also identified the region with higher probability of occurrence around the Central Indian Ridge hotspot extending to Mascarene plateau hotspots, which remain relatively stable throughout the four periods with an observed slight increase during the summer monsoon period.

The yearly prediction maps for devil rays (Figure 6, FSC; Figure S11, FADs) show the same distinct four hotspot with higher habitat suitability persisting over time and only their intensity changes interannually. We found that each hotspot has different intensities in different years. The Western Arabian Sea hotspots peaks in years 2010, 2011, 2013, 2014 and 2020. While the Mascarene plateau and Central Indian Ridge hotspots peaks in 2011-2013. The equatorial hotspots remained constant across all the years. The year 2010 shows the highest suitability areas in the northeastern side of Socotra Island while Mascarene Plateau and Central Indian Ridge hotspots had relatively lower probability. During 2011 the hotspot area in the Western Arabian Sea moves North and there is an increased probability in the South region in the Central Indian ridge. In 2012 the North hotspot decreases in probability and the southern hotspots also decreases in magnitude. In 2013, there is a westward shift of highest suitability in the west side of Mascarene plateau. Both the Mascarene plateau and Central Indian Ridge hotspots are permanent between year 2014-2020 while there is a minor shift in habitat suitability in the Western Arabian Sea hotspot. For spinetail devil ray *Mobula mobular* (Fig 7, FSC; Figure S12, FADs) the highest habitat suitability is found in Mascarene plateau towards the Central Indian Ocean Ridge. Within this area, the area close to the ridge have higher habitat suitability relative to their surroundings in 2010 to 2013. From 2014-2018 it remains approximately similar. From 2019 to 2020, both the Mascarene plateau and Central Indian Ridge hotspots becomes prominent again. For spinetail devil ray *Mobula mobular*, only two hotspots (Mascarene plateau and Central Indian Ridge hotspots) with higher habitat suitability are identified which are similar to the two hotspots identified for modelling all devil rays. Both areas also peak in 2011-2013 and peak again in 2019 and 2020.

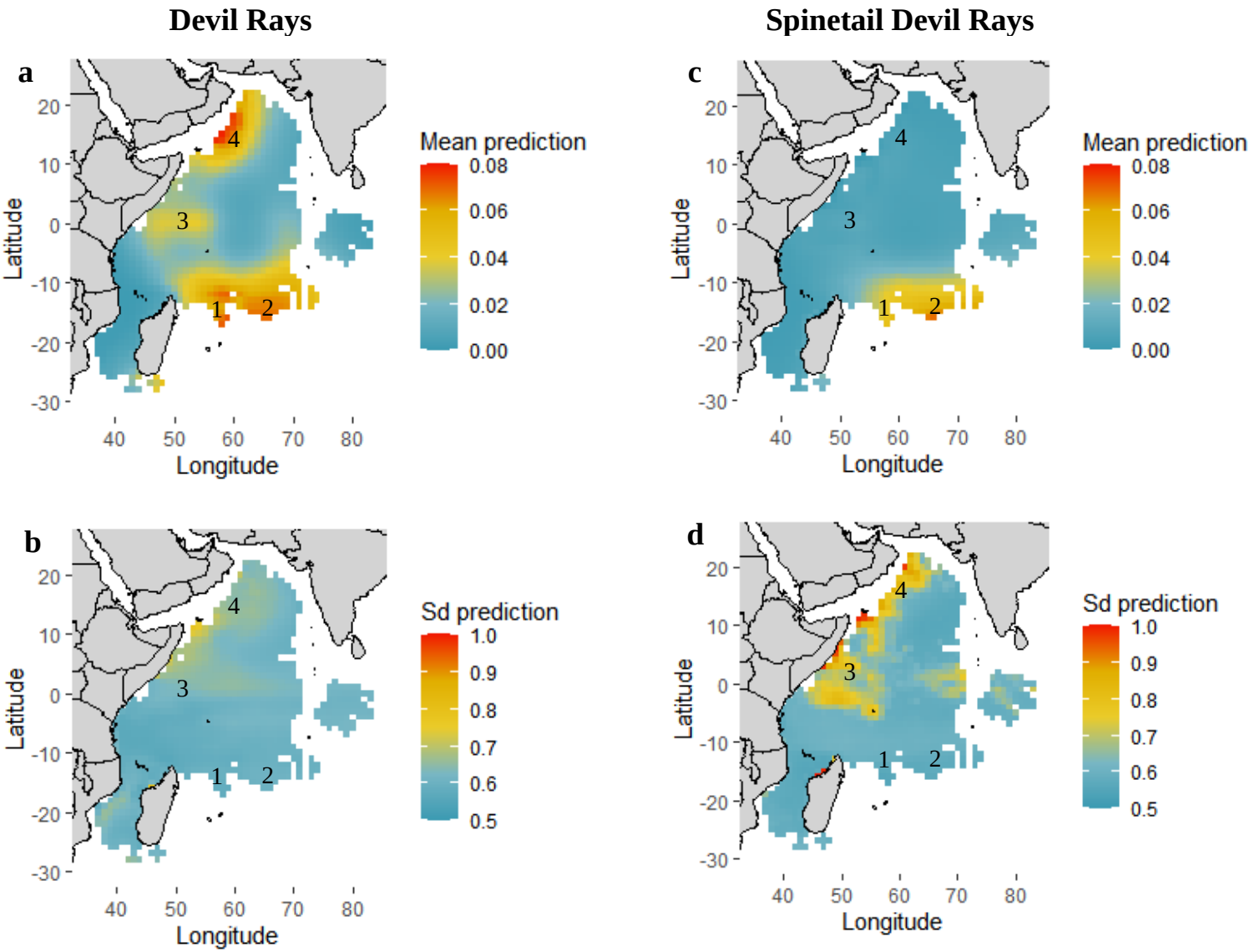

Figure 4 Mean prediction and standard deviation of the presence of devil rays between 2010 and 2020 in the Western Indian Ocean. FSC was used as the fishing set type for model predictions. a) Devil rays´ mean prediction, b) Devil rays' standard deviation, c) Spinetail devil ray *Mobula mobular* mean prediction, d) Spinetail devil ray *Mobula mobular* standard deviation. For FADs as a fishing set type *see* Figure S9. The main hotspots identified are 1) Mascarene plateau, 2) Central Indian Ridge, 3) Equatorial region, 4) Western Arabian Sea

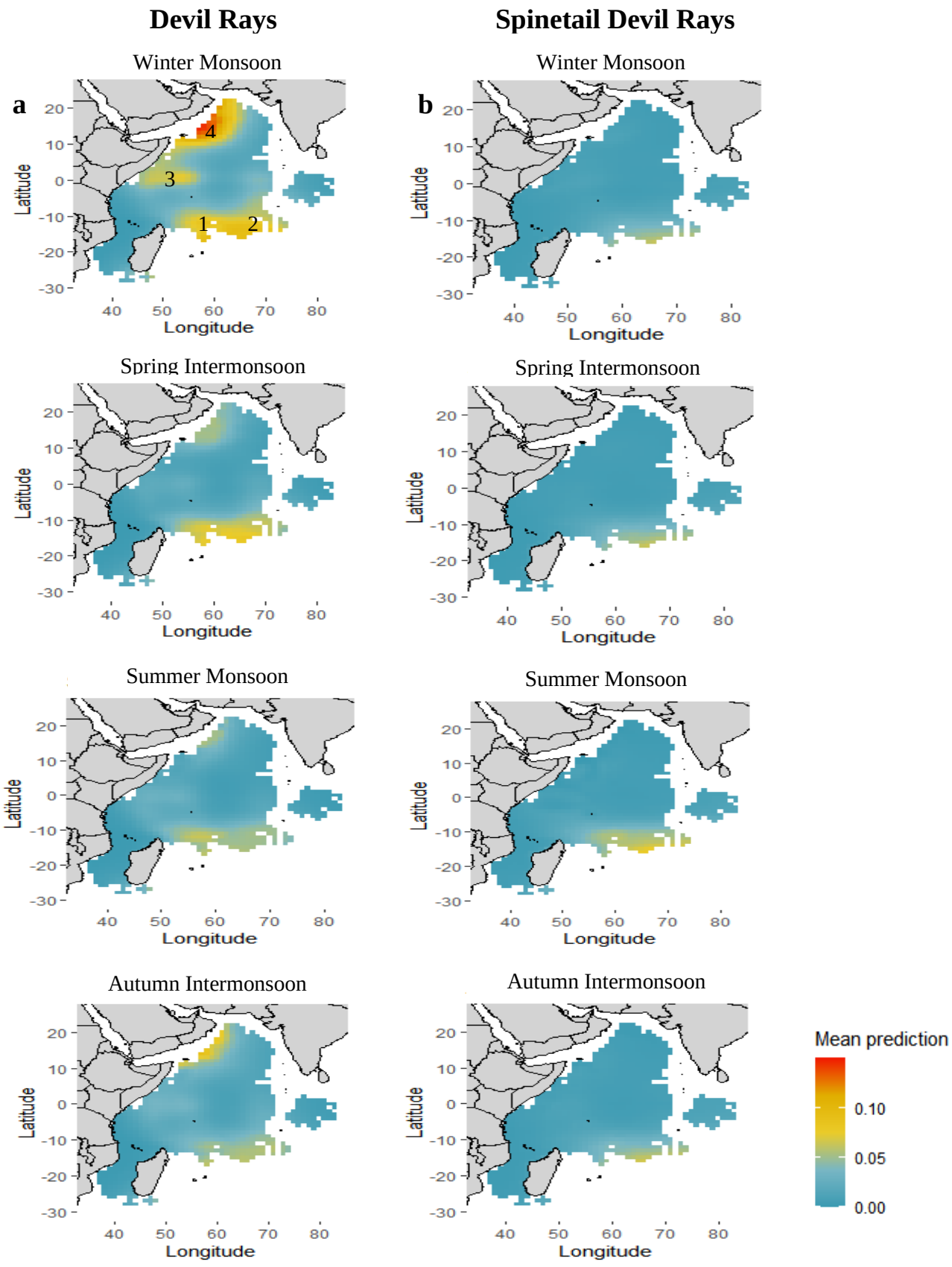

Figure 5 Mean prediction of the presence of all devil rays between 2010 and 2020 in the Western Indian Ocean by monsoon regime. FSC was used as the fishing set type for model predictions. a) devil ray's prediction in winter monsoon, spring intermonsoon, summer monsoon, autumn intermonsoon; b) spinetail devil rays *Mobula mobular* during winter monsoon, spring intermonsoon, summer monsoon, autumn intermonsoon. For FADs as fishing set type *see* Figure S10. The main hotspots identified are 1) Mascarene plateau, 2) Central Indian Ridge, 3) Equatorial region, 4) Western Arabian Sea

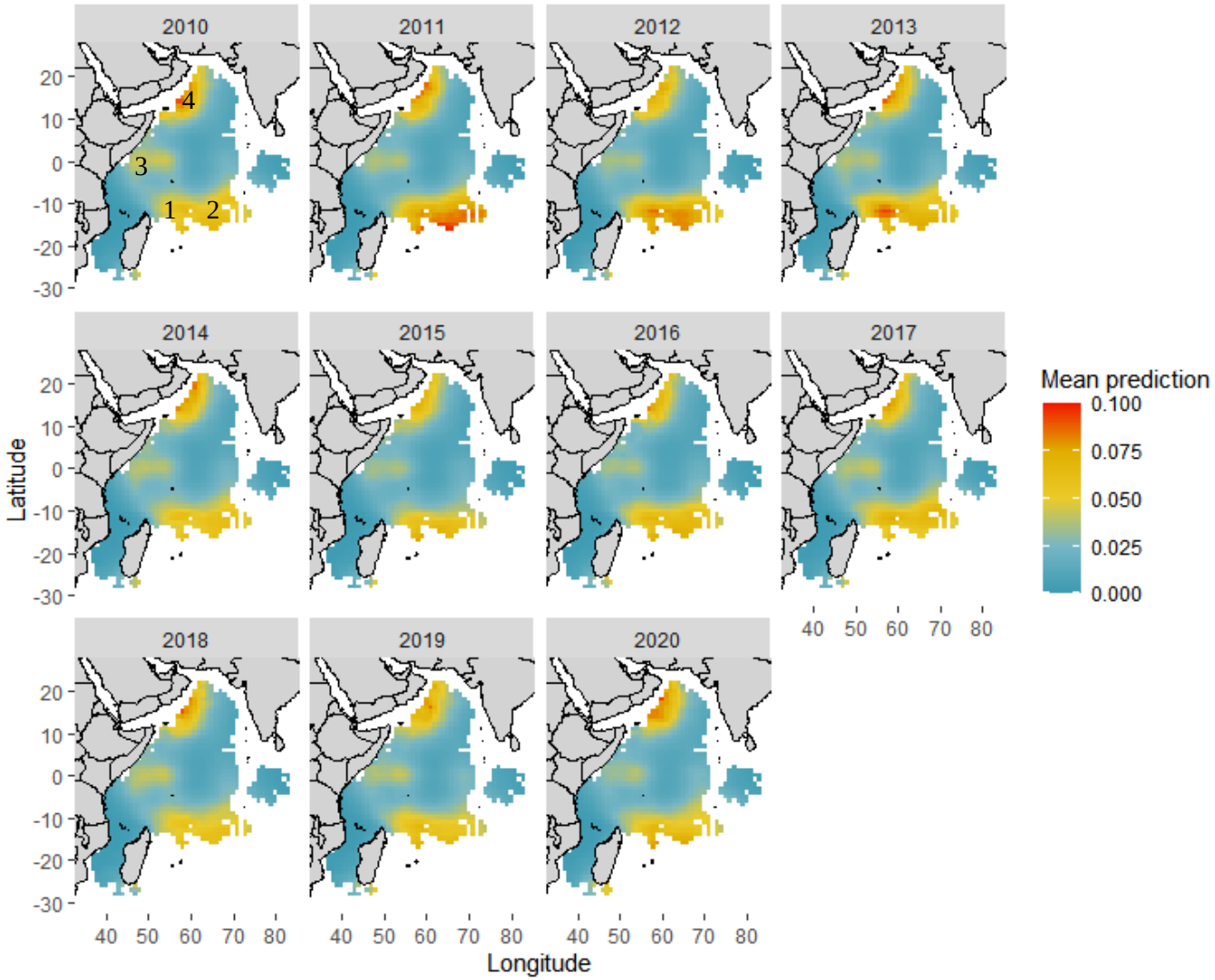

Figure 6 Mean annual prediction of the presence of devil rays between 2010 and 2020 in the Western Indian Ocean. FSC was used as the fishing set type for model predictions. For FADs as the main fishing set type *see* Figure S11. The main hotspot identified are 1) Mascarene plateau and 2) Central Indian Ocean ridge, 3) equatorial regions near ITCZ, 4) Western Arabian Sea.

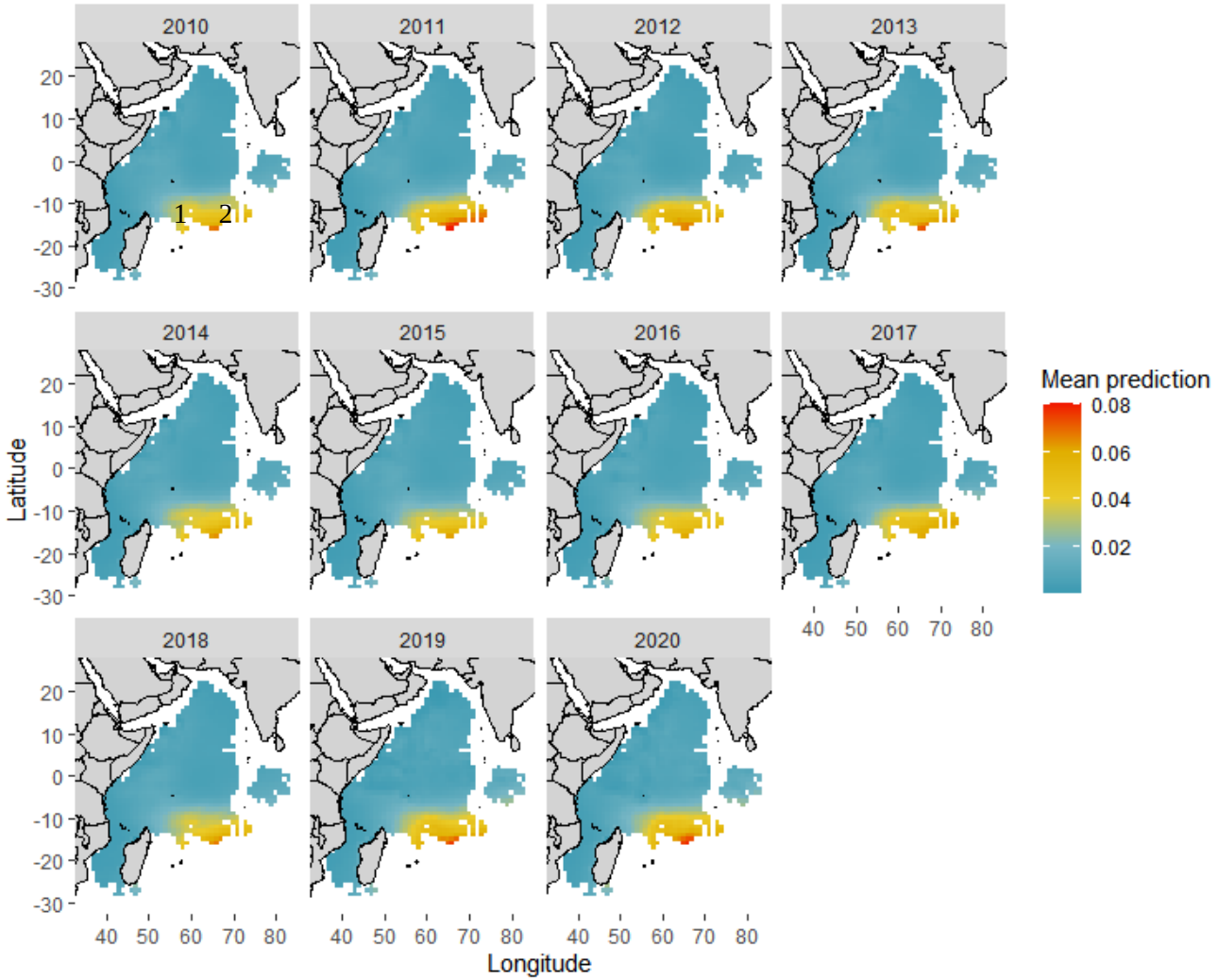

Figure 7 Mean annual prediction of the presence of spinetail devil rays *Mobula mobular* between 2010 and 2020 in the Western Indian Ocean. FSC was used as the fishing set type for model predictions. For FADs as a fishing set type for model prediction *see* Figure S12. The main hotspot identified are 1) Mascarene plateau and 2) Central Indian Ocean ridge, 3) equatorial regions near ITCZ, 4) Western Arabian Sea.

4. Discussion

In this study we modelled the habitat suitability of devil rays in the Western Indian Ocean using the observer bycatch data collected in the EU tropical tuna purse-seine fishery from 2010-2020. Occurrences of devil rays as bycatch in the EU purse seine fishery can in part be explained by environmental variables corresponding to well-identified oceanographic processes and features characteristic of the Western Indian Ocean. Moreover, we found that devil rays are generally observed in high prevalence in sets of tuna schools (FSC) which are usually located in highly productive regions (Coletto et al., 2019; Davies et al., 2014). The environmental variables associated with the presence of devil rays (*Mobula mobular, M. tarapacana, M. thurstoni*) were chlorophyll, sea surface height and sea surface temperature fronts. When modelling the habitat suitability for spinetail devil rays (*M. mobular*) the most influential environmental variables were net primary production of phytoplankton and sea surface temperature fronts. In addition, the spatial predictions identified four hotspots (Figure 4) with higher habitat suitability and higher probability of incidentally catching devil rays. The permanent hotspots were found in the Mascarene Plateau and Central Indian Ridge that remain relatively stable throughout the year. Seasonal hotspots were identified in the Western Arabian Sea and equatorial regions that become prominent during winter monsoon. For spinetail devilray *Mobula mobular* only the permanent hotspots in the Mascarene Plateau and Central Indian Ridge were identified. We hypothesize these four main hotspots may be linked to seasonal productive areas in the western Indian Ocean. As devil rays commonly target high-productivity regions that are ideal for foraging, it is expected that devil rays (Figure 3) will be associated to areas with relatively high chlorophyll and net primary production of phytoplankton. Devil rays have also been recorded to be attracted to areas with low sea surface height which explains the association of the species to cyclonic eddies (Lezama-Ochoa et al. 2019; Lezama-Ochoa et al. 2020a) and sea surface temperature fronts (Graham et al. 2012). We therefore suggest that the main drivers for devil ray aggregations in these areas may be explained by their foraging behavior as they are attracted to high productive regions, and their oceanic migrations which are believed to be linked to the circulation of water masses (Lezama-Ochoa et al. 2019; Lezama-Ochoa et al. 2020b; Lezama-Ochoa et al. 2020a).

Low sea surface height (with values close to zero) was the most important environmental predictor of devil ray´s occurrence. Low sea surface height (with values close to zero) can be associated to upwelling areas and ultimately to cyclonic eddies, while high sea surface height is usually associated with downwelling and anticyclonic eddies. Previous researchers have also associated the presence of devil rays in the Pacific and Atlantic Ocean with low and negative sea surface height, respectively, which was also associated to upwelling regions and cyclonic eddies (Lezama-Ochoa et al. 2019; Lezama-Ochoa et al. 2020a). In this study, we observed that devil rays were notably absent in anticyclonic eddies (Animation S1, Animation S2), which are commonly found in the Arabian sea and North Somalia fishing area during summer monsoon regime, and only become present when these eddies dissipate or decrease in magnitude during winter monsoon regime. In Arabian sea, North and South Somalia, and Northwest Seychelles fishing area, the sea surface height is generally low however during summer with the formation of anticyclonic eddies such as Great whirl and Socotra eddy, and the presence of Southern gyre, there is an increase in sea surface height in the areas where these eddies and gyre are formed (Animation S1) (Schott et al. 2009). In contrast, in the Southeast Seychelles fishing area where the Mascarene plateau and Central Indian Ridge hotspot are located, the sea surface height is generally higher than in the rest of the fishing areas, but it remains relatively constant throughout the year. Thus, we hypothesized that the reason why devil rays are absent in Western Arabian Sea hotspot (Arabian sea fishing area) during summer but are still predicted in Mascarene plateau and Central Indian Ridge hotspots (Southeast Seychelles fishing area), is due to the relatively constant values of sea surface height in Southeast Seychelles fishing area throughout the year. This mean that the Southeast Seychelles fishing area is relatively calmer than the other fishing areas. Moreover, productivity in these areas could also be linked to sea surface height anomalies. Sea surface height anomalies refer to the changes in the average sea surface height of an area in a given time (Song et al. 2018). The study of Meng and colleagues showed that the northwestern Indian ocean have a negative sea surface height anomaly in areas of Western Arabian Sea and equatorial regions hotspots while positive sea surface height anomalies happens in the southwestern Indian ocean in Mascarene plateau and Central Indian ridge hotspots (Meng et al. 2020). This is supported by study of Song and colleagues which revealed that negative sea surface anomalies have higher chlorophyll concentration in winter and lower in summer, while for areas with positive sea surface heigh anomalies have higher chlorophyll during summer and low during winter (Song et al. 2018). Therefore, this study suggests a higher devil ray's occurrence in close to zero sea surface height which is associated to upwelling areas but it also highlights that the sea surface height covariate may also have different ecological meaning under different oceanographic processes in different areas of the Western Indian Ocean (Mannocci et al. 2020)

Chlorophyll was the second most important environmental predictor variable of devil ray occurrence. Devil rays' occurrences were observed in areas with chlorophyll concentration of 0.3 - 0.5 $mg.m^{-3}$. We hypothesize that the association to chlorophyll might be linked to the devil ray foraging activity in productive areas. However, the chlorophyll values seen here are relatively lower than the observed values in the Pacific (between 0.5-1 mg.m3) and Atlantic (between 0.2-1 mg.m3) in which the presence of *M. mobular* was predicted (Lezama-Ochoa et al. 2019; Lezama-Ochoa et al. 2020b; Lezama-Ochoa et al. 2020a). The lower chlorophyll values associated with the higher probabilities of incidental catches of devil rays could also be reflecting the relative low number of occurrences of devil rays in the EU observer fisheries dataset and the limited spatial coverage of the EU observer program in the productive coastal areas within the EEZs of Somalia (Figure S3a) (Martin 2020). Even though the Somali area have high chlorophyll values especially during the summer monsoon, this area was not identified as a main hotspot. We suggest that it may be because this region was not covered by the EU observer program between the years 2010 and 2013 (Figure S3b) and because of the existing piracy in region (Chassot et al. 2010; Báez et al. 2020). Moreover, the differences in oceanographic conditions (productive regions, mesoscale processes) among different regions of the Western Indian Ocean may also be in part explained by the different oceanographic processes unique in each region, its characteristic oligotrophic southern region, the lack of equatorial upwelling and the monsoon driven upwelling in the north (Vinayachandran et al. 2021). Yet, the habitat model for devil ray, even with the relatively low number of occurrences, was able to establish an association with chlorophyll that can be linked to their foraging behavior (Stewart et al. 2018).

Net primary production of phytoplankton (NPPV) was also chosen to best describe the occurrence of spinetail devil ray *Mobula mobular*. Net primary production of phytoplankton is the new biomass produced by phytoplankton from photosynthesis and respiration (Girondot et al. 2015). Therefore, net primary production of phytoplankton is a function of chlorophyll, which is supported by the high correlation ($p > 0.6$) between the two (Figure S8). The association of spinetail devil ray with net primary production of phytoplankton has also been observed in its relative species, the giant oceanic manta *Mobula birostris (*formerly *Manta birostris),* which presences have been associated with high net primary production in French Guiana waters (Girondot et al. 2015). Similar to the predictor variables of sea surface height and chlorophyll in the modelling of devil rays, the net primary production of phytoplankton also suggested the Mascarene plateau and Central Indian Ridge hotspots (Figure 4) as areas of high probability of occurrence of spinetail devil ray. However, it did not identify the equatorial and Western Arabian Sea hotspots as areas of high probability of occurrence for spinetail devil ray. This might be explained primarily because the Mascarene Plateau and Central Indian Ridge hotspots are found in an ocean region, which is more oligotrophic, as it is more influenced by the Southern Ocean circulation where the Indian ocean gyre serve as a vector circulating the water masses (Stellema et al. 2019). In contrast, the Western Arabian Sea and Equatorial Region hotspots are located in an ocean region that is highly influence by the monsoon (Schott et al. 2009) and varying sea surface height changes through time (Animation S1). Thus, either the net primary production or the combination of chlorophyll and sea surface height, with the rest of the other selected variables (Figure 3) could be used to describe the Mascarene Plateau and Central Indian Ridge hotspots. The habitat models attempt to identify environmental variables that explain devil rays' occurrences across the whole Western Indian Ocean, and this may be challenging because of the large spatial scale of the study region which encompasses diverse oceanographic conditions. At the end, this study associated the presence of spinetail devil ray with net primary production, which is also a good proxy for chlorophyll and sea surface height and predicted the presence of spinetail devil ray in Mascarene plateau and Central Indian Ridge hotspots (Animation S3).

Both the devil rays and spinetail devil ray habitat suitability models showed a strong positive relationship between occurrences and sea surface temperature fronts. We hypothesize that devil rays are attracted to sea surface temperature fronts because these are areas of zooplankton aggregation and areas used for thermoregulation. This has been observed in its relative species, giant oceanic manta ray *Mobula birostris* (formerly *Manta birostris*), which distribution has been associated to temperature fronts and linked to its foraging activity (Graham et al. 2012). The presence of other elasmobranchs such as the basking shark *Cetorhinus maximus* has also been linked to sea surface temperature fronts (Finucci et al. 2021). Moreover, fronts are considered hot spots of marine life, as they often are loci of maximum biodiversity and elevated primary and secondary production (Belkin 2021). Typically, weak fronts contain smaller phytoplankton and zooplankton such as dinoflagellates and microzooplankton. Instead, strong fronts lead to a size structure shift from smaller phytoplankton and microzooplankton to larger zooplankton and phytoplankton such as diatoms. The results suggest a higher probability of occurrence of devil rays in areas where there are sea surface temperature fronts, which can be linked to high surface zooplankton concentration and therefore, areas where devil rays may exploit phytoplankton patches (Graham et al. 2012; Woodson et al. 2015).

Sea surface temperature was selected as a predictor environmental variable in one of the habitat suitability models evaluated for devil rays (Table S1). However, this model showed lower model sensitivity when subjected to cross validation compared to the final model, which selected instead chlorophyll and sea surface height. When

modelling spinetail devil ray occurrences, the habitat model selecting sea surface temperature had also lower model performance (AIC, Table S1) than when net primary production of phytoplankton was selected. Previous work has suggested that devil rays' occurrences can also be associated with low values of sea surface temperature, which are directly describing the presence of upwelling systems (Couturier et al. 2018; Harris et al. 2020). However, our results suggest that chlorophyll, sea surface height and net primary productivity are better predictor variables than sea surface temperature for predicting devil rays occurrence (Lezama-Ochoa et al. 2019; Lezama-Ochoa et al. 2020a; Lezama-Ochoa et al. 2020b)

We found that "Year" is not significant ($p>0.05$) either as smooth term or as factor in the habitat models. This suggested there is no annual trend or a year effect explaining the interannual variability in the occurrences of devil rays or spinetail devil ray. We hypothesize that this lack of relationship may be explained by two main reasons. Firstly, the relative low number of occurrences of devil rays (369 presences; 118 spinetail devil ray) recorded in the EU observer program between year 2010-2020 might make it difficult to detect any year effect. Secondly, the areas with high occurrences of devil rays may be consistent throughout the years with little annual differences. Consequently, only changes in the environmental variables between 2010 and 2020 drives the interannual changes in the probability of devil rays' occurrences. Although the variable "Year" was not a significant variable in the final model, it can still be observed that the devil ray incidental catch has been declining during the 10 years of the study (Figure S7b). The observed decline in the incidental catch may be linked to the current observed population declines in these species in the Indian Ocean (Lewis et al. 2015; O'Malley et al. 2017; Rohner et al. 2017b; Flounders 2020; Moazzam 2018). Therefore, we recommended for future studies to explore further the potential declines observed in the incidental catches recorded in the EU observer program.

With respect to the type of fishing set used in the fishing operations, the habitat suitability models suggested a higher probability of occurrence and incidental catch of devil rays in FSC sets than in sets associated to FADs. We suggest that this might be explained because the school sets follow tuna schools which are mostly located in high productivity areas for foraging (Druon et al. 2017). Aggregation of tuna schools in productive area are observed in skipjack tuna *Katsuwonus pelamis* and yellowfin tuna *Thunnus albacares* (Richardson et al. 2018). These proposed that the potential overlap of devil rays and tuna schools could be a result of foraging activity on zooplankton in high-productivity regions (Davies et al. 2014). In contrast, the probability of occurrence of devil rays was lower in sets associated to FADs which differs to other species of tunas, sharks such as silky sharks and oceanic whitetip sharks and sea turtles which tend to aggregate in FADs, increasing their incidental catches (Davies et al. 2014; Lezama-Ochoa et al. 2015). Though, FADs contribute lesser to explaining the presence of devil rays, it is worth mentioning that during winter monsoon there is a higher probability of devil ray's occurrence in the Western Arabian Sea hotspot where there is a high aggregation of FADs. FADs drift with the currents and tend to get trapped in the gyres and eddies within this region, specifically during winter monsoon (Schott et al. 2009; Martin 2020). We hypothesize that release of large numbers of FADs to increase the catchability of tuna species in the ocean could potentially change the natural environment of tuna species and other species also aggregating underneath the FADs (Dagorn et al. 2013). This has been referred as the ecological trap hypothesis, which states that drifting FADs deployed in large numbers could be taking species to areas where they would not normally occur therefore having an impact on their migrations and also consequences for their conditions, growth and reproductive potential (Dagorn et al. 2013; Martin 2020). Therefore, we suggest further studies regarding the impact of FADs on the migration, condition, and behavior on devil rays.

The total catch of "Tuna" made in each set was also selected as a predictor variable explaining both the occurrence of devil rays and spinetail devil ray (Figure 3e for devil rays, Figure 3j for spinetail devil ray). A relatively small set size (<50 tons) showed a higher probability of occurrence of devil rays, then the probability decreased with larger catches of tunas. The model showed that when the total catch was approximately 50 tons or more there was a decrease of 20% probability of capture of devil rays. Our results coincide with the findings of Dagorn and colleagues where it was suggested that tropical tuna purse seine fisheries could target large schools of tunas to decrease bycatch not only of devil rays but also of other vulnerable species such as sharks and turtles (Dagorn et al. 2012; Dagorn et al. 2013). This same study shows that the ratios of bycatch of devil rays are higher when sets are made in small schools of tunas. Therefore, we suggest that targeting large schools of tuna could reduce the number of fishing sets or effort while maintaining the same total yield, contributing to a substantial reduction in the impacts of fishing on threatened species (Dagorn et al., 2012).

Both the devil rays and spinetail ray habitat suitability models revealed an interaction of latitude-longitude as a significant predictor variable. The predicted habitat maps showed seasonal hotspots (Western Arabian Sea, equatorial region) and permanent hotspots (Mascarene plateau and Central Indian ridge) with higher probabilities of occurrence of devil rays (Figure 4a). These regions are associated with Chlorophyll and phytoplankton net primary production, and low sea surface height and are great importance for the ecology of devil rays. We suggest two opposing hypotheses that may explain the aggregations of devil rays in Western Arabian Sea. First, this region

could play an important role in the distribution of devil rays being an important winter migration pathway for this species, as they aggregate in this area only during a short period (December-March) (Figure 5). Secondly, the high numbers of FADs deployed in this area may be having an impact on the distribution and migrations of this species, by retaining them in not their natural environment (Martin 2020). Due to limited number of presences recorded in the fisheries observer dataset in this area, the current data is not sufficient to ascertained which of the two hypothesis is more plausible (Figure 1). Moreover, in summer (June-September), the highest probability of occurrence of devil rays was found to be in Mascarene Plateau and Central Indian Ridge hotspots. We hypothesize that it may be explained by the high presence of seamounts and submerge ridges in Mascarene Plateau and Central Indian Ridge. These elevated areas are a perfect habitat for devil ray species, since they can be used for protection, reproduction, cleaning, or breeding (Stevens et al. 2018). Oceanic manta rays *Mobula birostris*, a relative species belonging to the same genus, also has been found to aggregate around oceanic island groups and offshore pinnacles, seamounts, and submarine ridge systems, where they are known to engage in courtship (Stevens et al., 2018). Moreover, other studies have shown a hotspot for the aggregations of silvertip shark (*Carcharhinus albimarginatus*) adjacent to the southern hotspot (Mascarene Plateau and Central Indian Ridge) in the Chagos Archipelago in the British Indian Ocean Territories seamounts (Hosegood et al. 2019). Moreover, aside from the association of this species to these areas for their foraging activity, these hotspots could also be a potential migratory corridor for devil rays serving as a pathway connecting different regions. Previous tagging studies on sea turtles on the Mascarene Islands and Mozambique Channel showed their extensive migrations in all directions across open ocean areas (Dalleau et al. 2019) suggesting that this area might be an important migratory corridor not only for turtles and devil rays but also for other migratory species. Furthermore another study investigating the filter feeder whale shark connectivity concluded that Mascarene plateau as the largest underwater oceanic bank in the whole Indian ocean, could potentially a stopover for whale sharks to an unidentified breeding habitat (Dulau et al. 2017). The high occurrence of devil rays in the equatorial regions during winter but not during summer might be explained by the chlorophyll bloom events occurring from December to March and the influence of the Madden-Julian Oscillation (MJO). During this period is when the shallowing thermocline cause the blooms to be more efficient during the early stage of the winter monsoon (December–January), while the deeper thermocline in the later monsoon period becomes less favourable to phytoplankton blooms (Liao et al. 2017). Consequently, we propose the existence of hotspots for devil rays which are closely linked to productive oceanic areas and areas associated with ridges and seamounts that could act as a foraging locations and migration corridors.

Limitation and future perspective

Limitation of this study includes the use of fishery dependent data which might create some bias due to the way the sampling data is made. The sampling of the data collected in the EU purse seine observer program are often influenced by their preferential sampling because fisheries are commercially driven and not focused on conducting scientific random sampling (Pennino et al. 2016; Orue et al. 2020). Though this may be the case, Pennino and colleagues stressed that fishery dependent and independent data can complement each other. The restricted time coverage of the fishery-independent data could be complemented by using fishery dependent data that are collected annually, and the spatial uncertainty of fishery-dependent sites may be corrected using fishery-independent data (Pennino et al. 2016). Thus, this study will be the basis of future studies using more restricted fishery independent studies to investigate the importance of the identified permanent and temporal hotspots for the ecology of devil rays (Figure 5).

The difficulty in identifying devil rays at the species level in the EU purse seine observer program is another important limitation in this study. Species of devil rays share various morphological similarities which makes their identification difficult. This is reflected in EU purse seine observer data set which contains a high number of devil rays records assigned to the genus level (Figure S5d). This is a widespread challenge across multiple fisheries in the Indian Ocean. A recent report of Flounder and Martin in IOTC also stressed the difficulties to correctly identify species up to species level in multiple IOTC fisheries (Flounders 2020; Martin 2020). Yet it is important that species are correctly identified to the species level to support the development of species distribution models in the future (Ward-Paige et al. 2013). Further genetic studies are also needed so the population structure can be better understood in these species and to help with their correct identification (Couturier et al. 2012; White et al. 2018; Hosegood et al. 2020).

The partial spatial coverage of the observer program also creates limitations in how the results can be interpreted in areas where the fleet does not operate or partially operates such as in the coastal areas off the Africa and Arabia coast where devil ray species are known to aggregate (Figure S3a).Therefore, the results in this study provide a preliminary overview of the potential environmental characteristics associated with the presences of devil rays and their seasonally preferred habitats. We highly suggest using fisheries independent data and studies including satellite and acoustic tagging data to account for potential biases when modeling the habitat suitability of species

and to validate the current models. Further research using telemetry, stable isotope, and genetic studies could also be used to validate the current habitat suitability models obtained in this study, and provide additional information on biology and ecology of devil rays species in the Indian Ocean (Lezama-Ochoa et al. 2019)

The habitat models produced here using GAMs explained a low percent of the total deviance. This means that the presence of devil rays' species may be explained by diverse factors not considered, unknown, or not included in the models. These additional external factors not accounted in the models could be any additional physical, chemical, or biological environmental characteristics explaining the habitat suitability of devil rays and zooplankton distribution. In comparison to the habitat models for devil rays, a single or two environmental variables are usually enough to explain the distribution and habitat suitability of targeted species such as tunas (Davies et al. 2014; Orue et al. 2020), which might be driven by the higher quality and the quantity of the data used in the habitat modelling for the main commercial tuna species. Previous work modelling habitat suitability for other bycatch species in purse seine fisheries targeting tuna species also found a low deviance explained in their models (Birkmanis et al. 2020; Lezama-Ochoa et al. 2020a; Lopez et al. 2020). Although the low level of explained deviance in our models are in line with previous research (Couturier et al. 2012; Couturier et al. 2018; Lezama-Ochoa et al. 2019; Lezama-Ochoa et al. 2020a; Lopez et al. 2020; Martin 2020), it should be interpreted with caution (Lezama-Ochoa et al. 2020a). Yet despite the low deviance explained in the models, the information obtained from the observer program is still deemed useful, since it contributes to improving the knowledge about the most vulnerable bycatch species in the EU purse seine fleet. Moreover, based on the different statistics indices (AUC, sensitivity, specificity, etc.) calculated in this study, the performance of the model is considered acceptable. Thus, the habitat model produced here can still provide basic and preliminary information about devil rays distribution and their preferred habitat preferences.

This study modelled the relationship between characteristics of the environment and fishing behaviors, and the occurrences of multiple devil ray species. Future studies should also explore modelling the abundance of devil rays, instead of occurrence, as well as explore other modelling techniques such as Maximum Entropy Models, Bayesian Approaches (INLA), and Random Forests to model both the presence and abundance of these species (Lezama-Ochoa et al. 2019; Lezama-Ochoa et al. 2020a). Additionally, since the presence or abundance of devil rays may also be linked to foraging opportunities, the inclusion of a variable describing zooplankton abundance could also improve model fit and performance. A variable for zooplankton was not included in this study because such information and data are not collected as part of the observer program and it is not readily available in other external data collection programs (Lezama-Ochoa et al. 2019). Therefore, alternative sources to get and access zooplankton datasets could be explored in future modelling studies (Montero et al. 2016).

We suggest that the hotspot areas predicted in the habitat models showing those areas with a higher probability of occurrence in devil rays could be potentially important in helping researchers to plan strategic research work such as implementing successful tagging programs.

5. Conclusion

This study gives insights on the environmental conditions of suitable habitats for devil rays in the Western Indian Ocean using the EU tropical tuna purse seine fisheries observer data and generalized additive models. We revealed that these species are generally attracted to productive areas with relatively high in chlorophyll and net primary production, low sea surface height, and sea surface temperature fronts. Devil rays were also found to be associated with permanent hotspots in the Mascarene Plateau and Central Indian Ridge and associated with seasonal hotspots in the Western Arabian Sea and Equatorial regions during winter monsoon. We found that there is no annual trend or a year effect explaining the interannual variability in the occurrences of devil rays or spinetail devil ray. Only the yearly variability of selected environmental variables affects the observe changes in the habitat suitability of both devil ray and spinetail devil ray, interannually. Moreover, chlorophyll and sea surface height were good predictor variables of the presence of devil rays (all three mobula species combined), explaining the high occurrences in both temporal hotspots such as Western Arabian Sea and equatorial regions, and permanent hotspots such as Mascarene Plateau and Central Indian Ridge in Western Indian Ocean. While net primary production of phytoplankton was a good predictor variable of the occurrence of spinetail devil rays (*Mobula mobular*), explaining the high occurrences of this species in Mascarene Plateau and Central Indian Ridge hotspots. We also suggest setting in big schools of tuna to reduce the probability of catching devil rays. Both the devil rays and the spinetail devil ray habitat models predicted a higher probability of incidental catch in free school sets than in sets associated to FADs. This information should be considered when designing management measures that aim to minimize the interactions of purse seine fisheries with vulnerable bycatch species, given that some vulnerable species are more frequently caught in FSC sets while others are more frequently caught in sets using FADs. Therefore, trade-offs need be closely evaluated among these two types of fishing operations when designing management and conservation measures for protecting vulnerable bycatch species. In addition, this study is the first to investigate and identify biological hotspots of devil rays in the Western Indian Ocean. Accurate knowledge of the habitat preferences of the species at relevant spatial resolutions is vital to minimize the interaction of fisheries with the most vulnerable species (Hahlbeck et al. 2017b). Therefore, the permanent and temporal hotspots of high incidental catch of devil rays identified in this study could inform the development of future spatial management measures, including time-area closures, to minimize the interaction of fisheries with these species (Lezama-Ochoa et al. 2019; Lezama-Ochoa et al. 2020a; Lopez et al. 2020)

References

Alfaro-Cordova E, Del Solar A, Alfaro-Shigueto J, Mangel JC, Diaz B, Carrillo O, Sarmiento D. 2017. Captures of manta and devil rays by small-scale gillnet fisheries in northern Peru. Fish Res. 195:28–36. doi:10.1016/j.fishres.2017.06.012.

Amandè MJ, Chassot E, Chavance P, Murua H, de Molina AD, Bez N. 2012. Precision in bycatch estimates: the case of tuna purse-seine fisheries in the Indian Ocean. ICES J Mar Sci. 69(8):1501–1510. doi:10.1093/icesjms/fss106.

Arrizabalaga H, Dufour F, Kell L, Merino G, Ibaibarriaga L, Chust G, Irigoien X, Santiago J, Murua H, Fraile I, et al. 2015. Global habitat preferences of commercially valuable tuna. Deep Sea Res Part II Top Stud Oceanogr. 113:102–112. doi:10.1016/j.dsr2.2014.07.001.

Báez JC, Ramos ML, Herrera M, Murua H, Cort JL, Déniz S, Rojo V, Ruiz J, Pascual-Alayón PJ, Muniategi A, et al. 2020. Monitoring of Spanish flagged purse seine fishery targeting tropical tuna in the Indian ocean: Timeline and history. Mar Policy. 119. doi:10.1016/j.marpol.2020.104094. [accessed 2021 Aug 1]. https://linkinghub.elsevier.com/retrieve/pii/S0308597X19307559.

Barr Y, Abelson A. 2019. Feeding – Cleaning Trade-Off: Manta Ray "Decision-Making" as a Conservation Tool. Front Mar Sci. 6:88. doi:10.3389/fmars.2019.00088.

Beale CS, Stewart JD, Setyawan E, Sianipar AB, Erdmann MV. 2019. Population dynamics of oceanic manta rays (*Mobula birostris*) in the Raja Ampat Archipelago, West Papua, Indonesia, and the impacts of the El Niño–Southern Oscillation on their movement ecology. Embling C, editor. Divers Distrib. 25(9):1472–1487. doi:10.1111/ddi.12962.

Belkin IM. 2021. Remote Sensing of Ocean Fronts in Marine Ecology and Fisheries. Remote Sens. 13(5):883. doi:10.3390/rs13050883.

Belkin IM, O'Reilly JE. 2009. An algorithm for oceanic front detection in chlorophyll and SST satellite imagery. J Mar Syst. 78(3):319–326. doi:10.1016/j.jmarsys.2008.11.018.

Birkmanis CA, Partridge JC, Simmons LW, Heupel MR, Sequeira AMM. 2020. Shark conservation hindered by lack of habitat protection. Glob Ecol Conserv. 21:e00862. doi:10.1016/j.gecco.2019.e00862.

Boerder K, Schiller L, Worm B. 2019. Not all who wander are lost: Improving spatial protection for large pelagic fishes. Mar Policy. 105:80–90. doi:10.1016/j.marpol.2019.04.013.

Brodie S, Hobday AJ, Smith JA, Everett JD, Taylor MD, Gray CA, Suthers IM. 2015. Modelling the oceanic habitats of two pelagic species using recreational fisheries data. Fish Oceanogr. 24(5):463–477. doi:10.1111/fog.12122.

Burt WJ, Westberry TK, Behrenfeld MJ, Zeng C, Izett RW, Tortell PD. 2018. Carbon: Chlorophyll Ratios and Net Primary Productivity of Subarctic Pacific Surface Waters Derived From Autonomous Shipboard Sensors. Glob Biogeochem Cycles. 32(2):267–288. doi:10.1002/2017GB005783.

Chassot E, Dewals P, Floch L, Lucas V, Morales-Vargas M, Kaplan DM. 2010. Analysis of the effects of Somali piracy on the European tuna purse seine fisheries of the Indian Ocean. https://www.iotc.org/documents/analysis-effects-somali-piracy-european-tuna-purse-seine-fisheries-indian-ocean.

Clarke S, Sato M, Small C, Sullivan B, Inoue Y, Ochi D. 2014. Bycatch in longline fisheries for tuna and tuna-like species: a global review of status. Rome, Italy: FAO FAO Fisheries and Aquaculture Technical Paper Report No.: 588.

CMS. 2016. Mobula thurstoni | CMS. [accessed 2021 Aug 1]. https://www.cms.int/es/node/7434.

Couturier L, Newman P, Jaine F, Bennett M, Venables W, Cagua E, Townsend K, Weeks S, Richardson A. 2018. Variation in occupancy and habitat use of Mobula alfredi at a major aggregation site. Mar Ecol Prog Ser. 599:125–145. doi:10.3354/meps12610.

Couturier LIE, Marshall AD, Jaine FRA, Kashiwagi T, Pierce SJ, Townsend KA, Weeks SJ, Bennett MB, Richardson AJ. 2012. Biology, ecology and conservation of the Mobulidae. J Fish Biol. 80(5):1075–1119. doi:10.1111/j.1095-8649.2012.03264.x.

Croll DA, Dewar H, Dulvy NK, Fernando D, Francis MP, Galván-Magaña F, Hall M, Heinrichs S, Marshall A, Mccauley D, et al. 2016. Vulnerabilities and fisheries impacts: the uncertain future of manta and devil rays. Aquat Conserv Mar Freshw Ecosyst. 26(3):562–575. doi:10.1002/aqc.2591.

Cruz MJ, Machete M, Menezes G, Rogan E, Silva MA. 2018. Estimating common dolphin bycatch in the pole-and-line tuna fishery in the Azores. PeerJ. 6:e4285. doi:10.7717/peerj.4285.

Dagorn L, Filmalter JD, Forget F, Amandè MJ, Hall MA, Williams P, Murua H, Ariz J, Chavance P, Bez N. 2012. Targeting bigger schools can reduce ecosystem impacts of fisheries. Hilborn R, editor. Can J Fish Aquat Sci. 69(9):1463–1467. doi:10.1139/f2012-089.

Dagorn L, Holland KN, Restrepo V, Moreno G. 2013. Is it good or bad to fish with FADs? What are the real impacts of the use of drifting FADs on pelagic marine ecosystems? Fish Fish. 14(3):391–415. doi:10.1111/j.1467-2979.2012.00478.x.

Dalleau M, Kramer-Schadt S, Gangat Y, Bourjea J, Lajoie G, Grimm V. 2019. Modeling the emergence of migratory corridors and foraging hot spots of the green sea turtle. Ecol Evol. 9(18):10317–10342. doi:10.1002/ece3.5552.

Davies TK, Mees CC, Milner-Gulland EJ. 2014. Modelling the Spatial Behaviour of a Tropical Tuna Purse Seine Fleet. Hazen EL, editor. PLoS ONE. 9(12):e114037. doi:10.1371/journal.pone.0114037.

Díaz-Delgado E, Crespo-Neto O, Martínez-Rincón RO. 2021. Environmental preferences of sharks bycaught by the tuna purse-seine fishery in the Eastern Pacific Ocean. Fish Res. 243:106076. doi:10.1016/j.fishres.2021.106076.

Dörner H, Casey J, Carvalho N, Damalas D, Graham N, Guillen J, Holmes S, Natale F, Osio G, Rätz H, et al. 2018. Collection and dissemination of fisheries data in support of the EU Common Fisheries Policy. Ethics Sci Environ Polit. 18:15–25. doi:10.3354/esep00183.

Druon J-N, Chassot E, Murua H, Lopez J. 2017. Skipjack Tuna Availability for Purse Seine Fisheries Is Driven by Suitable Feeding Habitat Dynamics in the Atlantic and Indian Oceans. Front Mar Sci. 4:315. doi:10.3389/fmars.2017.00315.

Duffy LM, Lennert-Cody CE, Olson RJ, Minte-Vera CV, Griffiths SP. 2019. Assessing vulnerability of bycatch species in the tuna purse-seine fisheries of the eastern Pacific Ocean. Fish Res. 219:105316. doi:10.1016/j.fishres.2019.105316.

Dulau V, Pinet P, Geyer Y, Fayan J, Mongin P, Cottarel G, Zerbini A, Cerchio S. 2017. Continuous movement behavior of humpback whales during the breeding season in the southwest Indian Ocean: on the road again! Mov Ecol. 5(1):11. doi:10.1186/s40462-017-0101-5.

Dulvy NK, Fowler SL, Musick JA, Cavanagh RD, Kyne PM, Harrison LR, Carlson JK, Davidson LN, Fordham SV, Francis MP. 2014. Extinction risk and conservation of the world's sharks and rays. eLife. https://elifesciences.org/articles/00590.

Elith J, Leathwick JR. 2009. Species Distribution Models: Ecological Explanation and Prediction Across Space and Time. Annu Rev Ecol Evol Syst. 40(1):677–697. doi:10.1146/annurev.ecolsys.110308.120159.

Fadool B. 2020. Anthropogenic Change on the Distribution of Marine Megafauna and Their Prey. Honors Theses Univ Neb-Linc.:278.

Finucci B, Duffy CAJ, Brough T, Francis MP, Milardi M, Pinkerton MH, Petersen G, Stephenson F. 2021. Drivers of Spatial Distributions of Basking Shark (Cetorhinus maximus) in the Southwest Pacific. Front Mar Sci. 8:665337. doi:10.3389/fmars.2021.665337.

Flounders L. 2020. The impact of the IOTC fisheries on mobulid rays: status and interactions, data availability, and recommendations for management. https://iotc.org/documents/WPEB/16/18.

Forrestal FC, Goodyear CP, Schirripa M. 2019. Applications of the longline simulator (LLSIM) using US pelagic longline logbook data and Atlantic blue marlin. Fish Res. 211:331–337. doi:10.1016/j.fishres.2018.11.029.

Fortuna CM, Kell L, Holcer D, Canese S, Filidei Jr. E, Mackelworth P, Donovan G. 2014. Summer distribution and abundance of the giant devil ray (Mobula mobular) in the Adriatic Sea: Baseline data for an iterative management framework. Sci Mar. 78(2):227–237. doi:10.3989/scimar.03920.30D.

Francis MP, Jones EG. 2017. Movement, depth distribution and survival of spinetail devilrays (*Mobula japanica*) tagged and released from purse-seine catches in New Zealand: Movement, depth distribution and survival of spinetail devilrays. Aquat Conserv Mar Freshw Ecosyst. 27(1):219–236. doi:10.1002/aqc.2641.

Freeman E. 2012. Presence-Absence Model Evaluation.

Galland G, Rogers A, Nickson A. 2016. Netting Billions: A Global Valuation of Tuna. Washington, D.C.: The Pew Charitable Trusts.

Gallienne CP, Conway DVP, Robinson J, Naya N, William JS, Lynch T, Meunier S. 2004. Epipelagic mesozooplankton distribution and abundance over the Mascarene Plateau and Basin, south-western Indian Ocean. J Mar Biol Assoc UK. 84(1):1–8. doi:10.1017/S0025315404008835h.

Giannoulaki M, Iglesias M, Tugores MP, Bonanno A, Patti B, De Felice A, Leonori I, Bigot JL, Tičina V, Pyrounaki MM, et al. 2013. Characterizing the potential habitat of European anchovy *Engraulis encrasicolus* in the Mediterranean Sea, at different life stages: *Habitat of anchovy in the Mediterranean*. Fish Oceanogr. 22(2):69–89. doi:10.1111/fog.12005.

Gilman E, Passfield K, Nakamura K. 2014. Performance of regional fisheries management organizations: ecosystem-based governance of bycatch and discards. Fish Fish. 15(2):327–351. doi:10.1111/faf.12021.

Giomi F, Barausse A, Duarte CM, Booth J, Agusti S, Saderne V, Anton A, Daffonchio D, Fusi M. 2019. Oxygen supersaturation protects coastal marine fauna from ocean warming. Sci Adv. 5(9):eaax1814. doi:10.1126/sciadv.aax1814.

Girondot M, Bédel S, Delmoitiez L, Russo M, Chevalier J, Guéry L, Ben Hassine S, Féon H, Jribi I. 2015. Spatio-temporal distribution of *Manta birostris* in French Guiana waters. J Mar Biol Assoc U K. 95(1):153–160. doi:10.1017/S0025315414001398.

Graham RT, Witt MJ, Castellanos DW, Remolina F, Maxwell S, Godley BJ, Hawkes LA. 2012. Satellite Tracking of Manta Rays Highlights Challenges to Their Conservation. Browman H, editor. PLoS ONE. 7(5):e36834. doi:10.1371/journal.pone.0036834.

Hacohen-Domené A, Martínez-Rincón RO, Galván-Magaña F, Cárdenas-Palomo N, Herrera-Silveira J. 2017. Environmental factors influencing aggregation of manta rays (*Manta birostris*) off the northeastern coast of the Yucatan Peninsula. Mar Ecol. 38(3):e12432. doi:10.1111/maec.12432.

Hahlbeck N, Scales KL, Dewar H, Maxwell SM, Bograd SJ, Hazen EL. 2017a. Oceanographic determinants of ocean sunfish (Mola mola) and bluefin tuna (Thunnus orientalis) bycatch patterns in the California large mesh drift gillnet fishery. Fish Res. 191:154–163. doi:10.1016/j.fishres.2017.03.011.

Hahlbeck N, Scales KL, Dewar H, Maxwell SM, Bograd SJ, Hazen EL. 2017b. Oceanographic determinants of ocean sunfish (Mola mola) and bluefin tuna (Thunnus orientalis) bycatch patterns in the California large mesh drift gillnet fishery. Fish Res. 191:154–163. doi:10.1016/j.fishres.2017.03.011.

Hall M, Roman M. 2013. Bycatch and non-tuna catch in the tropical tuna purse seine fisheries of the world. Rome, Italy: FAO FAO Fisheries and Aquaculture Technical Paper Report No.: 568. http://www.fao.org/3/i2743e/i2743e00.htm.

Harms NC, Lahajnar N, Gaye B, Rixen T, Dähnke K, Ankele M, Schwarz-Schampera U, Emeis K-C. 2019. Nutrient distribution and nitrogen and oxygen isotopic composition ofnitrate in water masses of the subtropical South Indian Ocean. Biogeochemistry: Open Ocean. [accessed 2021 Aug 1]. https://bg.copernicus.org/preprints/bg-2018-511/bg-2018-511.pdf.

Harris JL, McGregor PK, Oates Y, Stevens GMW. 2020. Gone with the wind: Seasonal distribution and habitat use by the reef manta ray (*Mobula alfredi*) in the Maldives, implications for conservation. Aquat Conserv Mar Freshw Ecosyst. 30(8):1649–1664. doi:10.1002/aqc.3350.

Hosegood J, Humble E, Ogden R, de Bruyn M, Creer S, Stevens GMW, Abudaya M, Bassos-Hull K, Bonfil R, Fernando D, et al. 2020. Phylogenomics and species delimitation for effective conservation of manta and devil rays. Mol Ecol. 29(24):4783–4796. doi:10.1111/mec.15683.

Hosegood PJ, Nimmo-Smith WAM, Proud R, Adams K, Brierley AS. 2019. Internal lee waves and baroclinic bores over a tropical seamount shark 'hot-spot.' Prog Oceanogr. 172:34–50. doi:10.1016/j.pocean.2019.01.010.

ICCAT. 2019. REPORT OF THE STANDING COMMITTEE ON RESEARCH AND STATISTICS (SCRS). Spain: ICCAT 2019 SCRS REPORT. https://www.iccat.int/Documents/Meetings/Docs/2019/REPORTS/2019_SCRS_ENG.pdf.

IOTC. 2019a. RESOLUTION 19/03 ON THE CONSERVATION OF MOBULID RAYS CAUGHT IN ASSOCIATION WITH FISHERIES IN THE IOTC AREA OF COMPETENCE. https://www.iotc.org/cmm/resolution-1903-conservation-mobulid-rays-caught-iin-association-fisheries-iotc-area-competence.

IOTC. 2019b. REGIONAL OBSERVER SCHEME – DRAFT PROGRAMME STANDARDS. https://www.iotc.org/documents/regional-observer-scheme-programme-standards.

IUCN. 2018a. Mobula mobular: Marshall, A., Barreto, R., Carlson, J., Fernando, D., Fordham, S., Francis, M.P., Herman, K., Jabado, R.W., Liu, K.M., Rigby, C.L. & Romanov, E.: The IUCN Red List of Threatened Species 2020: e.T110847130A176550858. doi:10.2305/IUCN.UK.2020-3.RLTS.T110847130A176550858.en. [accessed 2021 Aug 1]. https://www.iucnredlist.org/species/110847130/176550858.

IUCN. 2018b. Mobula alfredi: Marshall, A., Barreto, R., Carlson, J., Fernando, D., Fordham, S., Francis, M.P., Herman, K., Jabado, R.W., Liu, K.M., Pacoureau, N., Rigby, C.L., Romanov, E. & Sherley, R.B.: The IUCN Red List of Threatened Species 2019: e.T195459A68632178. doi:10.2305/IUCN.UK.2019-3.RLTS.T195459A68632178.en. [accessed 2021 Aug 1]. https://www.iucnredlist.org/species/195459/68632178.

IUCN. 2018c. Mobula thurstoni: Marshall, A., Barreto, R., Bigman, J.S., Carlson, J., Fernando, D., Fordham, S., Francis, M.P., Herman, K., Jabado, R.W., Liu, K.M., Pardo, S.A., Rigby, C.L., Romanov, E., Smith, W.D. & Walls, R.H.L.: The IUCN Red List of Threatened Species 2019: e.T60200A124451622. doi:10.2305/IUCN.UK.2019-3.RLTS.T60200A124451622.en. [accessed 2021 Aug 1]. https://www.iucnredlist.org/species/60200/124451622.

IUCN. 2018d. Mobula tarapacana: Marshall, A., Barreto, R., Bigman, J.S., Carlson, J., Fernando, D., Fordham, S., Francis, M.P., Herman, K., Jabado, R.W., Liu, K.M., Pardo, S.A., Rigby, C.L., Romanov, E. & Walls, R.H.L.: The IUCN Red List of Threatened Species 2019: e.T60199A124451161. doi:10.2305/IUCN.UK.2019-3.RLTS.T60199A124451161.en. [accessed 2021 Aug 1]. https://www.iucnredlist.org/species/60199/124451161.

IUCN. 2019. Mobula birostris: Marshall, A., Barreto, R., Carlson, J., Fernando, D., Fordham, S., Francis, M.P., Derrick, D., Herman, K., Jabado, R.W., Liu, K.M., Rigby, C.L. & Romanov, E.: The IUCN Red List of Threatened Species 2020: e.T198921A68632946. doi:10.2305/IUCN.UK.2020-3.RLTS.T198921A68632946.en. [accessed 2021 Aug 1]. https://www.iucnredlist.org/species/198921/68632946.

Jiménez-Valverde A, Lobo JM. 2007. Threshold criteria for conversion of probability of species presence to either–or presence–absence. Acta Oecologica. 31(3):361–369. doi:10.1016/j.actao.2007.02.001.

Juan-Jordá MJ, Murua H, Arrizabalaga H, Dulvy NK, Restrepo V. 2018. Report card on ecosystem-based fisheries management in tuna regional fisheries management organizations. Fish Fish. 19(2):321–339. doi:10.1111/faf.12256.

Lan K-W, Shimada T, Lee M-A, Su N-J, Chang Y. 2017. Using Remote-Sensing Environmental and Fishery Data to Map Potential Yellowfin Tuna Habitats in the Tropical Pacific Ocean. Remote Sens. 9(5):444. doi:10.3390/rs9050444.

Lawson JM, Fordham SV, O'Malley MP, Davidson LNK, Walls RHL, Heupel MR, Stevens G, Fernando D, Budziak A, Simpfendorfer CA, et al. 2017. Sympathy for the devil: a conservation strategy for devil and manta rays. :30.

Lewis SA, Setiasih N, Fahmi, Dharmadi D, O'Malley MP, Campbell SJ, Yusuf M, Sianipar AB. 2015. Assessing Indonesian manta and devil ray populations through historical landings and fishing community interviews. PeerJ Preprints. [accessed 2021 Aug 1]. https://peerj.com/preprints/1334v1.

Lezama-Ochoa N, Hall MA, Pennino MG, Stewart JD, López J, Murua H. 2019. Environmental characteristics associated with the presence of the Spinetail devil ray (Mobula mobular) in the eastern tropical Pacific. Kimirei IA, editor. PLOS ONE. 14(8):e0220854. doi:10.1371/journal.pone.0220854.

Lezama-Ochoa N, Lopez J, Hall M, Bach P, Abascal F, Murua H. 2020a. Spatio-temporal distribution of spinetail devil ray Mobula mobular in the eastern tropical Atlantic Ocean. Endanger Species Res. 43:447–460. doi:10.3354/esr01082.

Lezama-Ochoa N, Murua H, Chust G, Ruiz J, Chavance P, de Molina AD, Caballero A, Sancristobal I. 2015. Biodiversity in the by-catch communities of the pelagic ecosystem in the Western Indian Ocean. Biodivers Conserv. 24(11):2647–2671. doi:10.1007/s10531-015-0951-3.

Lezama-Ochoa N, Murua H, Chust G, Van Loon E, Ruiz J, Hall M, Chavance P, Delgado De Molina A, Villarino E. 2016. Present and Future Potential Habitat Distribution of Carcharhinus falciformis and Canthidermis maculata By-Catch Species in the Tropical Tuna Purse-Seine Fishery under Climate Change. Front Mar Sci. 3. doi:10.3389/fmars.2016.00034. [accessed 2021 Aug 1]. http://journal.frontiersin.org/Article/10.3389/fmars.2016.00034/abstract.

Lezama-Ochoa N, Pennino MG, Hall MA, Lopez J, Murua H. 2020b. Using a Bayesian modelling approach (INLA-SPDE) to predict the occurrence of the Spinetail Devil Ray (Mobular mobular). Sci Rep. 10(1):18822. doi:10.1038/s41598-020-73879-3.

Liao X, Du Y, Zhan H, Wang T, Feng M. 2017. Wintertime Phytoplankton Blooms in the Western Equatorial Indian Ocean Associated With the Madden-Julian Oscillation. J Geophys Res Oceans. 122(12):9855–9869. doi:10.1002/2017JC013203.

Liu C, Berry PM, Dawson TP, Pearson RG. 2005. Selecting thresholds of occurrence in the prediction of species distributions. Ecography. 28(3):385–393. doi:10.1111/j.0906-7590.2005.03957.x.

Lopez J, Alvarez-Berastegui D, Soto M, Murua H. 2020. Using fisheries data to model the oceanic habitats of juvenile silky shark (Carcharhinus falciformis) in the tropical eastern Atlantic Ocean. Biodivers Conserv. 29(7):2377–2397. doi:10.1007/s10531-020-01979-7.

Mandrekar JN. 2010. Receiver Operating Characteristic Curve in Diagnostic Test Assessment. J Thorac Oncol. 5(9):1315–1316. doi:10.1097/JTO.0b013e3181ec173d.

Mannocci L, Forget F, Tolotti MT, Bach P, Bez N, Demarcq H, Kaplan D, Sabarros P, Simier M, Capello M, et al. 2020. Predicting bycatch hotspots in tropical tuna purse seine fisheries at the basin scale. Glob Ecol Conserv. 24:e01393. doi:10.1016/j.gecco.2020.e01393.

Martin S. 2020. A review of mobulid ray interactions with fisheries for tuna and tuna-like species in the Indian Ocean. https://www.iotc.org/documents/WPEB/16/19.

Martinez-Rincon RO, Ortega-Garcia S, Vaca-Rodriguez JG, Griffiths SP. 2015. Development of habitat prediction models to reduce by-catch of sailfish (Istiophorus platypterus) within the purse-seine fishery in the eastern Pacific Ocean | Bycatch Management Information System (BMIS). http://dx.doi.org/101071/MF14062. [accessed 2021 Jul 5]. https://www.bmis-bycatch.org/references/8amrfh9t.

Martiny AC, Lomas MW, Fu W, Boyd PW, Chen YL, Cutter GA, Ellwood MJ, Furuya K, Hashihama F, Kanda J, et al. 2019. Biogeochemical controls of surface ocean phosphate. Sci Adv. 5(8):eaax0341. doi:10.1126/sciadv.aax0341.

Maufroy A, Gamon A, Vernet A-L, Goujon M. 2020. 8 YEARS OF BEST PRACTICES ONBOARD FRENCH AND ASSOCIATED FLAGS TROPICAL TUNA PURSE SEINERS: AN OVERVIEW IN THE ATLANTIC AND INDIAN OCEANS.

McKinney R, Gibbon J, Wozniak E, Galland G. 2020. Netting Billions 2020: A Global Tuna Valuation. Washington, D.C.: The Pew Charitable Trusts. https://www.pewtrusts.org/en/research-and-analysis/reports/2020/10/netting-billions-2020-a-global-tuna-valuation.

Mendonça SA, Macena BCL, Afonso AS, Hazin FHV. 2018. Seasonal aggregation and diel activity by the sicklefin devil ray *MOBULA TARAPACANA* off a small, equatorial outcrop of the Mid-Atlantic Ridge. J Fish Biol. 93(6):1121–1129. doi:10.1111/jfb.13829.

Meng L, Zhuang W, Zhang W, Yan C, Yan X. 2020. Variability of the Shallow Overturning Circulation in the Indian Ocean. J Geophys Res Oceans. 125(2). doi:10.1029/2019JC015651. [accessed 2021 Aug 2]. https://onlinelibrary.wiley.com/doi/10.1029/2019JC015651.

Miller DL, Wood SN. 2014. Finite area smoothing with generalized distance splines. Environ Ecol Stat. 21(4):715–731. doi:10.1007/s10651-014-0277-4.

Moazzam M. 2018. Unprecedented decline in the catches of mobulids: an important component of tuna gillnet fisheries of the Northern Arabian Sea. :7.

Montero JT, Martinez-Rincon RO, Heppell SS, Hall M, Ewal M. 2016. Characterizing environmental and spatial variables associated with the incidental catch of olive ridley (*Lepidochelys olivacea*) in the Eastern Tropical Pacific purse-seine fishery. Fish Oceanogr. 25(1):1–14. doi:10.1111/fog.12130.

Murua H, Fiorellato F, Ruiz J, Chassot E, Restrepo V. 2020. Minimum standards for designing and implementing Electronic Monitoring systems in Indian Ocean tuna fisheries. https://www.iotc.org/documents/SC/23/12E.

Naimi B. 2017. R: Uncertainty analysis for SDMs. [accessed 2021 Aug 2]. https://search.r-project.org/CRAN/refmans/usdm/html/usdm-package.html.

Navarro M, Hailu A, Langlois T, Ryan KL, Kragt ME. 2020. Determining spatial patterns in recreational catch data: a comparison of generalized additive mixed models and boosted regression trees. Hyder K, editor. ICES J Mar Sci. 77(6):2216–2225. doi:10.1093/icesjms/fsz123.

O'Malley M p., Townsend KA, Hilton P, Heinrichs S, Stewart JD. 2017. Characterization of the trade in manta and devil ray gill plates in China and South-east Asia through trader surveys: The Manta and Devil Ray Gill Plate Trade. Aquat Conserv Mar Freshw Ecosyst. 27(2):394–413. doi:10.1002/aqc.2670.

Orue B, Lopez J, Pennino MG, Moreno G, Santiago J, Murua H. 2020. Comparing the distribution of tropical tuna associated with drifting fish aggregating devices (DFADs) resulting from catch dependent and independent data. Deep Sea Res Part II Top Stud Oceanogr. 175:104747. doi:10.1016/j.dsr2.2020.104747.

Oyafuso ZackS, Drazen JC, Moore CH, Franklin EC. 2017. Habitat-based species distribution modelling of the Hawaiian deepwater snapper-grouper complex. Fish Res. 195:19–27. doi:10.1016/j.fishres.2017.06.011.

Palacios MD, Hoyos-Padilla EM, Trejo-Ramírez A, Croll DA, Galván-Magaña F, Zilliacus KM, O'Sullivan JB, Ketchum JT, González-Armas R. 2021. Description of first nursery area for a pygmy devil ray species (Mobula munkiana) in the Gulf of California, Mexico. Sci Rep. 11(1):132. doi:10.1038/s41598-020-80506-8.

Pearson RG. 2010. Species' Distribution Modeling for Conservation Educators and Practitioners. Lessons Conserv. 3:54–89.

Peel LR, Stevens GMW, Daly R, Keating Daly CA, Collin SP, Nogués J, Meekan MG. 2020. Regional Movements of Reef Manta Rays (Mobula alfredi) in Seychelles Waters. Front Mar Sci. 7:558. doi:10.3389/fmars.2020.00558.

Pennino MG, Conesa D, López-Quílez A, Muñoz F, Fernández A, Bellido JM. 2016. Fishery-dependent and -independent data lead to consistent estimations of essential habitats. ICES J Mar Sci. 73(9):2302–2310. doi:10.1093/icesjms/fsw062.

Poisson F, Vernet AL, Séret B, Dagorn L. 2012. Good practices to reduce the mortality of sharks and rays caught incidentally by tropical tuna purse seiners. http://ebfmtuna-2012.sciencesconf.org/conference/ebfmtuna-2012/pages/D6.2_Practices_to_reduce_shark_mortality_purse_seiners.pdf.

Prasanna Kumar S, Narvekar J, Nuncio M, Gauns M, Sardesai S. 2009. What drives the biological productivity of the northern Indian Ocean? In: Wiggert JD, Hood RR, Naqvi SWA, Brink KH, Smith SL, editors. Geophysical Monograph Series. Vol. 185. Washington, D. C.: American Geophysical Union. p. 33–56. [accessed 2021 Aug 1]. https://onlinelibrary.wiley.com/doi/10.1029/2008GM000757.

Putri A, Zainuddin M. 2019. Application of remotely sensed satellite data to identify Skipjack Tuna distributions and abundance in the coastal waters of Bone Gulf. IOP Conf Ser Earth Environ Sci. 241:012012. doi:10.1088/1755-1315/241/1/012012.

R Core Team. 2020. R: A Language and Environment for Statistical Computing. Vienna, Austria: R Foundation for Statistical Computing. [accessed 2021 Aug 2]. https://www.r-project.org/.

Richardson AJ, Downes KJ, Nolan ET, Brickle P, Brown J, Weber N, Weber SB. 2018. Residency and reproductive status of yellowfin tuna in a proposed large-scale pelagic marine protected area. Aquat Conserv Mar Freshw Ecosyst. 28(6):1308–1316. doi:10.1002/aqc.2936.

Rohner C, Pierce S, Marshall A, Weeks S, Bennett M, Richardson A. 2013. Trends in sightings and environmental influences on a coastal aggregation of manta rays and whale sharks. Mar Ecol Prog Ser. 482:153–168. doi:10.3354/meps10290.

Rohner CA, Burgess KB, Rambahiniarison JM, Stewart JD, Ponzo A, Richardson AJ. 2017a. Mobulid rays feed on euphausiids in the Bohol Sea. R Soc Open Sci. 4(5):161060. doi:10.1098/rsos.161060.

Rohner CA, Flam AL, Pierce SJ, Marshall AD. 2017b. Steep declines in sightings of manta rays and devilrays (Mobulidae) in southern Mozambique. PeerJ Preprints. [accessed 2021 Aug 1]. https://peerj.com/preprints/3051v1.

Ruiz J, Abascal FJ, Bach P, Baez JC, Cauquil P, Grande M, Lucas J, Murua H, Alonso MLR, Sabarros PS. 2018. BYCATCH OF THE EUROPEAN, AND ASSOCATED FLAG, PURSE-SEINE TUNA FISHERY IN THE INDIAN OCEAN FOR THE PERIOD 2008-2017. IOTC. IOTC-2018-WPEB14-15:15.

Ruiz J, Batty A, Chavance P, McElderry H, Restrepo V, Sharples P, Santos J, Urtizberea A. 2015. Electronic monitoring trials on in the tropical tuna purse-seine fishery. ICES J Mar Sci. 72(4):1201–1213. doi:10.1093/icesjms/fsu224.

Schott FA, McCreary JP. 2001. The monsoon circulation of the Indian Ocean. Prog Oceanogr. 51(1):1–123. doi:10.1016/S0079-6611(01)00083-0.

Schott FA, Xie S-P, McCreary JP. 2009. Indian Ocean circulation and climate variability. Rev Geophys. 47(1):RG1002. doi:10.1029/2007RG000245.

Sequeira AMM, Mellin C, Fordham DA, Meekan MG, Bradshaw CJA. 2014. Predicting current and future global distributions of whale sharks. Glob Change Biol. 20(3):778–789. doi:10.1111/gcb.12343.

Shahid U, Moazzam M, Kiszka JJ, Fernando D, Rambahiniarison J, Harvey A, Rosady V, Cornish AS. 2018. Shahid et al., 2018 (IOTC).pdf. https://www.iotc.org/documents/regional-perspective-mobulid-ray-interactions-surface-fisheries-indian-ocean.

Somavilla R, González-Pola C, Fernández-Diaz J. 2017. The warmer the ocean surface, the shallower the mixed layer. H ow much of this is true? J Geophys Res Oceans. 122(9):7698–7716. doi:10.1002/2017JC013125.

Song H, Long MC, Gaube P, Frenger I, Marshall J, McGillicuddy DJ. 2018. Seasonal Variation in the Correlation Between Anomalies of Sea Level and Chlorophyll in the Antarctic Circumpolar Current. Geophys Res Lett. 45(10):5011–5019. doi:10.1029/2017GL076246.

Sospedra J, Niencheski LFH, Falco S, Andrade CFF, Attisano KK, Rodilla M. 2018. Identifying the main sources of silicate in coastal waters of the Southern Gulf of Valencia (Western Mediterranean Sea). Oceanologia. 60(1):52–64. doi:10.1016/j.oceano.2017.07.004.

Stellema A, Sen Gupta A, Taschetto AS. 2019. Projected slow down of South Indian Ocean circulation. Sci Rep. 9(1):17705. doi:10.1038/s41598-019-54092-3.

Stevens GMW, Hawkins JP, Roberts CM. 2018. Courtship and mating behaviour of manta rays *Mobula alfredi* and *M. BIROSTRIS* in the Maldives. J Fish Biol. 93(2):344–359. doi:10.1111/jfb.13768.

Stewart JD, Jaine FRA, Armstrong AJ, Armstrong AO, Bennett MB, Burgess KB, Couturier LIE, Croll DA, Cronin MR, Deakos MH, et al. 2018. Research Priorities to Support Effective Manta and Devil Ray Conservation. Front Mar Sci. 5:314. doi:10.3389/fmars.2018.00314.

Stock BC, Ward EJ, Eguchi T, Jannot JE, Thorson JT, Feist BE, Semmens BX. 2020. Comparing predictions of fisheries bycatch using multiple spatiotemporal species distribution model frameworks. Can J Fish Aquat Sci. 77(1):146–163. doi:10.1139/cjfas-2018-0281.

Stock BC, Ward EJ, Thorson JT, Jannot JE, Semmens BX. 2019. The utility of spatial model-based estimators of unobserved bycatch. Anderson E, editor. ICES J Mar Sci. 76(1):255–267. doi:10.1093/icesjms/fsy153.

Swimmer Y, Zollett E, Gutierrez A. 2020. Bycatch mitigation of protected and threatened species in tuna purse seine and longline fisheries. Endanger Species Res. 43:517–542. doi:10.3354/esr01069.

Temple AJ, Wambiji N, Poonian CNS, Jiddawi N, Stead SM, Kiszka JJ, Berggren P. 2019. Marine megafauna catch in southwestern Indian Ocean small-scale fisheries from landings data. Biol Conserv. 230:113–121. doi:10.1016/j.biocon.2018.12.024.

Thorne LH, Baird RW, Webster DL, Stepanuk JE, Read AJ. 2019. Predicting fisheries bycatch: A case study and field test for pilot whales in a pelagic longline fishery. Embling C, editor. Divers Distrib. 25(6):909–923. doi:10.1111/ddi.12912.

Thovyan AI, Tapilatu RF, Sabariah V. 2020. Plankton abundance and community structure in reef manta ray (Mobula alfredi) feeding habitat in the Dampier Strait, Raja Ampat, West Papua, Indonesia. 13(5):15.

Velasco J, Gutiérrez-Cánovas C, Botella-Cruz M, Sánchez-Fernández D, Arribas P, Carbonell JA, Millán A, Pallarés S. 2019. Effects of salinity changes on aquatic organisms in a multiple stressor context. Philos Trans R Soc B Biol Sci. 374(1764):20180011. doi:10.1098/rstb.2018.0011.

Venables SK, Duinkerken DI van, Rohner CA, Marshall AD. 2020. Habitat use and movement patterns of reef manta rays Mobula alfredi in southern Mozambique. Mar Ecol Prog Ser. 634:99–114. doi:10.3354/meps13178.

Villarino E, Chust G, Licandro P, Butenschön M, Ibaibarriaga L, Larrañaga A, Irigoien X. 2015. Modelling the future biogeography of North Atlantic zooplankton communities in response to climate change. Mar Ecol Prog Ser. 531:121–142. doi:10.3354/meps11299.

Vinayachandran PNM, Masumoto Y, Roberts M, Hugget J, Halo I, Chatterjee A, Amol P, Gupta GVM, Singh A, Mukherjee A, et al. 2021. Reviews and syntheses: Physical and biogeochemical processes associated with

upwelling in the Indian Ocean. Biogeochemistry: Coastal Ocean. [accessed 2021 Aug 1]. https://bg.copernicus.org/preprints/bg-2020-486/.

Vonnahme TR, Leroy M, Thoms S, van Oevelen D, Harvey HR, Kristiansen S, Gradinger R, Dietrich U, Völker C. 2021. Modeling silicate–nitrate–ammonium co-limitation of algal growth and the importance of bacterial remineralization based on an experimental Arctic coastal spring bloom culture study. Biogeosciences. 18(5):1719–1747. doi:10.5194/bg-18-1719-2021.

Ward-Paige CA, Davis B, Worm B. 2013. Global Population Trends and Human Use Patterns of Manta and Mobula Rays. Stergiou KI, editor. PLoS ONE. 8(9):e74835. doi:10.1371/journal.pone.0074835.

White WT, Corrigan S, Yang L, Henderson AC, Bazinet AL, Swofford DL, Naylor GJP. 2018. Phylogeny of the manta and devilrays (Chondrichthyes: mobulidae), with an updated taxonomic arrangement for the family. Zool J Linn Soc. 182(1):50–75. doi:10.1093/zoolinnean/zlx018.

Wood S. 2021. Mixed GAM Computation Vehicle with Automatic Smoothness Estimation. CRAN.

Wood SN. 2017. Generalized Additive Models An Introduction with R. 2nd ed. US: Chapman and Hall/CRC.

Woodson CB, Litvin SY. 2015. Ocean fronts drive marine fishery production and biogeochemical cycling. Proc Natl Acad Sci. 112(6):1710–1715. doi:10.1073/pnas.1417143112.

Supplementary Materials

Table S 1 Combination of variable sets subjected to forward variable selection and the final variable selection. The final variables ($p < 0.05$) selected for each candidate model are listed in column 3 for devil rays and column 5 for spinetail devil ray. Corresponding Akaike information criterion (AIC) is provided.

Model	Variables*	Devil Rays	AIC	Spinetail devil ray	AIC
1	Chl, Ke	Type, (Longitude x Latitude), Week, Chl, SSH, Tuna, SSTfronts	3658	Type + (Longitude x Latitude) + Tuna + Chl + SSTfronts	1433
2	NPPV, Ke	Type, (Longitude x Latitude), Week, NPPV, SSH, Tuna, SSTfronts	3661	Type + (Longitude x Latitude) + Tuna + NPPV, SSTfronts	1429
3	SST, NO3, Ke	Type, (Longitude x Latitude), Week, SST, Tuna, SSTfronts	3658	Type, SST, Tuna, Week, SSTfronts	1434
4	O2, NO3, Ke	Type + (Longitude x Latitude), Week, O2, SSH, Tuna, SSTfronts	3663	Type + (Longitude x Latitude) + Tuna + O2 + SSTfronts	1430
5	Chl, Vel	Same as 1	3658	Same as 1	
6	NPPV, Vel	Same as 2	3661	Same as 2	
7	SST, NO3, Vel	Same as 3	3658	Same as 3	
8	O2, NO3, Vel	Same as 4	3663	Same as 4	

*Variables Type, Year, Week, Longitude, Latitude, Sunrise, Chlfronts, PO4, Si, MLD, SSTfronts, SSH, Heading, Tuna are other variables subjected to model selection

Table S 2 Final candidate Generalized Additive Models (GAMs) for devil rays with the corresponding Akaike Information Criteria (AIC) values and the variables selected for each model. The piece-wise construction of the best model with each new variable improving the AIC value is also shown.

Variables	AIC
Longitude x Latitude	3815
Longitude x Latitude + Type	3734
Longitude x Latitude + Type + Week	3698
Longitude x Latitude + Type + Week + SSH	3682
Longitude x Latitude + Type + Week + SSH + Chl	3671
Longitude x Latitude + Type + Week + SSH + Chl + SSTfronts	3666
Longitude x Latitude + Type + Week + SSH + Chl + SSTfronts + Tuna	3659

Table S 3 Final candidate Generalized Additive Models (GAMs) for spinetail devil ray with the corresponding Akaike Information Criteria (AIC) values and the variables selected for each model. The piece-wise construction of the best model with each new variable improving the AIC value.

Variables	AIC
Longitude x Latitude	1487
Longitude x Latitude + Type	1450
Longitude x Latitude + Type+ NPPV	1438
Longitude x Latitude + Type+ NPPV+SST fronts	1436
Longitude x Latitude + Type+ NPPV+SST fronts + Tuna	1429

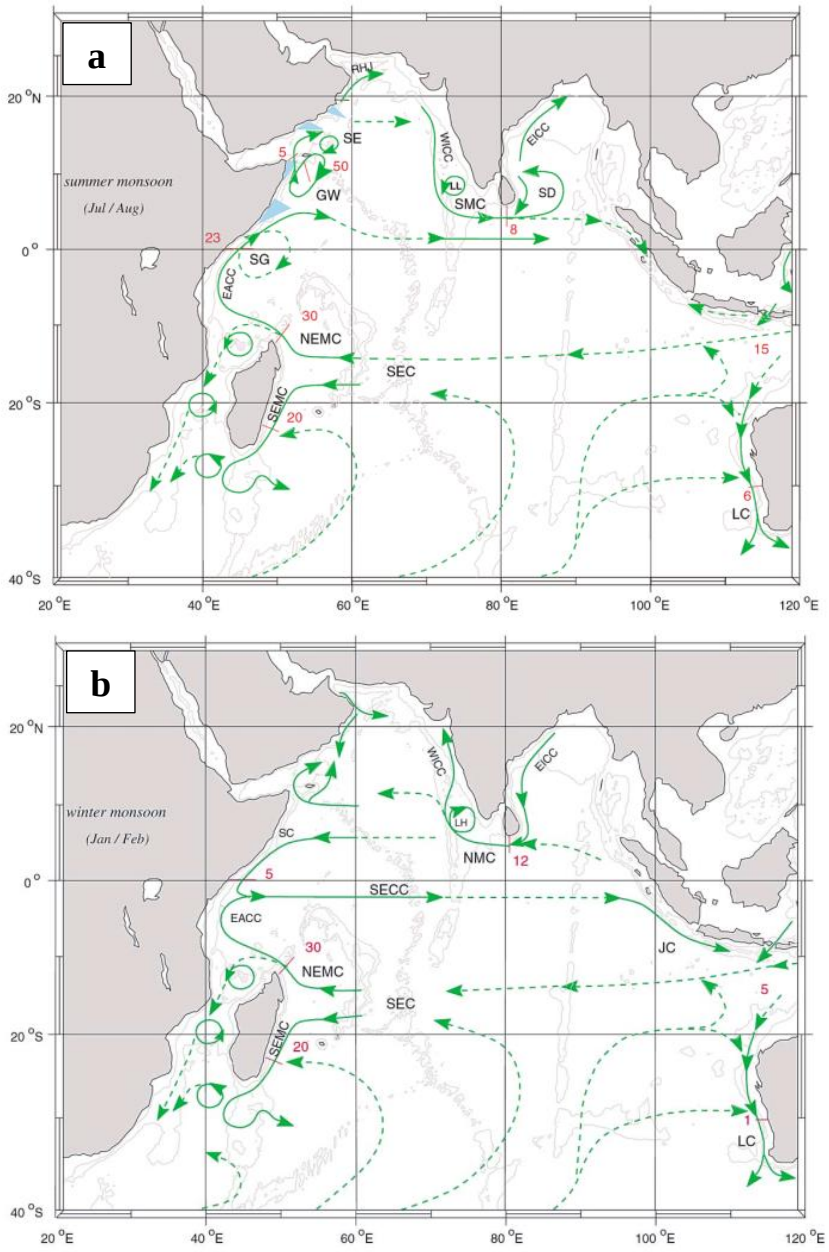

Figure S 1 Schematic representation of main circulation patterns in the Indian Ocean, including current branches and some choke point transport numbers (Sv=106m3s1). a) summer monsoon, b) winter monsoon. Current branches shown include the South Equatorial Current (SEC), South Equatorial Countercurrent (SECC), Northeast and Southeast Madagascar Current (NEMC and SEMC), East African Coast Current (EACC), Somali Current (SC), Southern Gyre (SG) and Great Whirl (GW) and associated upwelling wedges, Socotra Eddy (SE), Ras al Hadd Jet (RHJ) and upwelling wedges off Oman, West Indian Coast Current (WICC), Laccadive High and Low (LH and LL), East Indian Coast Current (EICC), Southwest and Northeast Monsoon Current (SMC and NMC), South Java Current (JC) and Leeuwin Current (LC). Source: (Schott et al. 2001; Schott et al. 2009)

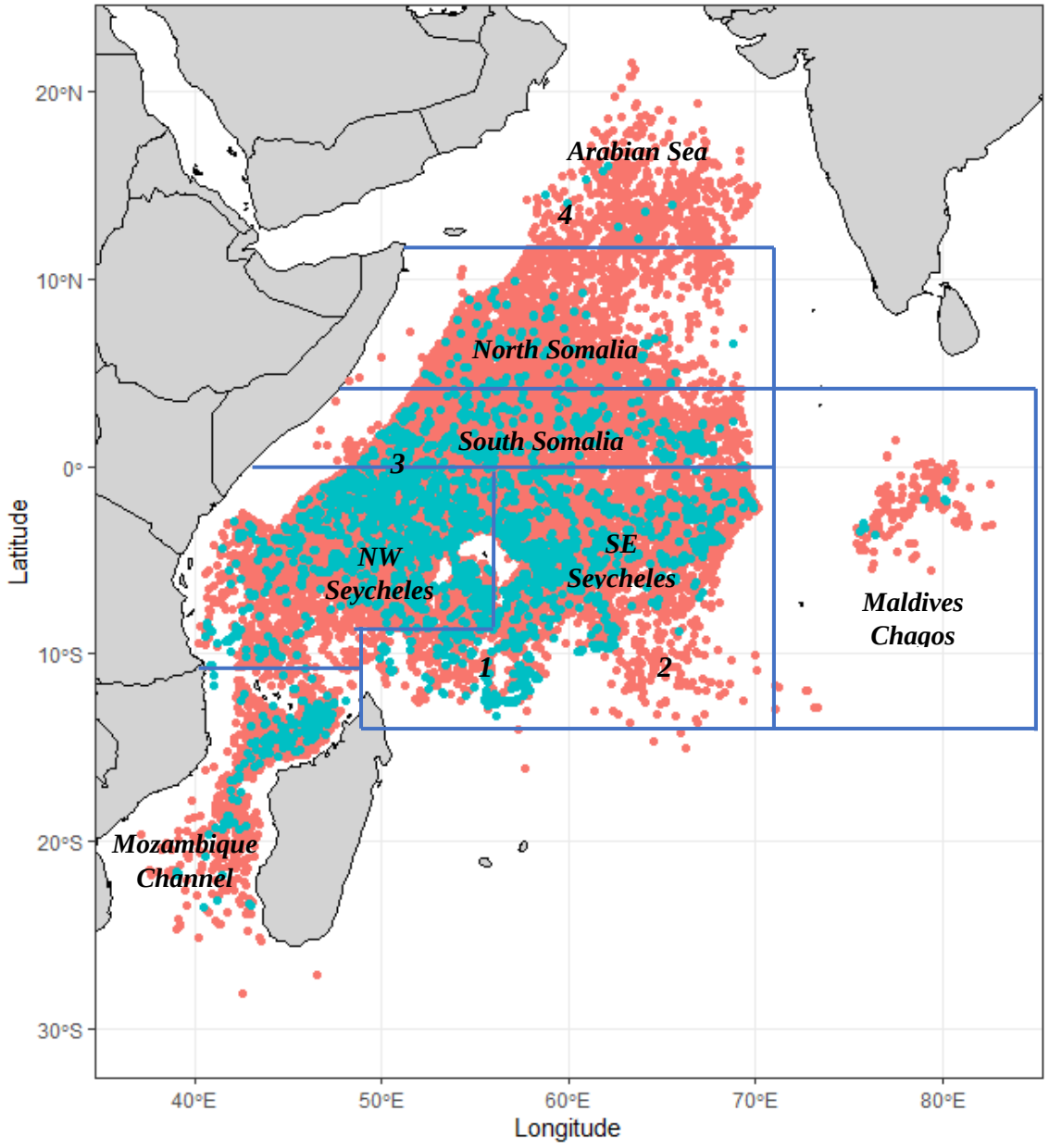

Figure S 2 Spatial distribution of the observed fishing sets of the EU tropical tuna purse seine fishery in the Western Indian Ocean between 2010 and 2020 and delineation of the main fishing areas. The partitioning of the fishing areas (blue rectangles) was derived from Lezama et al., 2015 with minor modifications. The observed sets are coloured by major fishing types with sets on Free School sets (FSC) in *skyblue points* and sets on fish aggregating devices (FADs) in *pink points*.

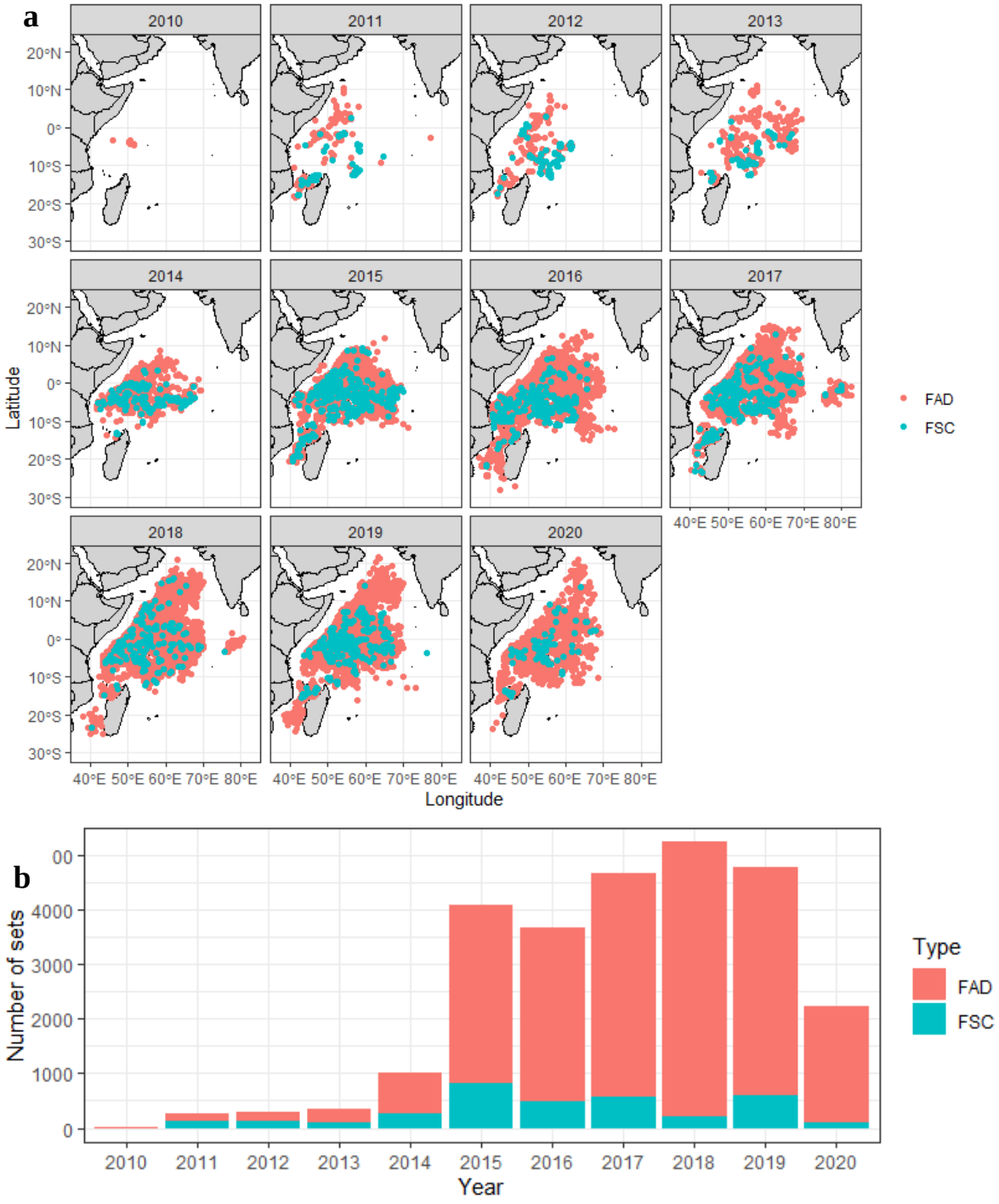

Figure S 3 Spatial and temporal distribution of the observed fishing sets in the EU tropical tuna purse seine fishery in the Western Indian Ocean between 2010 and 2020. a) Spatial distribution of observed sets across over time. b) Total number of sets observed over time. Fishing operations using sets associated to fish aggregation devices (FAD) (pink) and sets associated to free swimming schools of tunas (FSC) (skyblue).

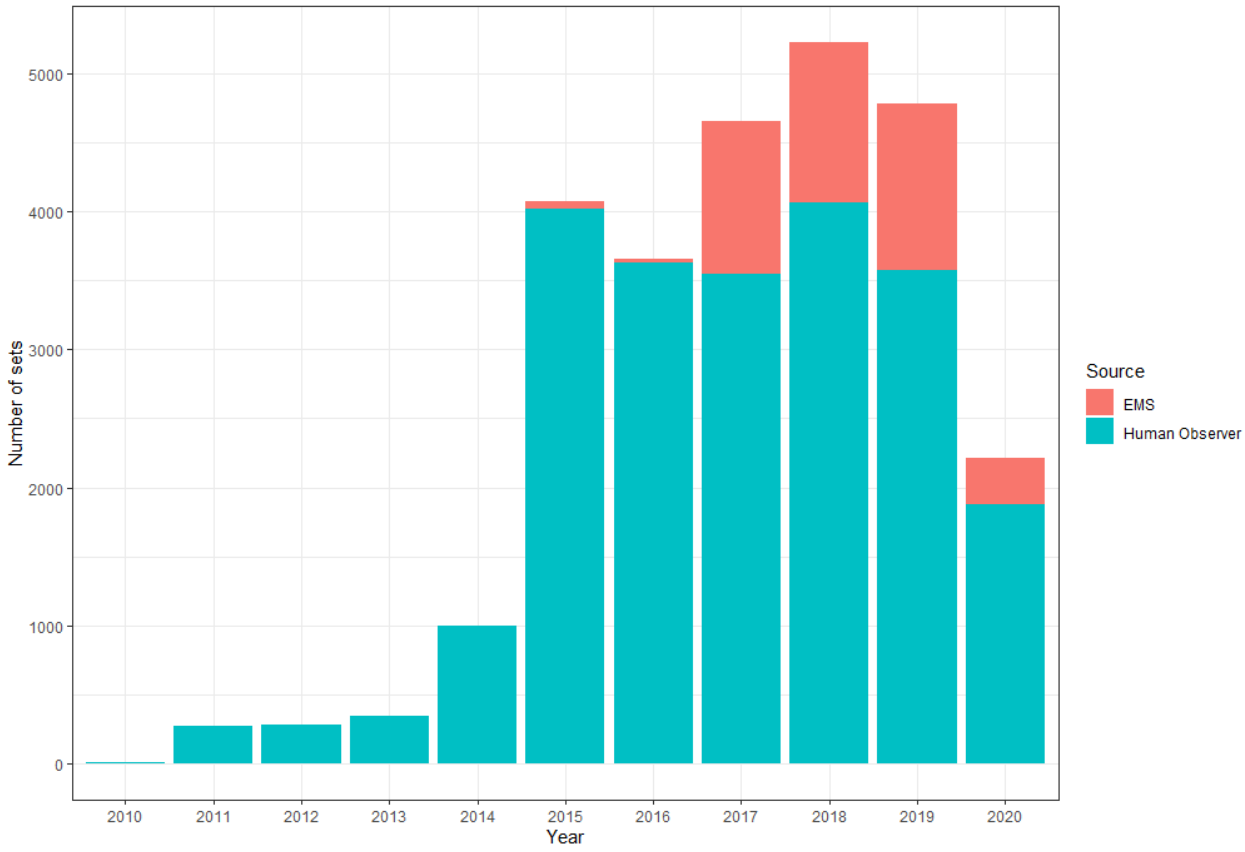

Figure S 4 Total number of observed fishing sets in the EU tropical tuna purse seine fishery in the Western Indian Ocean between 2010 and 2020 and the main source of data collection. Observer data is collected either with electronic monitoring systems (EMSs) or human observers.

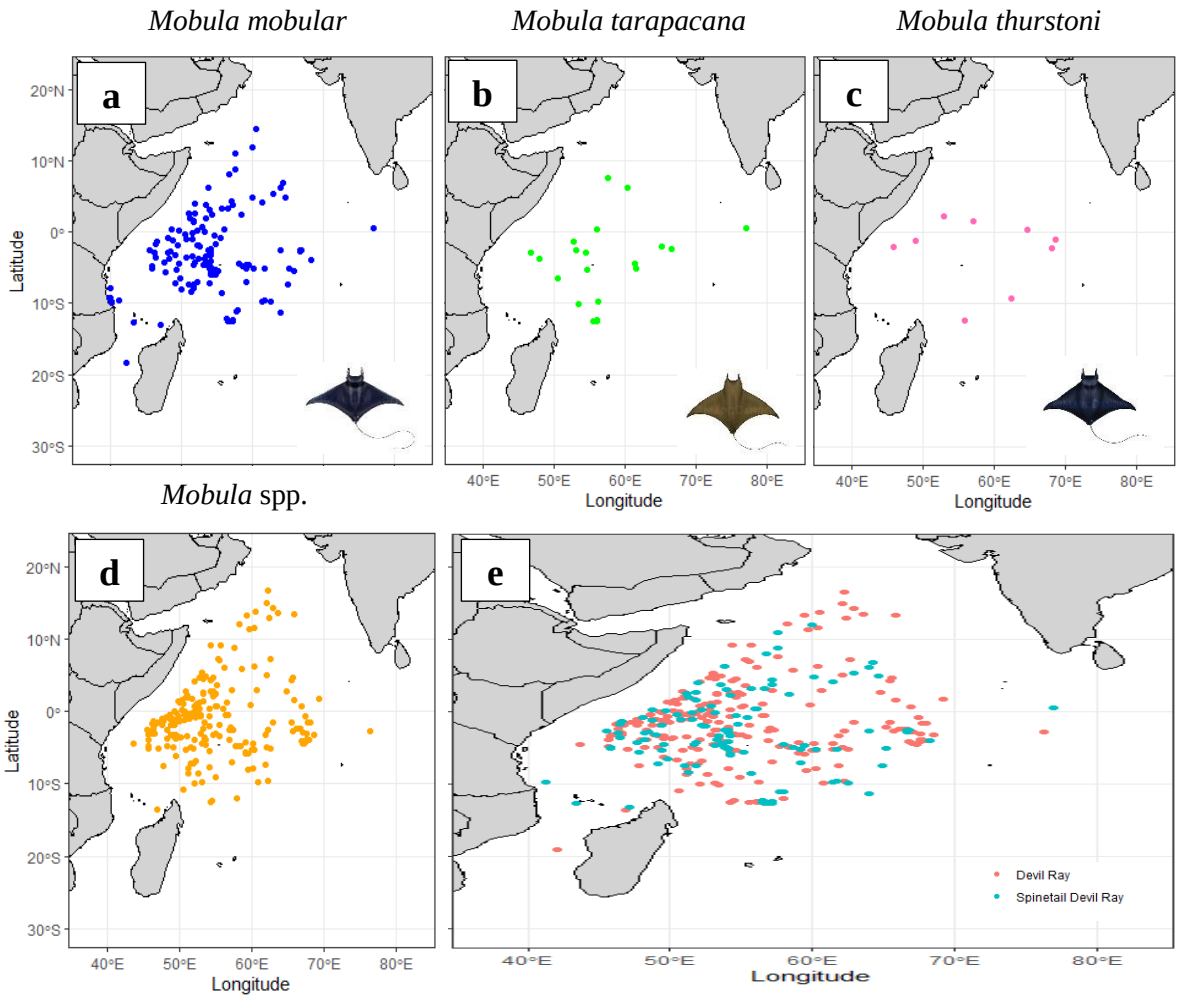

Figure S 5 Spatial distribution of presences of several species of devil rays in the EU tropical tuna purse seine fisheries in the Western Indian Ocean between 2010 and 2020. a) presences of Spinetail devil ray *Mobula mobular*, b. presences of Sicklefin devil ray *Mobula tarapacana*, c. presences of Bentfin devil ray name *Mobula thurstoni*, d. presences of devil rays identified to the genus level. e. presences of *Mobula mobular* (sky blue) and presences of rest of species and individuals identified to the genus level (in pink). Photos of devil ray are from Manta Trust.

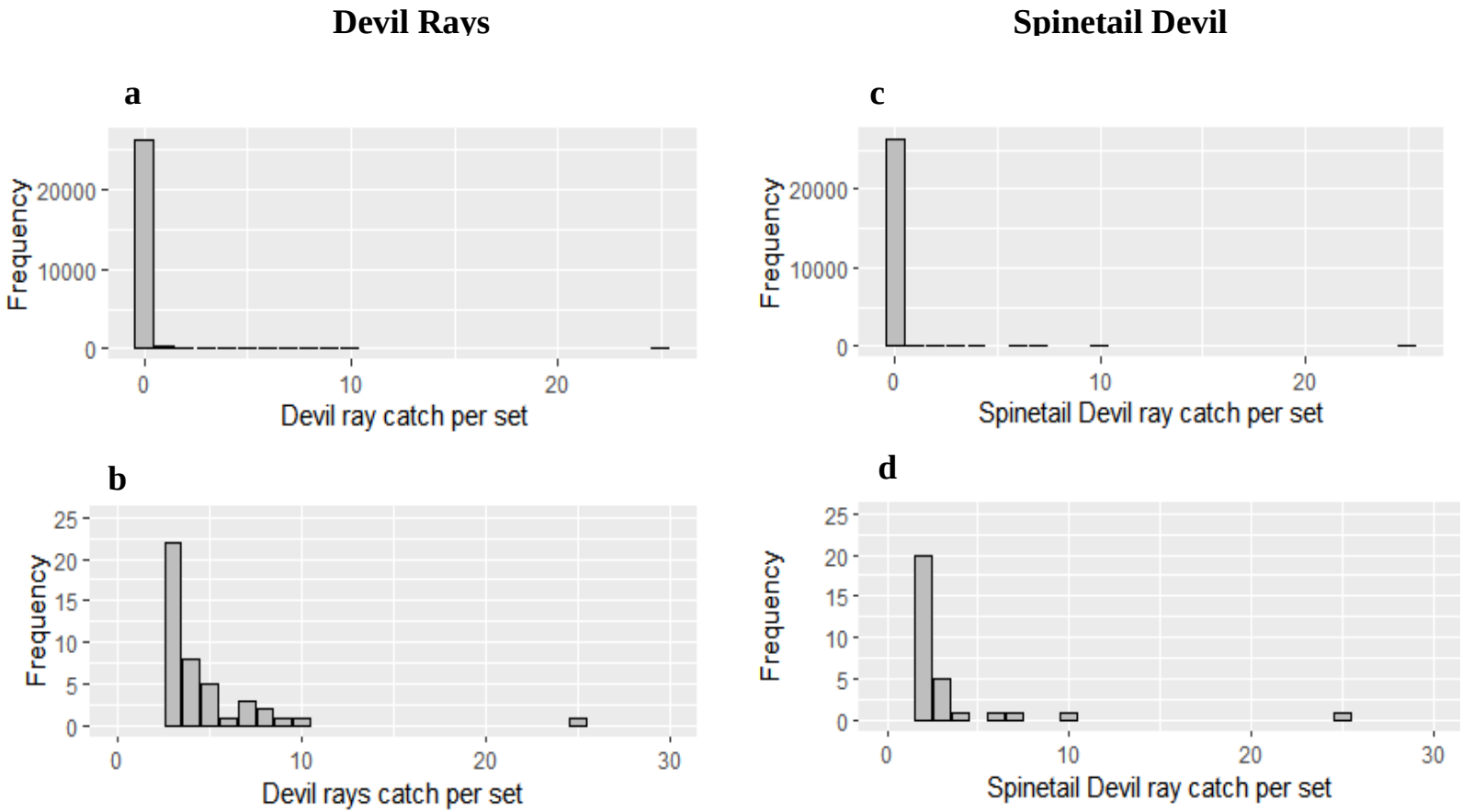

Figure S 6 The distribution of the number of devil rays captured per fishing set in the EU tropical tuna purse seine fishery in the Western Indian Ocean between 2010 and 2020. a) The distribution of the number of devil rays captured including the sets with zero catches. b) The distribution of the number of devil rays captured excluding the sets with zero catches. c) The distribution of the number of spinetail devil rays (*Mobula mobular*) captured including the sets with zero catches. d) The distribution of the number of spinetail devil rays (*Mobula mobular*) captured excluding the sets with zero catches.

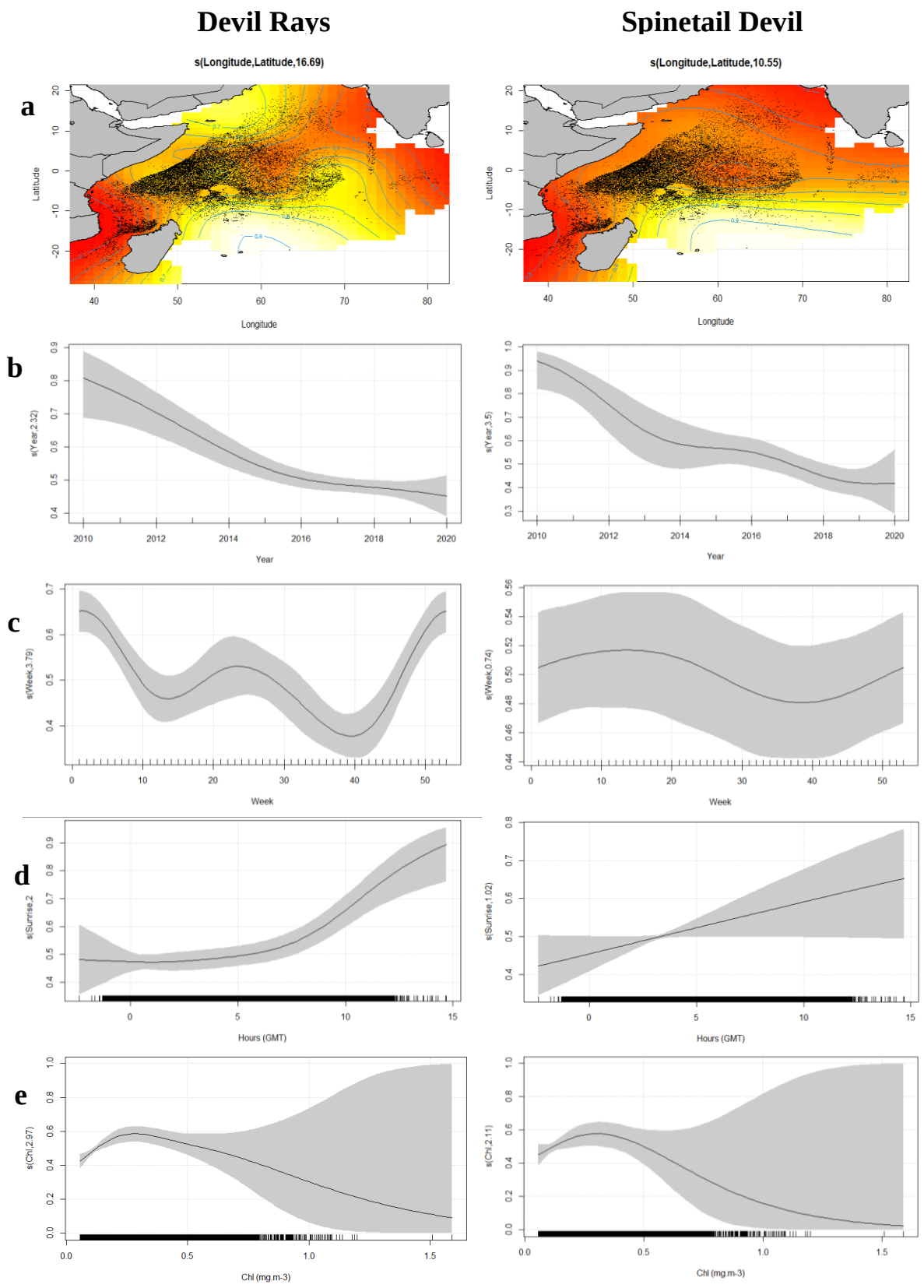

Figure S 7 Univariate smooth fits of covariates from modelling the presence of devil rays in the left column and spinetail devil ray in the right column. a) Interaction term of Latitude and Longitude, b) Year, c) Week, d) Hours from Sunrise (hours GMT), e) Chlorophyll (mmol.m^{-3}).

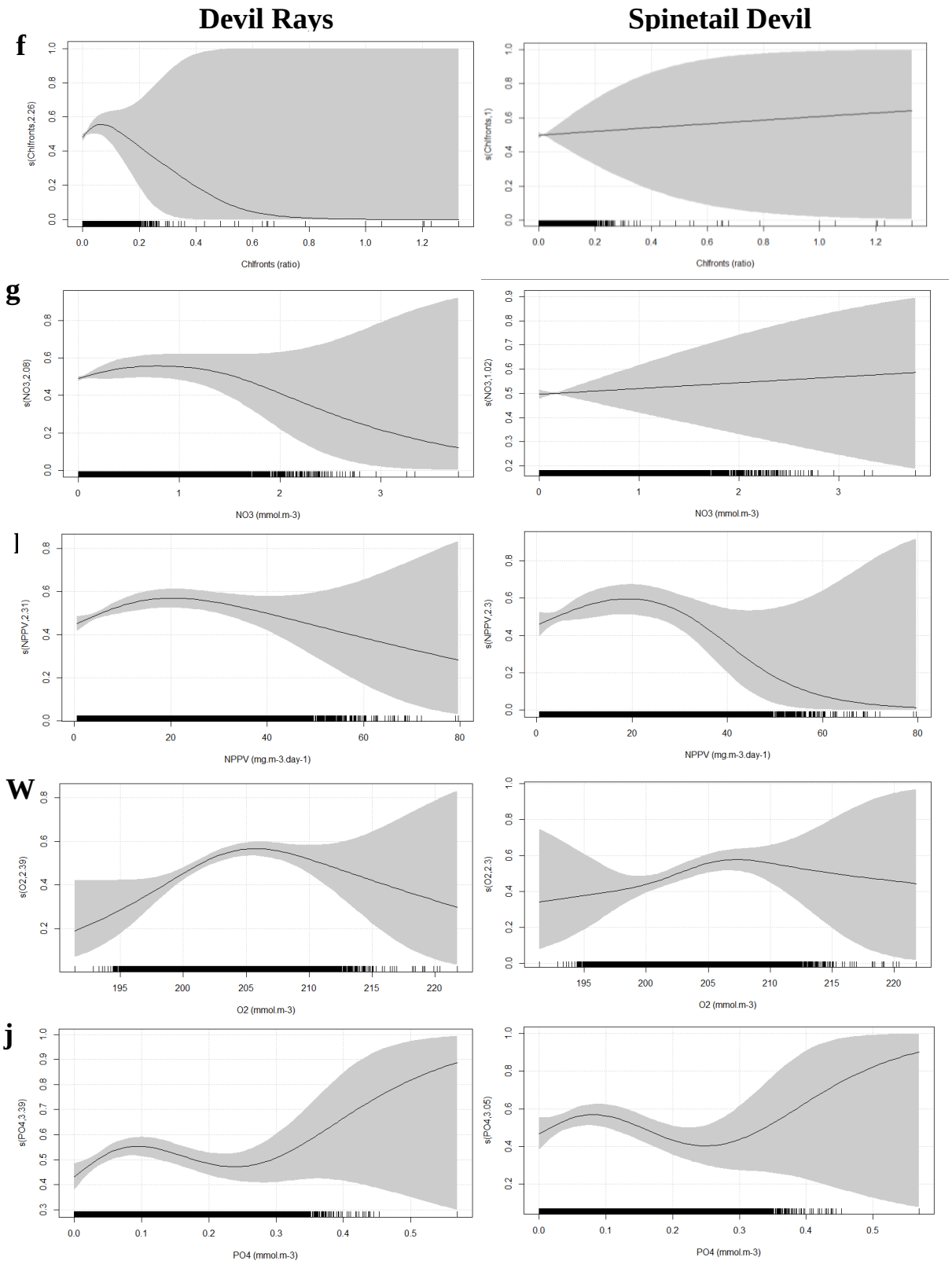

Figure S7 1 Univariate smooth fits of covariates from modelling the presence of devil rays in the left column and spinetail devil ray in the right column. f) Chlorophyll fronts (ratio), g) nitrate (mmol. m-3), h) net primary productivity (mg. m-3 day-1), We) Oxygen (mmol m-3), j) Phosphate (mmol m-3)

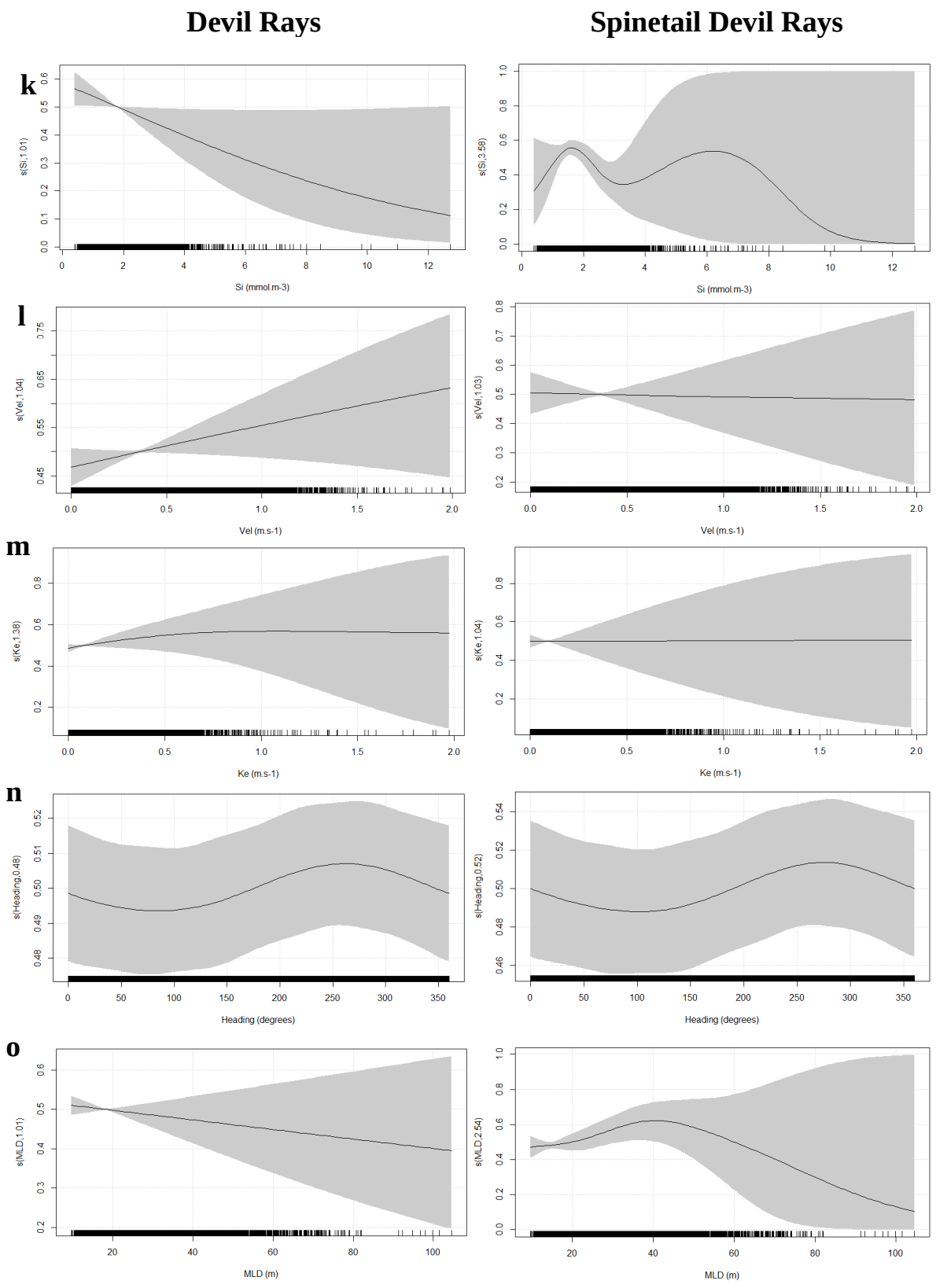

Figure S7 2 Univariate smooth fits of covariates from modelling the presence of devil rays in the left column and spinetail devil ray in the right column. k) Silicate (mmol m-3), l) current velocity ($m.s^{-1}$), m) eddy kinetic energy ($m.s^{-1}$), n) current heading (degrees), o) Mix layer depth (m).

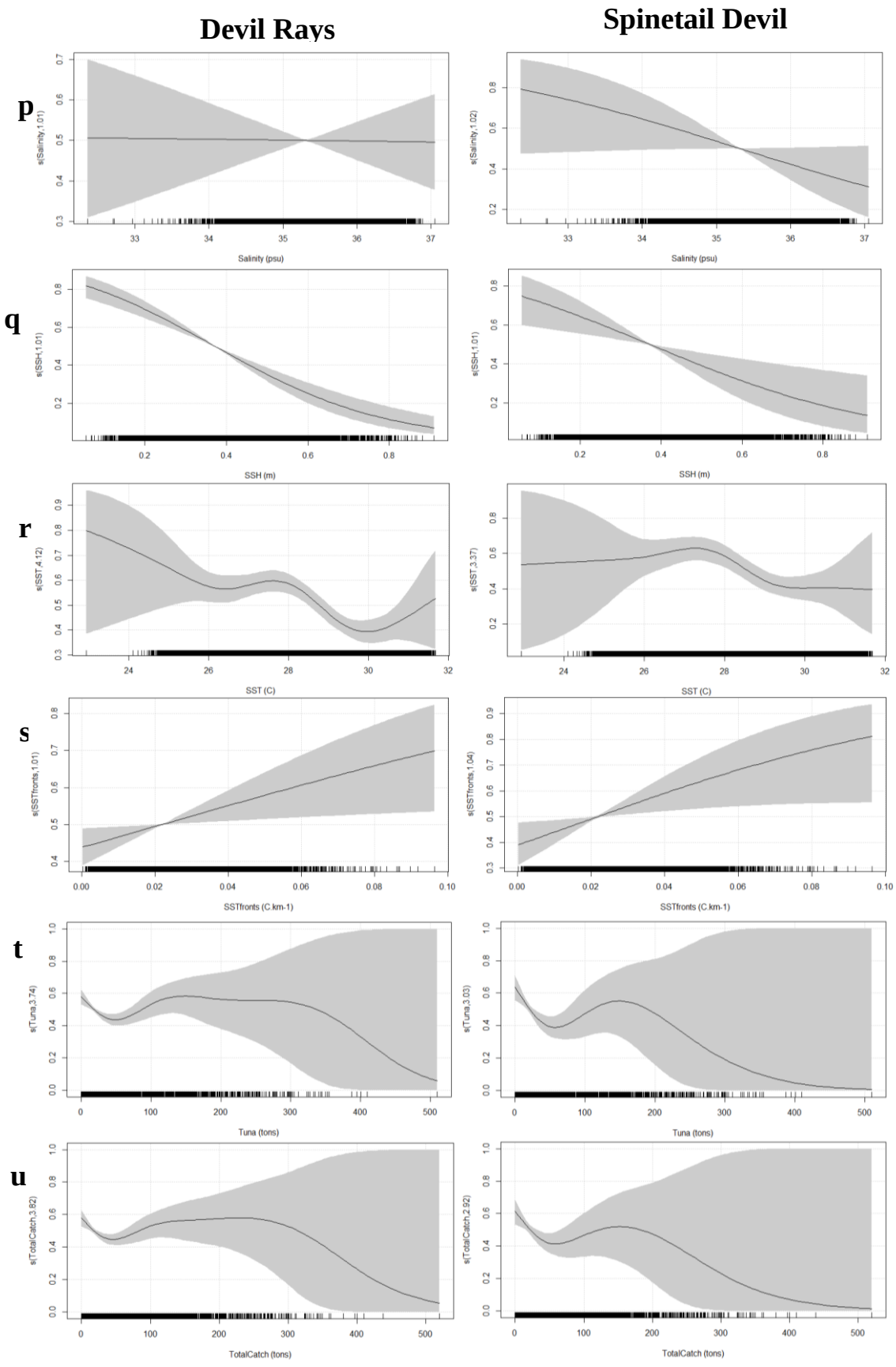

Figure S7 3 Univariate smooth fits of covariates from modelling the presence of devil rays in the left column and spinetail devil ray in the right column. p) Salinity (psu), q) Sea surface height (m), r) Sea surface temperature (^{o}C), s) Sea surface temperature fronts (^{o}C. km $^{-1}$), t) target tuna catch (tons), u) total catch including targeted species and bycatch species (tons).

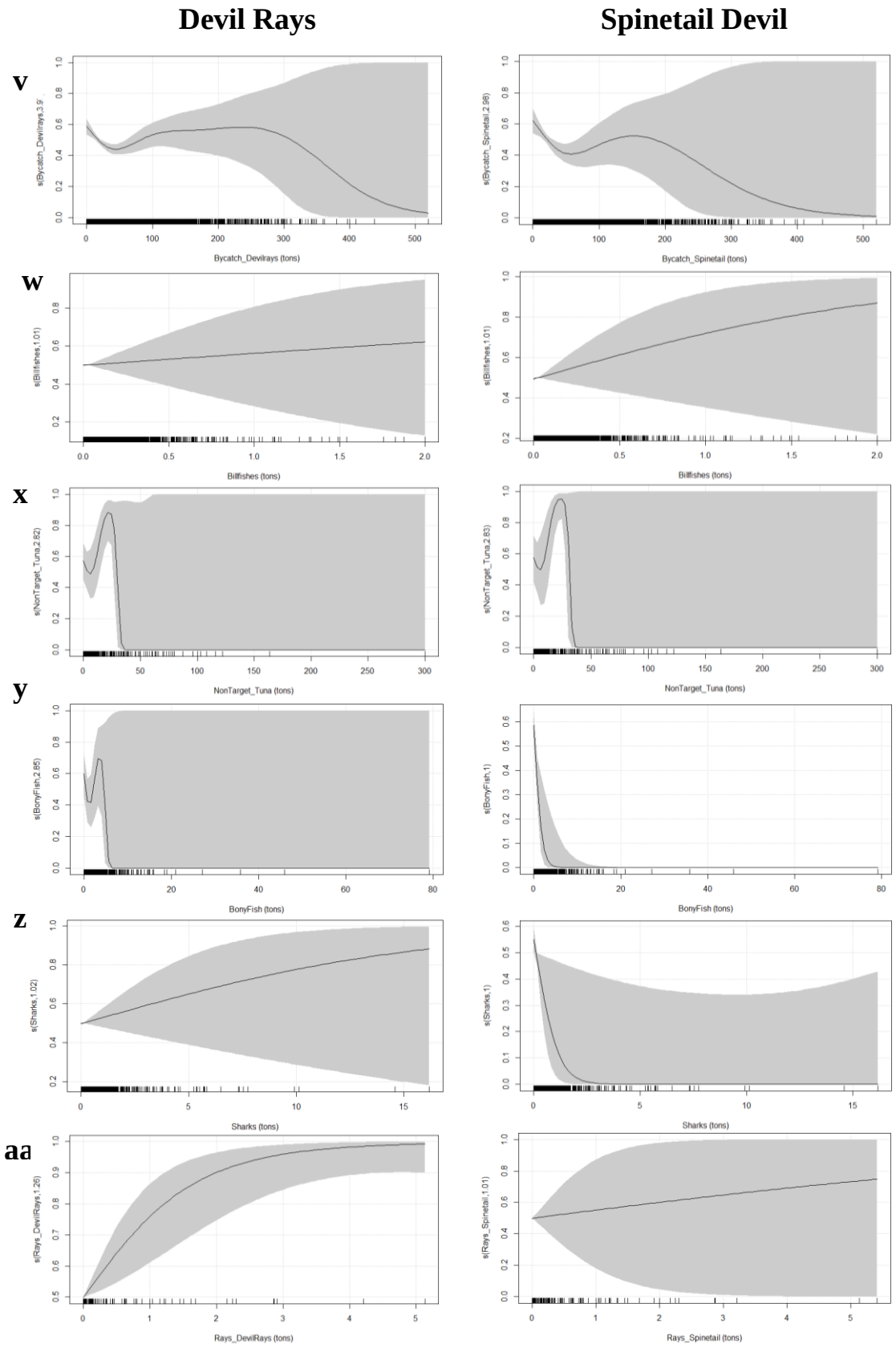

Figure S7 4 Univariate smooth fits of covariates from modelling the presence of devil rays in the left column and spinetail devil ray in the right column. v) total catch of bycatch species excluding devil ray and spinetail devil ray respectively (tons), w) total catch of Billfishes (tons), x) total catch of Non target tuna catch (tons), y) total catch of other bony fishes (tons), z) total catch of sharks (tons), aa) Total catch of rays excluding devil rays and spinetail devil rays respectively (tons).

a

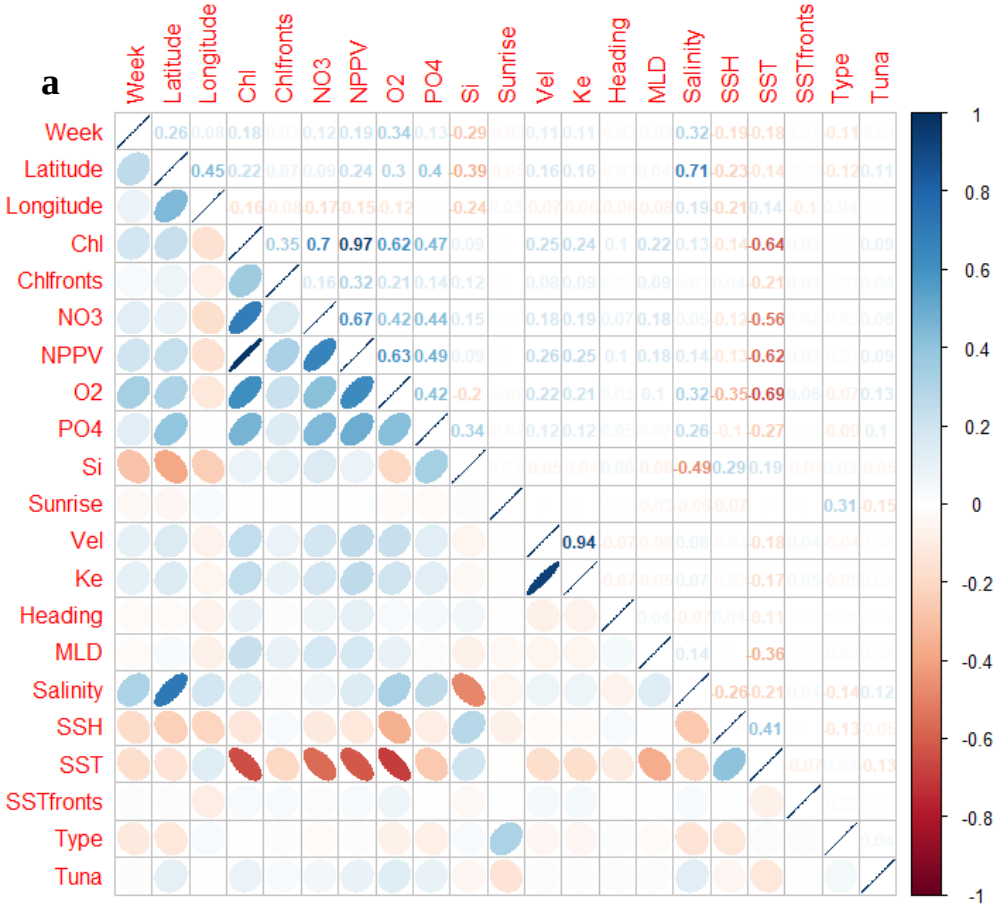

b

Variables	VIF
Week	1.28
Latitude	3.55
Longitude	1.61
Chl	23.33
Chlfronts	1.22
NO3	2.46
NPPV	20.99
O2	3.06
PO4	2.75
Si	2.73
Sunrise	1.17
Vel	8.23
Ke	8.20
Heading	1.05
MLD	1.38
Salinity	2.72
SSH	1.54
SST	3.74
SSTfronts	1.03
Type	1.23
Tuna	1.08

Figure S 8 Pearson correlations and variance inflation factor for measuring the correlation and collinearity between variables. a. Pearson correlation with correlation values p>0.6 considered to be highly correlated. b. vif of greater than 5 is considered highly collinear.

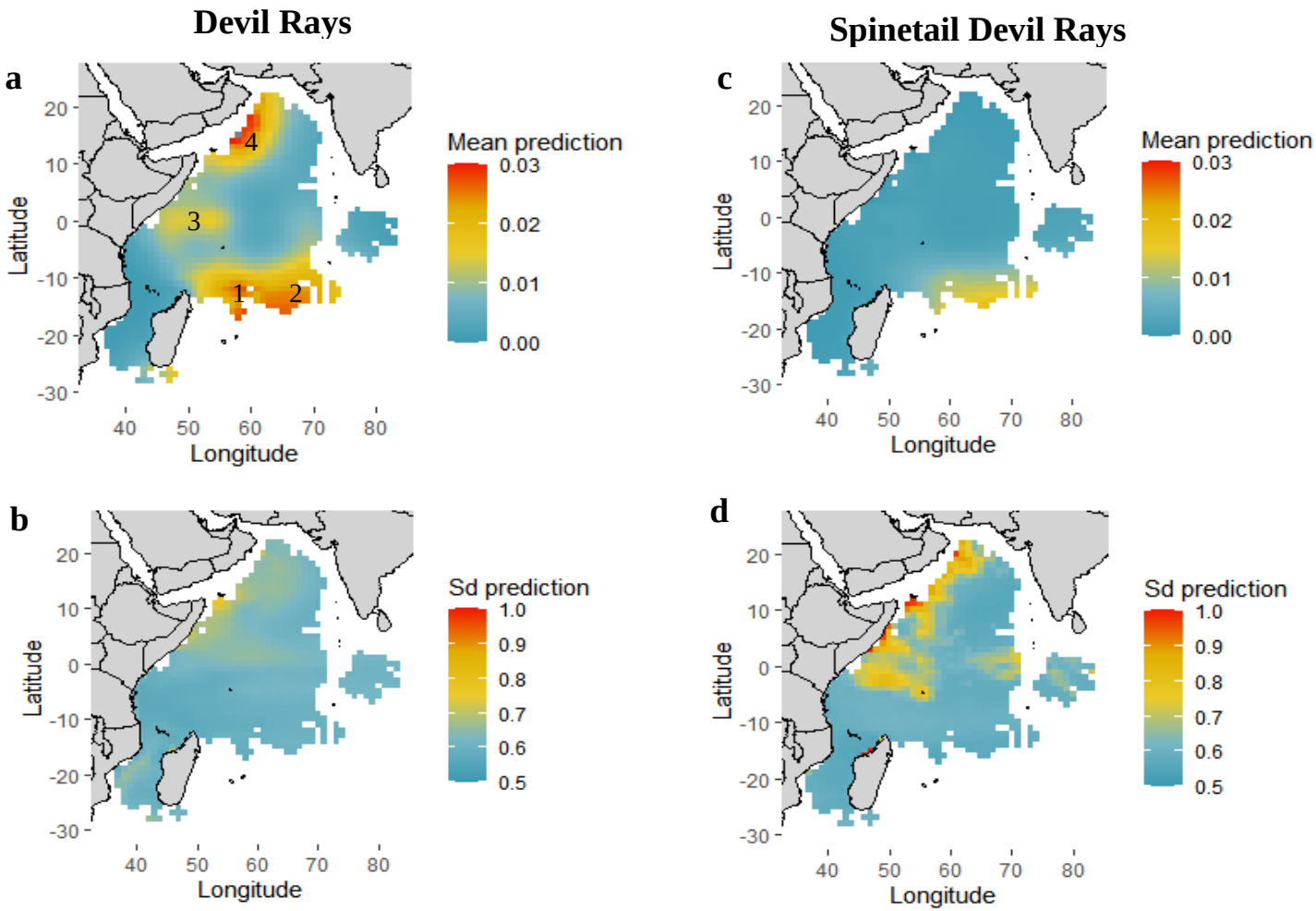

Figure S 9 Mean prediction and standard deviation of the presence of devil rays between 2010 and 2020 in the Western Indian Ocean. FADs were used as the fishing set type for model predictions. a. Devil rays´ mean prediction, b. Devil rays' standard deviation, c. Spinetail devil ray *Mobula mobular* mean prediction, d. Spinetail devil ray *Mobula mobular* standard deviation. For FSC as a fishing set type for model prediction *see* Figure S4. The main hotspots identified are 1) Mascarene plateau, 2) Central Indian Ridge, 3) Equatorial region, 4) Western Arabian Sea

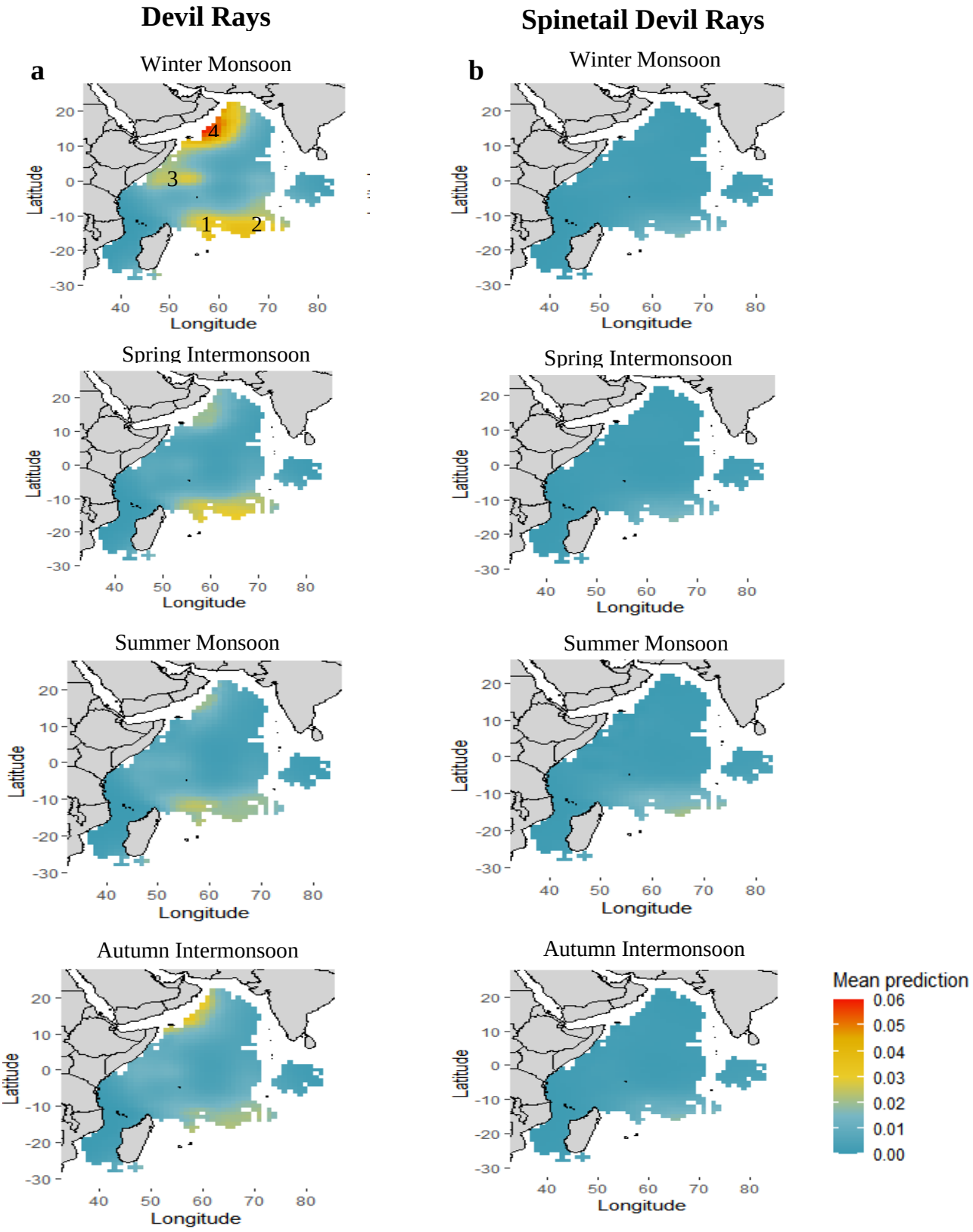

Figure S 10 Mean prediction of the presence of devil rays between 2010 and 2020 in the Western Indian Ocean by monsoon regime. FADs were used as the fishing set type for model predictions. a) devil ray's prediction in winter monsoon, spring intermonsoon, summer monsoon, autumn intermonsoon; b) spinetail devil rays *Mobula mobular* during winter monsoon, spring intermonsoon, summer monsoon, autumn intermonsoon. For FSC as the main fishing set type for model prediction *see* Figure S5. The main hotspots identified are 1) Mascarene plateau, 2) Central Indian Ridge, 3) Equatorial region, 4) Western Arabian Sea

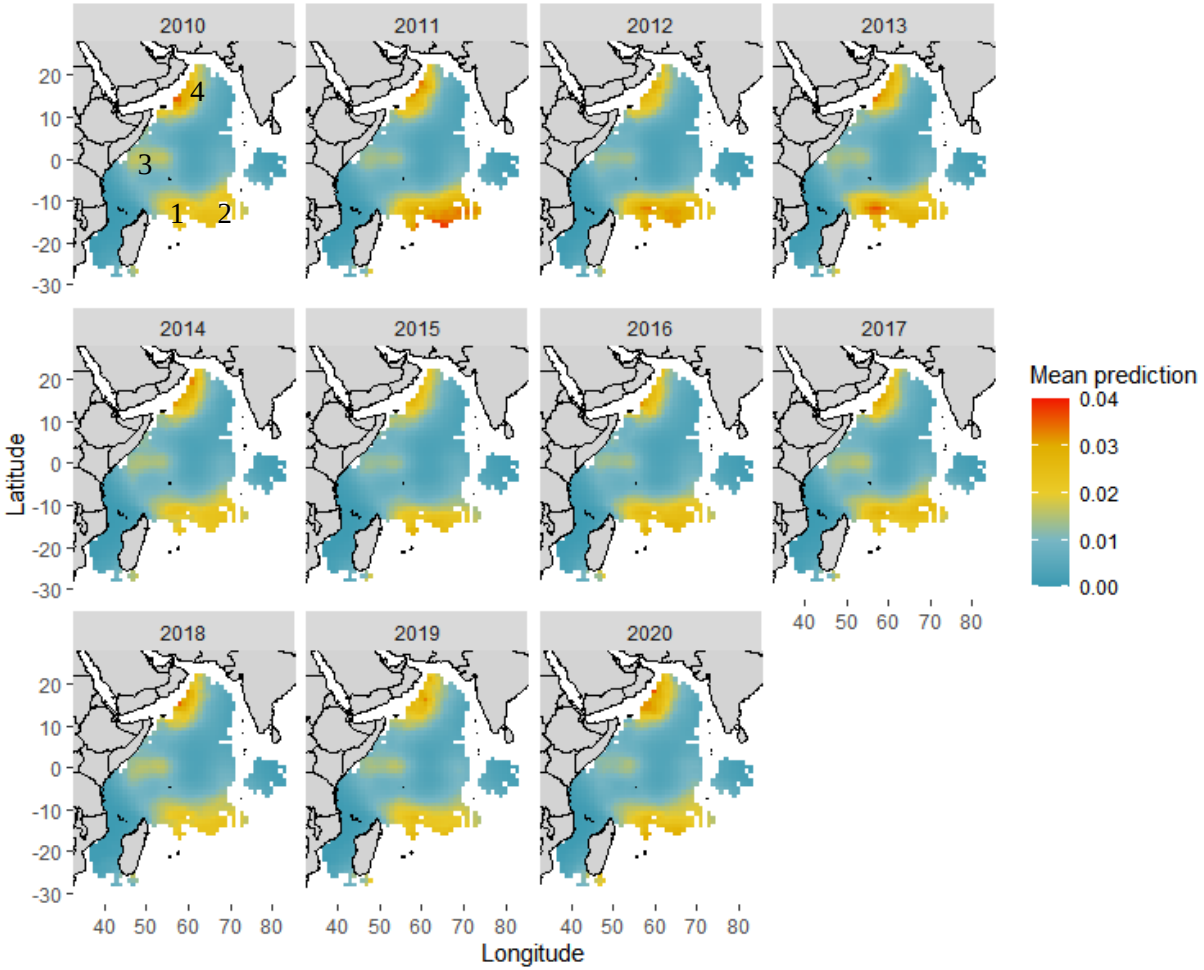

Figure S 11 Mean annual prediction of the presence of devil rays between 2010 and 2020 in the Western Indian Ocean. FADs was used as the fishing set type for model predictions. For FSC as the main fishing set type for model prediction *see* Figure S6. The main hotspot identified are 1) Mascarene plateau and 2) Central Indian Ocean ridge, 3) equatorial regions near ITCZ, 4) Western Arabian Sea.

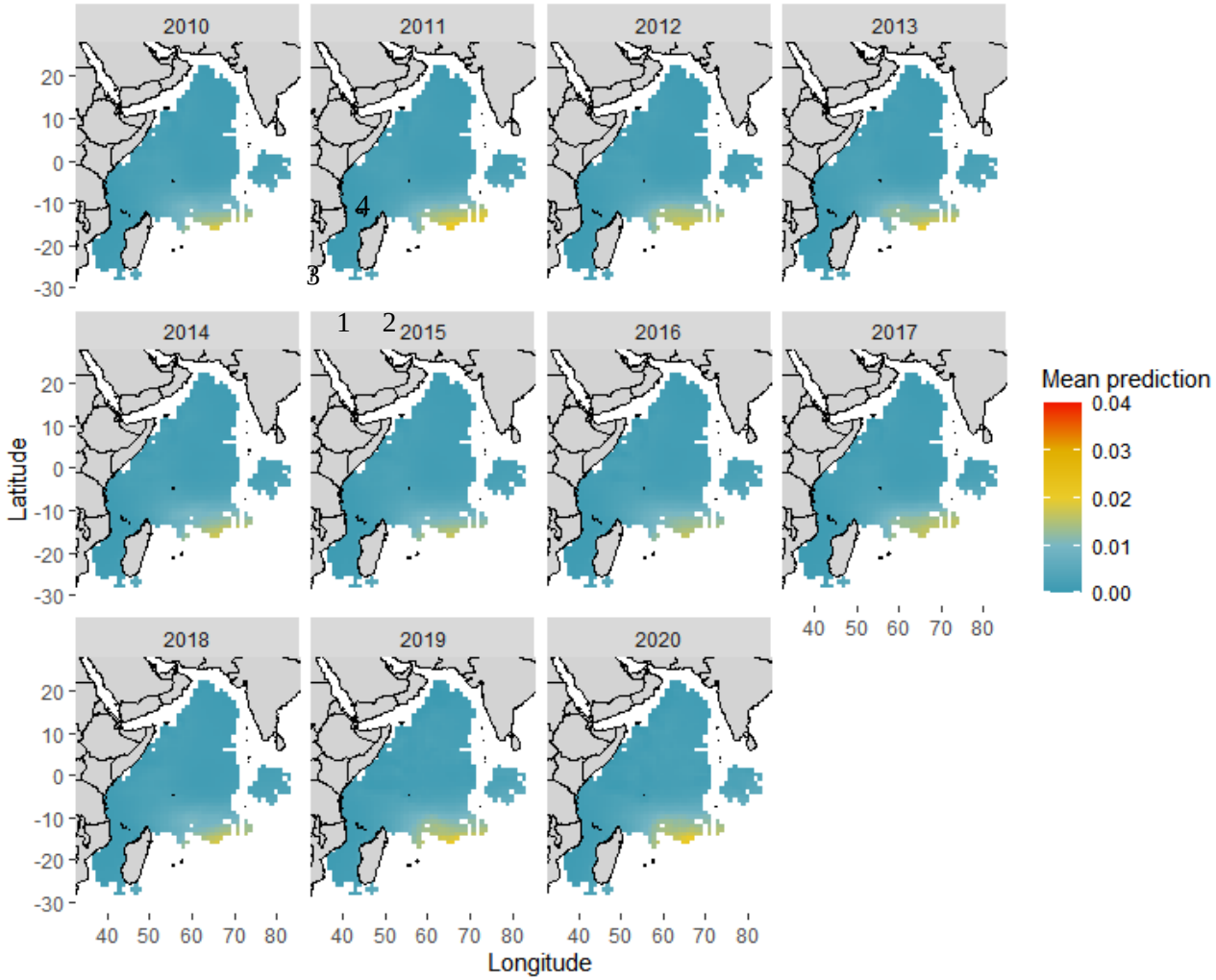

Figure S 12 Mean annual prediction of the presence of spinetail devil rays *Mobula mobular* between 2010 and 2020 in the Western Indian Ocean. FADs were used as the fishing set type for model predictions. For FSC as the main fishing set type for model prediction see Figure S7. The main hotspot identified are 1) Mascarene plateau and 2) Central Indian Ocean ridge, 3) equatorial regions near ITCZ, 4) Western Arabian Sea.

List of Animation

Animation S 1 Weekly Sea surface height values between 2010 and 2020 in the Western Indian Ocean

Animation S 2 Weekly habitat suitability predictions between 2010 and 2020 for Devil Rays in the Western Indian Ocean using FSC as the fishing set type for model prediction.

Animation S 3Weekly habitat suitability predictions between 2010 and 2020 for Spinetail Devil Ray *Mobula mobular* in the Western Indian Ocean using FSC as the fishing set type for model prediction.

https://drive.google.com/drive/folders/1l21ZNschXKhc5AYGdiV4WzrkM9-y9-gD?usp=sharing